2023-08-22

Estimating Hemispheric Specialization in Autistic and Neurotypical Individuals

Madeline Peterson
Brigham Young University

Estimating Hemispheric Specialization in Autistic and Neurotypical Individuals

Madeline Peterson

A dissertation submitted to the faculty of
Brigham Young University
in partial fulfillment of the requirements for the degree of

Doctor of Philosophy

Jared A. Nielsen, Chair
Derin Cobia
Rebecca A. Lundwall
C. Brock Kirwan

Department of Psychology

Brigham Young University

ABSTRACT

Estimating Hemispheric Specialization in Autistic and Neurotypical Individuals

Madeline Peterson
Department of Psychology, Brigham Young University
Doctor of Philosophy

While the brain appears to be symmetrical, macroscopic differences or asymmetries between the two hemispheres emerge through careful quantitative study. Functional asymmetries can accompany these structural asymmetries, and these can be a reflection of hemispheric specialization, or the predominant hosting of macroscale functional network and its accompanying functional properties by a given hemisphere. Prior work has identified the specialization of language to the left hemisphere, visuospatial attention to the right hemisphere, and a dual specialization of executive control to both hemispheres. However, it is largely unknown how specialization is characterized at an individual level, particularly in terms of identifying the specific connections that contribute to the specialization of a given network.

The present article-style dissertation explores human brain organization through the lens of specialization within individuals. Secondary to this goal is establishing reliable and valid methods for estimating specialization, as well as examining atypical patterns of specialization. Study 1 focuses on identifying specialized networks and investigating the relationships between these networks in neurotypical adults through the use of a novel, surface area-based measure of specialization. After establishing this measure of specialization in neurotypical individuals, Study 2 explores functional specialization within a neurodevelopmental condition, including the potential ramifications of atypical specialization for specific behavioral phenotypes. Taking a different approach to estimating specialization, Study 3 replicates and expands on prior work, examining the underpinnings of network specialization and providing support for principles governing contributions to specialization. Collectively, these studies elucidate the particulars of functional specialization within individuals, illustrating the complexity of brain organization through large-scale networks.

Keywords: lateralization, specialization, asymmetry, brain networks, brain organization, network specialization, hemispheric specialization, neuroimaging, MRI, fMRI, precision neuroimaging, autism, autism spectrum conditions, neurodevelopment

ACKNOWLEDGEMENTS

I am grateful for the abundant support which I have received with this endeavor, particularly from my family, friends, cohort, labmates, committee chair, and committee members. I am especially thankful to my parents for the frequent disbursement of encouragement and wisdom.

TABLE OF CONTENTS

LIST OF FIGURES

LIST OF TABLES

Estimating Hemispheric Specialization in Autistic and Neurotypical Individuals

Overall Introduction

As a key principle of brain organization, hemispheric asymmetries are found at levels ranging from the cytoarchitectonic to the structurally macroscopic (for review, see Toga & Thompson, 2003). Often accompanying these structural asymmetries are functional asymmetries, which are reflections of hemispheric specialization. In this context, specialization refers to the predominant hosting of a macroscale functional network and its associated functional properties by one hemisphere (Hervé et al., 2013). This organizational design appears to hold evolutionary value and play key roles in brain development and processing. Rather than duplicate processing capacities across both hemispheres and waste neural space (Corballis, 1991; Güntürkün & Ocklenburg, 2017), it is thought that evolutionary pressures conspired to produce hemispheric specialties, resulting in greater overall efficiency (Levy, 1969) and processing speed (Ringo et al., 1994). Given the evident importance of specialization to brain organization, functional specialization findings within individuals are remarkably limited.

To ameliorate this gap, the present dissertation explores human brain organization through the lens of functional specialization within individuals. Secondary to this goal is the development of robust methods for estimating specialization within individuals, as well as the investigation of specialization within a neurodevelopmental population. In the following sections, three studies and associated supplementary materials achieving these aims are described (see the Appendix for deviations from the prospectus and accompanying justification).

Study 1 approaches the problem of estimating specialization within individuals through the use of a novel measure: the network surface area ratio. Following the development of this

measure, the networks with the greatest specialization were identified, and the nature of relationships between specialized networks was characterized.

After establishing a method of within-individual specialization in neurotypical adolescents and adults, this method was applied to a neurodevelopmental population in Study 2. Potential deviations in specialization in autism were explored, followed by the examination of hypothesized relationships between language specialization and three behavioral phenotypes: verbal ability, autism symptom severity, and language delay.

Finally, Study 3 characterizes within-individual specialization through the autonomy index, a method previously applied at the group level. After estimating specialization in seventeen networks, specialization was deconstructed through the identification of the connections contributing the most to a given networks specialization, unraveling principles governing network specialization.

Through the use of robust measures for estimating specialization, the three studies contribute to the overall goal of understanding individual human brain organization. Importantly, the following results highlight the potential consequences of atypical specialization patterns for a specific neurodevelopmental condition. Together, the findings illustrate the complexities of brain organization, evident even at the macroscale network level.

References

Corballis, M. C. (1991). *The lopsided ape: Evolution of the generative mind.* (pp. vii, 366). Oxford University Press.

Güntürkün, O., & Ocklenburg, S. (2017). Ontogenesis of lateralization. *Neuron*, *94*(2), 249–263. https://doi.org/10.1016/j.neuron.2017.02.045

Hervé, P.-Y., Zago, L., Petit, L., Mazoyer, B., & Tzourio-Mazoyer, N. (2013). Revisiting human hemispheric specialization with neuroimaging. *Trends in Cognitive Sciences*, *17*(2), 69–80. https://doi.org/10.1016/j.tics.2012.12.004

Levy, J. (1969). Possible basis for the evolution of lateral specialization of the human brain. *Nature*, *224*(5219), Art. 5219. https://doi.org/10.1038/224614a0

Ringo, J. L., Doty, R. W., Demeter, S., & Simard, P. Y. (1994). Time is of the essence: A conjecture that hemispheric specialization arises from interhemispheric conduction delay. *Cerebral Cortex*, *4*(4), 331–343. https://doi.org/10.1093/cercor/4.4.331

Toga, A. W., & Thompson, P. M. (2003). Mapping brain asymmetry. *Nature Reviews Neuroscience*, *4*(1), Art. 1. https://doi.org/10.1038/nrn1009

Study 1: Estimating Brain Network Specialization: The Development and Use of the Network Surface Area Ratio

Abstract

The two hemispheres of the brain are asymmetric in structure and function. On the network-level, the language network is known to exhibit left hemisphere lateralization while the visuospatial network is known to exhibit right hemisphere lateralization. However, it remains unknown which networks are the most functionally specialized when a greater number of networks are examined, as well as how network specialization is related between networks. In the present study, we estimated network specialization using a network surface area-based approach across four datasets. After examining the validity and reliability of individual network parcellations and this surface area-based measure of specialization, we addressed two hypotheses. First, we hypothesized that networks associated with language, visuospatial attention, and executive control would show the greatest specialization. Second, we hypothesized that network specialization relationships would follow one of three hypotheses: covariation, compensation, or independence. Exploratory factor analyses were used to examine relationships between networks' specialization.

Keywords: Lateralization, specialization, asymmetry, brain networks, network specialization, hemispheric specialization, neuroimaging, precision neuroimaging, MRI, fMRI

Introduction

Observations of the human brain have revealed significant differences in the gross anatomical morphometry between the two hemispheres (for review, see Toga & Thompson, 2003). These structural asymmetries are accompanied by functional asymmetries, such as language specialization. Famously, Paul Broca traced language specialization to the left hemisphere subsequent to identifying a lesion in the left inferior frontal gyrus of his patient as being responsible for his eponymous aphasia (Broca, 1861). This contribution launched an emphasis on regions specialized for language, which only recently shifted to a focus on a functional language network (Fedorenko & Thompson-Schill, 2014; Petersen & Sporns, 2015).

Contemporarily, the language network is regarded as a prototypical example of a lateralized network, with left-hemisphere language lateralization estimated to occur in most (Breier et al., 2000; Stippich et al., 2003) to more than 90% of the general population (Corballis, 2003). The canonical language network is a distributed network of regions across the frontal, temporal, and parietal lobes, and these regions were identified using a rigorously tested task-based fMRI approach (Fedorenko et al., 2010, 2011; Fedorenko, McDermott et al., 2012; Lipkin et al., 2022; Scott et al., 2017) and a functional connectivity-based approach (Braga et al., 2020). Remarkably, the overwhelmingly asymmetric organization of this network in neurotypical individuals continues to be replicated (Elin et al., 2022; Malik-Moraleda et al., 2022; Olulade et al., 2020; Reynolds et al., 2019).

This line of research has expanded to include additional specialized functional networks in both the right and left hemispheres, which support distinct cognitive processes and behaviors. In this context, “specialization” refers to the dominant hosting of a macroscale functional network and its associated functional properties by one hemisphere over the other (Hervé et al.,

2013). For example, a right-lateralized attention network composed of the temporoparietal junction and ventral frontal areas is hypothesized to process visuospatial information, particularly unexpected stimuli (Corbetta & Shulman, 2002). Of note, one study quantified specialization across seven functional networks and found that specialization was not restricted to a single left- or right-specialized network (Wang et al., 2014). Rather, the right frontoparietal network and right ventral and dorsal attention networks, as well as the left default and frontoparietal networks exhibited specialization as assessed via a functional connectivity-based metric (see Figure 5; Wang et al., 2014). While these and other studies have made significant contributions, much regarding network and hemispheric specialization within individuals remains unknown.

Methods of Examining Hemispheric Specialization

In humans, hemispheric specialization has historically been identified using a variety of methods including split-brain patients (for review, see Gazzaniga, 2000), lateralized brain lesions (Milner, 1971; Rasmussen & Milner, 1977), the Wada test (Wada & Rasmussen, 1960), and intraoperative brain stimulation mapping (Penfield & Jasper, 1954). These methods have since been extended to include a suite of neuroimaging metrics, many of which are functional connectivity-based. Of particular interest are the intrinsic laterality index (Liu et al., 2009), autonomy index (Wang et al., 2014), hemispheric contrast (Gotts et al., 2013), functional lateralization metric (Nielsen et al., 2013), classification metric (Friedrich et al., 2022), and network variants approach (Perez et al., 2023). Despite the unifying aim of estimating hemispheric specialization, each of the listed methods varies in terms of how it approaches structural asymmetries, the addition of covariates such as handedness and gender, and short- and long-range connectivity. However, with few exceptions, each relies upon group-based analyses

in estimating specialization, a tactic which is increasingly being exchanged for a within-individual "precision" approach.

A Precision Approach

The precision approach, which emphasizes individual-level analyses, has been intertwined with fMRI research since its early days, starting with a study in 1991 involving a single participant and a flickering lights paradigm (Kwong, 2012). Over three decades later, a return to this design is being heralded as a well-powered alternative to the large and costly sample sizes required for cross-sectional group and brain-wide association studies (Gratton et al., 2022; Marek et al., 2022). This method of densely sampling individuals can, as noted by Marek et al. (2022), generate precise brain maps as well as blueprints for reducing MRI artifacts. Moreover, when combined with functional localizers, individual approaches offer superior sensitivity, functional resolution, and interpretability (Fedorenko, 2021).

Precision Specialization

In line with the precision neuroimaging approach and previous efforts to understand brain network organization and specialization, the present study examines two open questions. First, we explore which networks exhibit the highest hemispheric specialization. A recent study involving 18 densely-sampled individuals demonstrated that among six networks, the language network displayed the greatest left hemisphere specialization, while a frontoparietal control network exhibited the greatest right hemisphere specialization (Braga et al., 2020). However, it remains unclear how these estimates might change in a larger sample with a greater number of examined networks. Building upon the work of Braga et al. (2020), we hypothesized that networks associated with language, visuospatial attention, and executive control would show the greatest hemispheric specialization.

Second, we investigate how specialization in one network may influence the specialization of other networks. We propose the following three hypotheses to guide our investigation. The first hypothesis suggests that if an individual possesses a highly specialized network, other networks for that individual will exhibit increased specialization (the covariation hypothesis). The second hypothesis suggests that if one network is highly specialized, other networks will be less specialized (the compensatory hypothesis). The third hypothesis proposes that network specialization is unrelated between networks within an individual (the independent hypothesis).

Methods

Datasets and Overview

Three independent datasets were used for these analyses: The Human Connectome Project (HCP; split into discovery and replication datasets), the Human Connectome Project-Development (HCPD; Somerville et al., 2018), and the Natural Scenes Dataset (NSD; Allen et al., 2022). Each dataset was selected for its relatively high quantity of low-motion data per participant (see Figure 1).

HCP Discovery and Replication

The HCP S1200 release consists of 1206 subjects (1113 with structural MRI scans) collected at 13 different data acquisition sites with informed consent (Van Essen et al., 2013). Additional details regarding HCP scanning protocols are available online (https://humanconnectome.org/storage/app/media/documentation/s1200/HCP_S1200_Release_Appendix_I.pdf; Uğurbil et al., 2013; Van Essen et al., 2012). With a relatively large quantity of data available per individual, this dataset is ideally suited for taking a within-individual approach to specialization. Participants underwent four 15-minutes runs of a passive fixation task (resting-

state fMRI) during which they were asked to keep their eyes open while viewing a white cross on a dark background and think of nothing in particular while remaining awake (Smith et al., 2013). Exclusion criteria for the HCP S1200 release included removing participants with a mean framewise displacement greater than 0.2 mm and mean DVARS greater than 50, participants missing handedness data, and participants with less than 50% of volumes remaining after motion censoring. This resulted in a subsample of 553 participants, which was split into a discovery and replication dataset using random sampling without replacement. The two datasets were then compared using the R package MatchIt (Ho et al., 2023) on age, mean framewise displacement, sex, handedness, and percentage of volumes remaining following motion censoring. The HCP-Discovery dataset consisted of 276 participants 22-36 years old (M = 28.48, SD = 3.58) with 167 females, while the HCP-Replication dataset consisted of 277 participants 22-36 years old (M = 28.7, SD = 3.77) with 173 females.

HCPD

With a younger sample and smaller quantity of data per individual, the HCPD dataset was used as an additional replication dataset for primary analyses. Since data collection for the HCPD project is ongoing, cross-sectional data from the latest release were included, and these were composed of 652 healthy participants. All data were obtained with informed assent or consent. As a part of the HCPD protocol, participants underwent four 6.5-minute runs of resting-state fMRI, with an exception for participants 5-7 years old, which had six 3.5-minute runs each (Harms et al., 2018). Participants were instructed to view a small white fixation crosshair on a black background and blink normally. Exclusion criteria for HCPD included removing participants with less than 50% of volumes remaining after motion censoring, participants missing handedness data, and participants with a mean framewise displacement greater than 0.2

mm and mean DVARS greater than 50 (see Figure 1). Following the exclusion criteria, the dataset consisted of 343 individuals ages 11-21.92 (M = 15.93, SD = 2.97) of which 189 were female.

NSD

With a large quantity of resting-state and task fMRI data available per individual, the NSD was included to examine potential task effects on estimating individual network parcellations and specialization. The NSD is composed of eight individuals (two males and six females; age range 19–32 years). All data were obtained with informed written consent according to the University of Minnesota institutional review board. As detailed in Allen et al. (2022), participants averaged two hours of resting state fMRI and 39.5 hours of task-based fMRI. For the resting-state runs, participants were instructed to stay awake and fixate on a white cross placed on a gray background but otherwise rest. During the task-based runs, participants were shown distinct natural scenes taken from the Microsoft Common Objects in Context database (Lin et al., 2014). Images were presented for 3 s with 1-s gaps in between images. Subjects fixated centrally and performed a long-term continuous recognition task on the images. Exclusion criteria for NSD included removing participants with less than 50% of volumes remaining after motion censoring, and participants with a mean framewise displacement greater than 0.2 mm and mean DVARS greater than 50. No subjects were excluded from the analysis; however, following motion correction, a minimum of 12 resting-state fMRI runs (approximately 60 minutes) remained. In order to compare resting-state and task data on equal grounds, only the first 12 available resting-state runs and the first 12 available task fMRI runs from each participant were utilized.

Figure 1

Participant Age, Data Quality, and Data Availability

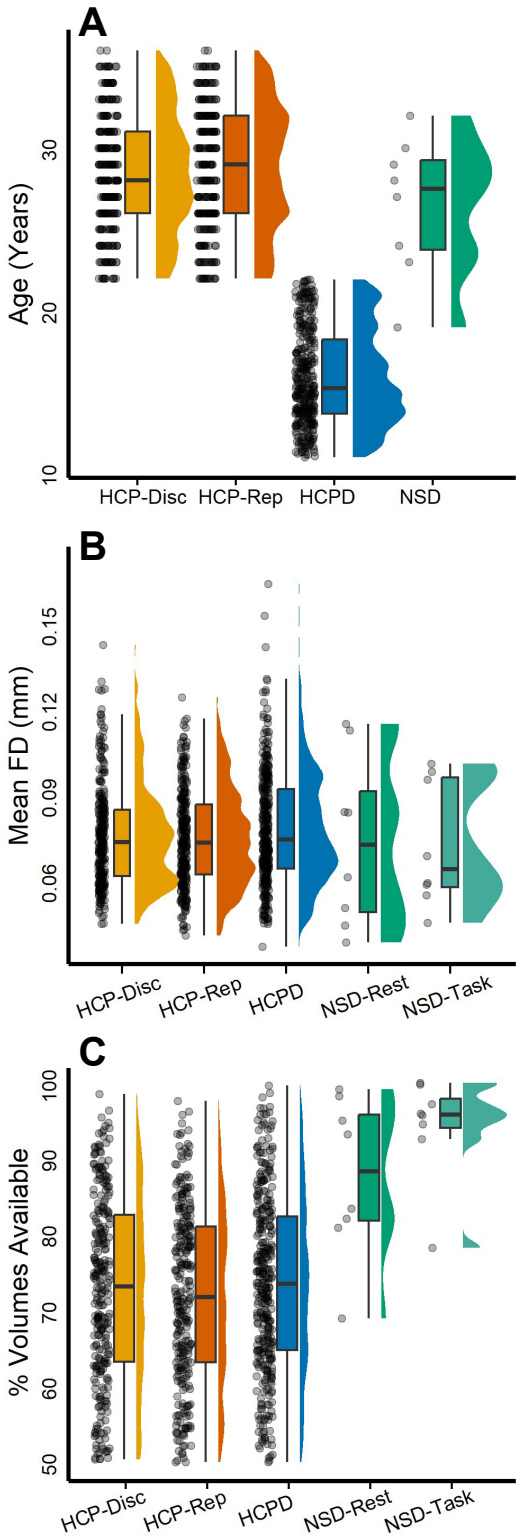

Note. Panel A depicts participant age across each dataset following the implementation of exclusion criteria. HCP-Discovery participants included 276 individuals 22-36 years of age, HCP-Replication participants included 277 individuals 22-36 years of age, HCPD participants included 343 individuals 11-22 years of age, and NSD participants included eight individuals 19-32 years of age. Panel B depicts the mean framewise displacement (FD) across each dataset following the implementation of exclusion criteria. HCP-Discovery mean FD was 0.08 mm (*SD* = 0.02 mm), range 0.04-0.14 mm; HCP-Replication mean FD was 0.07 mm (*SD* = 0.01 mm), range 0.04-0.12 mm; HCPD mean FD was 0.08 mm (*SD* = 0.02 mm), range 0.04-0.16 mm; NSD-Rest mean FD was 0.07 mm (*SD* = 0.03), range 0.04-0.11 mm; and NSD-Task mean FD was 0.07 mm (*SD* = 0.02 mm), range 0.04-0.1 mm. Panel C depicts the percentage of volumes remaining following motion-correction procedures for each dataset. HCP-Discovery mean percentage of volumes was 72.81% (*SD* = 12.12%), range 50.38-98.54%; HCP-Replication mean percentage of volumes was 72.09% (*SD* = 11.59%), range 50.04-97.62%; HCPD mean percentage of volumes was 73.6% (*SD* = 11.73%), range 50.05-99.63%; NSD-Rest mean percentage of volumes was 87.64% (*SD* = 10.51%), range 68.98-99.14%; and NSD-Task mean percentage of volumes was 94.27% (*SD* = 6.92), range 78.31-100%. Across each panel, a circle represents a single participant.

MRI Acquisition Parameters

HCP Discovery and Replication

The HCP dataset was acquired on a custom Siemens 3T Skyra with a 32-channel head coil. T1-weighted images were collected with a 3D MPRAGE sequence with isotropic 0.7 mm voxels (256 sagittal slices, repetition time [TR] = 2400 milliseconds, echo time [TE] = 2.14 milliseconds) as detailed in Glasser et al. (2013). Resting-state functional images were collected

using 2 mm isotropic voxels (72 sagittal slices, TR = 720 milliseconds, TE = 33 milliseconds, multiband accelerated pulse sequence with multiband factor = 8) as detailed in Glasser et al. (2013, 2016).

HCPD

The HCPD MRI data were acquired on Siemens 3T Prisma scanners with vendor 32-channel headcoils at four sites: Harvard University, University of California-Los Angeles, University of Minnesota, and Washington University in St. Louis (Harms et al., 2018). Structural T1-weighted scans were acquired with a multi-echo MPRAGE sequence (van der Kouwe et al., 2008) with 0.8 mm isotropic voxels (sagittal FOV = 256 × 240 × 166; matrix size = 320 × 300 × 208 slices; slice oversampling = 7.7%; 2-fold in-plane acceleration (GRAPPA); pixel bandwidth = 744 Hz/Px; Tr/TI = 2500/1000, TE = 1.9/3.6/5.4/7.2 ms, flip angle = 8°; water excitation employed for fat suppression; up to 30 TRs allowed for motion-induced reacquisition). T2*-weighted scans were used for rs-fMRI with 2D multiband gradient-recalled echo echo-planar imaging sequence (MB8, TR/TE = 800/37 ms, flip angle = 52°) and 2.0 mm isotropic voxels covering the whole brain (72 oblique-axial slices). Functional scans were acquired in pairs of two runs with opposite phase encoding polarity (anterior-to-posterior and posterior-to-anterior) so that fMRI data were not biased towards either phase encoding polarity. For all scans, Framewise Integrated Real-time MRI Monitoring (Dosenbach et al., 2017) was implemented to provide motion feedback to participants between fMRI runs.

NSD

The NSD dataset was acquired at the Center for Magnetic Resonance Research at the University of Minnesota (Allen et al., 2022). Anatomical data (such as T1-weighted volumes) were collected using a 3T Siemens Prisma scanner with a standard Siemens 32-channel RF head

coil while functional data were collected using a 7T Siemens Magnetom passively shielded scanner and a single-channel-transmit, 32-channel-receive RF head coil. T1-weighted images were acquired with a MPRAGE sequence (0.8-mm bandwidth 220 Hz per pixel, no partial Fourier, in-plane acceleration factor (iPAT) 2, TA = 6.6 min per scan). Functional data were collected using gradient-echo EPI at 1.8-mm isotropic resolution with whole-brain coverage (84 axial slices, slice thickness 1.8 mm, slice gap 0 mm, field-of-view 216 mm (FE) × 216 mm (PE), phase encode direction anterior-to-posterior, matrix size 120 × 120, TR = 1,600 milliseconds, TE = 22.0 milliseconds, flip angle 62°, echo spacing 0.66 milliseconds, bandwidth 1,736 Hz per pixel, partial Fourier 7/8, iPAT 2, multi-band slice acceleration factor 3). Full protocol printouts for the NSD dataset are available online (https://cvnlab.slite.page/p/NKalgWd__F/Experiments).

fMRI Preprocessing

Preprocessing took place on raw NIFTI files for the resting-state fMRI and task fMRI runs using a pipeline developed by the Computational Brain Imaging Group (CBIG; (Kong et al., 2019; Li et al., 2019); code is available online at https://github.com/ThomasYeoLab/CBIG/tree/c773720ad340dcb1d566b0b8de68b6acdf2ca505/stable_projects/preprocessing/CBIG_fMRI_Preproc2016). This CBIG2016 preprocessing pipeline was selected to process the fMRI data in order to more closely follow the processing steps used to implement the multi-session hierarchical Bayesian modeling parcellation method (Kong et al., 2019). As a prerequisite, this pipeline requires FreeSurfer recon-all output from the structural data (FreeSurfer 6.0.1; Dale et al., 1999). The fMRI data were then processed with the following steps: 1) removal of the first four frames and 2) motion correction using rigid body translation and rotation with the FSL package (Jenkinson et al., 2002; Smith et al., 2004). The structural and functional images are then aligned using boundary-based registration (Greve & Fischl, 2009)

using the FsFast software package (http://surfer.nmr.mgh.harvard.edu/fswiki/FsFast). FD and DVARS were computed using *fsl_motion_outliers* (Smith et al., 2004). Volumes with FD > 0.2 mm or DVARS > 50 were tagged as outliers. Uncensored segments of data lasting fewer than 5 contiguous volumes were also flagged as outliers (Gordon et al., 2016). BOLD runs with more than half of the volumes flagged as outliers were removed completely. Next, linear regression using multiple nuisance regressors was applied through a combination of CBIG in-house scripts and the FSL MCFLIRT tool (Jenkinson et al., 2002). Nuisance regressors consisted of global signal, six motion correction parameters, averaged ventricular signal, averaged white matter signal, and their temporal derivatives (totaling 18 regressors). The flagged outlier volumes were ignored during the regression procedure. Following the regression, a bandpass filter (0.009 Hz ≤ f ≤ 0.08 Hz) was applied using CBIG in-house scripts. At this point, the preprocessed fMRI data were projected onto the FreeSurfer fsaverage6 surface space (2 mm vertex spacing) with FreeSurfer's *mri_vol2surf* function. The projected fMRI data were then smoothed using a 6 mm full-width half-maximum kernel through FreeSurfer's *mri_surf2surf* function (Fischl et al., 1999). Surface space was selected for the following analyses in order to best follow the individual parcellation pipeline outlined in Kong et al. (2019), and following evidence that landmark surface-based registration outperforms volume-based registration (Anticevic et al., 2008; Argall et al., 2006; Desai et al., 2005; Van Essen, 2005).

Individual Network Parcellation

Following preprocessing, network parcellations were computed using a multi-session hierarchical Bayesian modeling (MS-HBM) pipeline. The MS-HBM pipeline is designed to generate parcellations for individuals with multiple sessions of fMRI data (Kong et al., 2019; Li et al., 2019) and is implemented in MATLAB R2018b (MATLAB, 2018). This particular model

has been selected because it accounts for intra-individual variation, allowing the model to better generalize to new fMRI data from the same participant. As an overview, this model uses a variational Bayes expectation-maximization algorithm to learn group-level priors from a training dataset and then apply those to estimate individual-specific parcellations (see Figure 2). This model estimates the following parameters: group-level network connectivity profiles, inter-subject functional connectivity variability, intra-subject functional connectivity variability, a spatial smoothness prior, and an inter-subject spatial variability prior. As recommended in the pipeline's GitHub documentation, subjects with a single available run post-preprocessing had that single run split in two and a connectivity profile was generated for each split. A k of 17 was selected for all participants (Yeo et al., 2011). Additionally, it has previously been demonstrated that MS-HBM parameters estimated from one dataset can be effectively applied to another dataset with significant differences in acquisition and preprocessing (Kong et al., 2021). Thus, to generate our model, priors trained on 40 Brain Genomics Superstruct Project (GSP) subjects were utilized (Holmes et al., 2015; Kong et al., 2019). Following the generation of individual parcellations, a Hungarian matching algorithm was used to match the parcellation labels with the Yeo et al. (2011) 17-network group parcellation labels.

Figure 2

Illustration of the Multi-Session Hierarchical Bayesian Modeling Individual Parcellation Pipeline

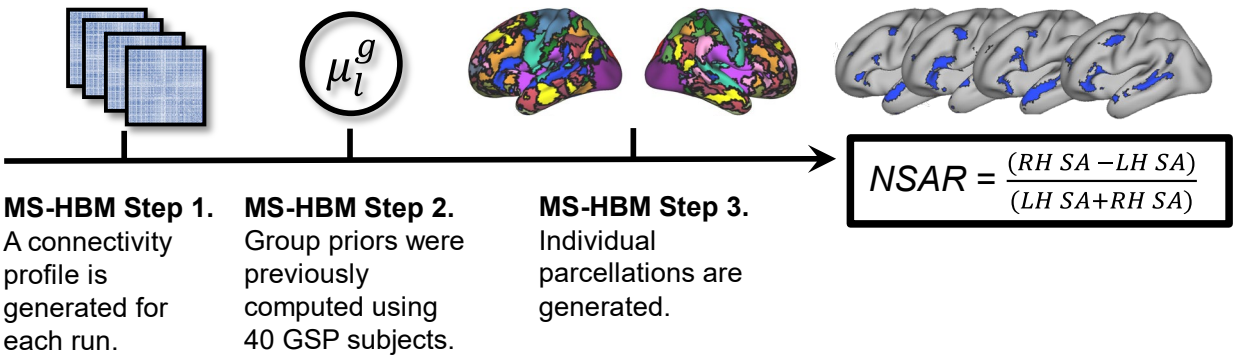

Note. First, a connectivity profile is generated for each available fMRI run on an individual basis (illustrated here as a functional connectivity matrix). Next, group priors previously estimated (Kong et al., 2019) from 40 Brain Genomics Superstruct Project (GSP) subjects were used. Third, the connectivity profiles from each available run and the group priors (more specifically, the inter-subject functional connectivity variability, intra-subject functional connectivity variability, spatial smoothness, and inter-subject spatial variability) are used to generate network parcellations for each participant. Finally, the network surface area ratio (NSAR) is calculated using the formula shown, where LH SA is the left hemisphere surface area for a given network and RH SA is the right hemisphere surface area for a given network. A negative NSAR value indicates left hemisphere specialization for a given network while a positive value indicates right hemisphere specialization.

Network Surface Area Ratio

Following the generation of individual network parcellations, specialization was estimated using a novel measure: the network surface area ratio (NSAR). This measure was

calculated within each individual for each of 17 networks by first extracting each network label as a region of interest using the Connectome Workbench wb_command functions *metric-label-import* and *gifti-label-to-roi* (Marcus et al., 2013). Next, the left and right hemisphere surface areas for a given network were calculated on an midthickness Conte69 surface in fsaverage6 resolution (Glasser & Essen, 2011) using the wb_command function *metric-stats*. Finally, NSAR was calculated as the difference between normalized left and right hemisphere surface areas as indicated in Figure 2. A scaling factor was not included in the denominator since asymmetry indices including a scaling factor deliver essentially the same findings as those without (X.-Z. Kong et al., 2022). NSAR values range from -1.0 to +1.0, with negative values indicating left hemisphere specialization for a given network and positive values indicating right hemisphere specialization. NSAR values closer to zero indicate less specialization (hemispheric symmetry). Additionally, while this measure of specialization is similar to several asymmetry indices previously implemented (Binder et al., 1996; Braga et al., 2020; Mahowald & Fedorenko, 2016), its specific validity and reliability stand untested.

Establishing the Validity of NSAR

Ecological validity for the parcellation method was first examined, since surface area estimates for NSAR rely exclusively upon the network parcellations. Since the language network has previously been established as a highly specialized network, the network parcellation for the language network was compared against a language task fMRI atlas (LanA atlas) derived from a large sample (N = 804; Lipkin et al., 2022). HCP participants with all four runs available were selected, and a group parcellation was generated by first computing the connectivity profiles from all four resting-state scans from each participant (N = 232; the first step of the MS-HBM pipeline), averaging those connectivity profiles, and then generating the group parcellation using

the Yeo et al. (2011) group parcellation algorithm. The network labels from this parcellation were then matched to the Yeo et al. (2011) 17-network group parcellation using a Hungarian matching algorithm. Following the matching, the parcellation was exported to the FreeSurfer annotation file format and then to the GIFTI file format, which is a file type compatible with Connectome Workbench. The LanA atlas is publicly available for download (see Lipkin et al., 2022), and was resampled to fsaverage6 resolution before being converted to the GIFTI file format. Both the HCP group parcellation and the LanA atlas were overlaid on semi-inflated surfaces in the Connectome Workbench's wb_view for visual comparison.

Convergent validity was also examined through a comparison of the NSAR against another measure of specialization: the autonomy index (Wang et al., 2014). The autonomy index approaches specialization from a functional connectivity perspective and is known to reliability estimate specialization across neurotypical and clinical samples (Mueller et al., 2015; Sun et al., 2022; Wang et al., 2014). First, individual functional connectivity matrices were calculated for each resting-state run and then averaged across runs within an individual at the fsaverage6 resolution in MATLAB R2018b (MATLAB, 2018). From here the autonomy index was computed. In summary, for each seed ROI obtained from a functional connectivity matrix, the degree of within-hemisphere connectivity and cross-hemisphere connectivity were computed by summing the number of vertices correlated to the seed in the ipsilateral hemisphere and in the contralateral hemisphere. This is then normalized by the total number of vertices in the corresponding hemisphere, thus the accounting for a potential brain size asymmetry between the two hemispheres. Finally, AI is calculated as the difference between normalized within- and cross-hemisphere connectivity as follows:

$$AI = N_i/H_i - N_c/H_c$$

where N_i and N_c are the number of vertices correlated to the seed ROI (using a threshold of |0.25|) in the ipsilateral hemisphere and contralateral hemisphere, respectively. H_i and H_c are the total number of vertices in the ipsilateral and contralateral hemisphere, respectively. To compute the specialization of each functional network, the AI was averaged within the boundary of each network on an individual basis. Subjects from the HCP dataset with all four runs available (N = 232) were again selected for this analysis of validity and all four runs from each individual were used to compute the autonomy index. To facilitate direct comparison with NSAR values, the sign for autonomy index values was reversed. A Spearman's rank correlation coefficient was then used to compare the autonomy index and NSAR on three right-specialized networks (Limbic-B, Visual-B, and Ventral Attention-A) and three left-specialized networks (Language, Dorsal Attention-A, and Control-B) determined *a priori*. In order to correct for multiple comparisons, a Bonferroni-corrected alpha level of 0.008 was used. This and all other statistical analyses took place in R 4.2.0 (R Core Team, 2022).

Establishing the Reliability of NSAR

Reliability analyses sought to address three questions: 1) How much data is needed to obtain a stable estimate of NSAR, 2) What is the test-retest reliability of NSAR, and 3) Is there a task effect on NSAR estimation?

Stable Estimate Analysis

Given that MRI scanning is costly, rendering it comparatively rare to have highly sampled individuals, it is important to understand how much data is needed to reliably estimate specialization. To address this concern, we utilized HCP participants with all four runs available (N = 232). Following preprocessing, the first and third scans from each participant were set aside to compose 30 minutes of independent data. Next, the second and fourth scans were each split

into three five-minute segments. Runs were split in MATLAB R2018b (MATLAB, 2018) using native MATLAB functions as well as the FreeSurfer functions *MRIread* and *MRIwrite*. The MS-HBM pipeline was then used to generate individual parcellations from 5, 10, 15, 20, 25, and 30 minutes of data from the segmented scans. The MS-HBM pipeline was also used to generate separate individual parcellations from 30 minutes of independent data. Of note, the reliability of the MS-HBM pipeline has been examined previously (see Kong et al. (2019) Figure 3B and Supplementary Figure S10C). The NSAR was then calculated for each iteration (5, 10, 15, etc. minutes) and the independent 30 minutes of data. An intraclass correlation between the NSAR from each iteration parcellation and the independent 30 minutes parcellation was assessed within each subject. Similarly, an intraclass correlation between the NSAR from each iteration parcellation and the independent 30 minutes parcellation was assessed for each network. For the NSAR and parcellation stable estimate analyses, the standard guidelines from Koo & Li (2016) regarding intraclass correlation values were implemented, with values less than 0.5 indicating poor reliability, values between 0.5 and 0.75 indicating moderate reliability, values between 0.75 and 0.9 indicating good reliability, and values greater than 0.9 indicating excellent reliability (based on a 95% confidence interval).

Test-Retest Reliability Analysis

The purpose of the test-retest reliability analysis is to measure the reliability of NSAR in a simpler fashion than the stable estimate analysis. For this analysis, the first two and second two runs from HCP participants with all four runs available were used to generate separate individual parcellations from which NSAR will be calculated. Outliers were fenced on a network basis to an upper limit of the third quartile plus 1.5 multiplied by the interquartile range, and a lower limit of the first quartile minus 1.5 multiplied by the interquartile range. An intraclass correlation

coefficient was calculated comparing the NSAR from the first half of the data with the NSAR from the second half for three right-specialized networks (Limbic-B, Visual-B, and Salience/Ventral Attention-A) and three left-specialized networks (Language, Dorsal Attention-A, and Control-B) determined *a priori*.

Task Effects Analysis

In the case that a large quantity of data is needed to derive a reliable estimate of specialization, one might consider including task data in addition to any resting-state data in order to increase the amount of available data per participant. However, in this situation it would be prudent to know if task data provides the same or similar estimates as those from resting-state data. To address this concern, the NSD dataset was selected since it has a large quantity of both resting-state and task-based fMRI data per participant. Following preprocessing, a minimum of 12 resting-state runs were available for each participant, so the first 12 available resting-state runs and the first 12 available task runs were utilized (resting-state and task runs were of the same duration). Individual parcellations were then generated based on various combinations of runs within task type: even-numbered runs, odd-numbered runs, the first half of runs, the second half of runs, and two random selections of runs (without replacement). A dice coefficient was then computed to compare parcellation label overlap within task (e.g., between even and odd-numbered resting-state runs) and between tasks (e.g., between odd-numbered runs from resting-state and task runs). This comparison procedure was repeated for the NSAR intraclass correlation coefficient. Due to the non-normal nature of such a small dataset, comparisons between the task and rest parcellation dice coefficients and NSAR intraclass correlations were formally made using paired Wilcoxon Signed Rank tests (R Core Team, 2011; Wilcoxon, 1945).

Identifying Specialized Networks

After establishing validity and reliability, we addressed the first hypothesis of determining whether any of the 17 networks exhibited specialization, and of those, which were the most specialized. The following analyses were first implemented in the HCP-Discovery dataset and then replicated in the HCP-Replication and HCPD datasets using all data available from each participant. First, to determine whether any networks exhibited specialization, multiple regressions were implemented for each of the 17 networks. Models consisted of the a given network's NSAR value and the covariates of mean-centered age, sex, mean-centered mean framewise displacement, and handedness (measured via the Edinburgh Handedness Inventory; Oldfield, 1971). A network was considered specialized if the model intercept was significant at the Bonferroni-corrected alpha level of 0.003. Next, to determine which networks were the most specialized, any networks exhibiting significant specialization in the previous tests with the same direction of specialization were compared against each other two at a time in multiple regressions with a binary variable for the two networks and the covariates of mean-centered age, sex, mean-centered mean framewise displacement, and handedness.

Identifying Network Relationships

To test the second hypothesis regarding how network specialization is potentially related between networks, correlation matrices and then separate exploratory factor analyses (EFAs) in the HCP-Discovery, HCP-Replication, and HCPD datasets were performed on the model-adjusted specialization values from any reliably specialized networks. For a network to be considered reliably specialized, it was significantly specialized across the HCP-Discovery, HCP-Replication, and HCPD datasets. The exploratory factor analysis was chosen for its ability to identify shared relationships between the items in a data-driven manner. The *fa* function from the psych package (Revelle, 2023) was used to conduct an iterated principal factors analysis and

subsequent parallel analysis. Criteria for the extraction of factors were: a minimum eigenvalue of one, visual inspection of a scree plot, and a parallel analysis. A four-factor model was hypothesized, similar to Liu et al. (2009), with each factor encompassing vision, internal thought, attention, and language.

Results

NSAR as a Valid Measure of Specialization

The ecological validity of NSAR was examined through the proxy of the network parcellation validity, by comparing an HCP group parcellation (see Figure 3 Panel A) with a task-based language atlas from a large population (see Figure 3 Panel B). Upon visual inspection of Figure 3 Panel B, the language network parcellations appears to be consistent with task-based language data.

Figure 3

The LanA Atlas and the HCP Group Parcellation Overlap

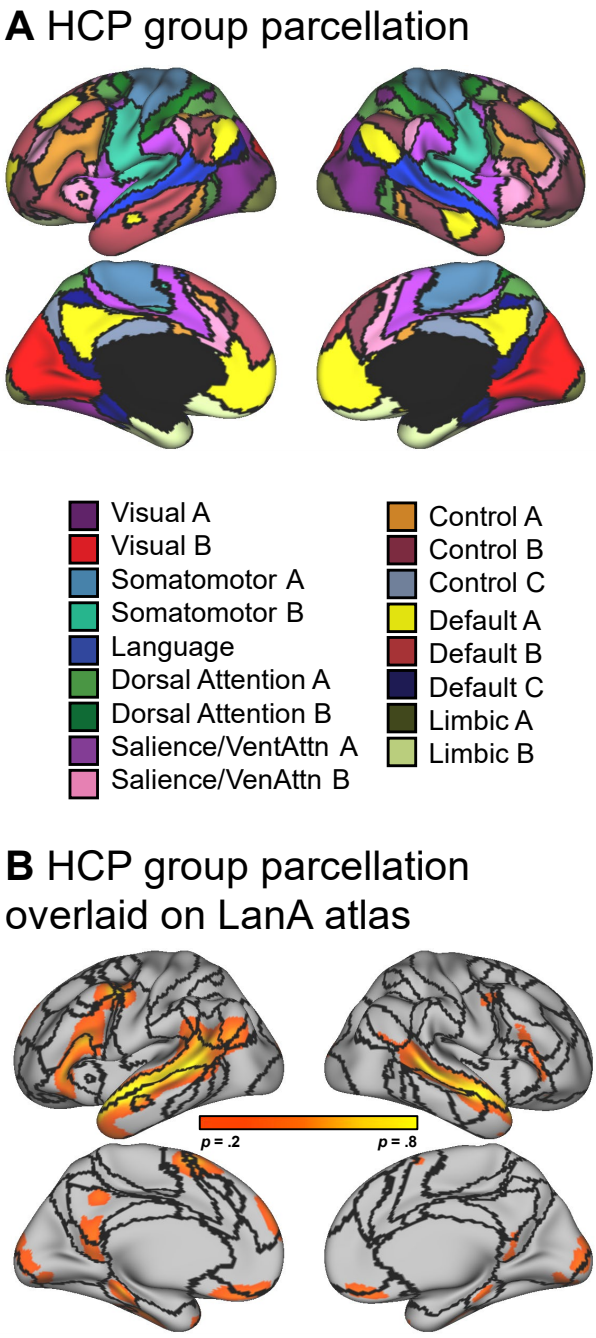

Note. Panel A depicts the group parcellation for a subset of the HCP dataset using participants with all four resting-state runs ($N = 232$). Panel B depicts that HCP group parcellation overlaid on the LanA atlas ($N = 804$).

The convergent validity of NSAR was assessed through comparison with an additional functional measure of specialization (the autonomy index) using the Spearman rank correlation. To facilitate direct comparison with NSAR values, the sign for autonomy index values was reversed. With the selected left-lateralized networks, significant relationships were found between the autonomy index and NSAR for the Language (Spearman rank correlation $r = 0.62$, $p < .001$), Dorsal Attention-A (Spearman rank correlation $r = 0.62$, $p < .001$), and the Control-B (Spearman rank correlation $r = 0.57$, $p < .001$) networks (see the top row of Figure 4). Significant relationships were also found between the autonomy index and NSAR for the selected right-lateralized networks including the Visual-B (Spearman rank correlation $r = -0.71$, $p < .001$), Salience/Ventral Attention-A (Spearman rank correlation $r = -0.61$, $p < .001$), and Limbic-B (Spearman rank correlation $r = -0.69$, $p < .001$) networks (see the second row of Figure 4). These findings indicate that NSAR and the autonomy index are measuring similar facets of specialization.

Figure 4

Evidence for Convergent Validity Between the Autonomy Index and NSAR in a Subset of the HCP Dataset

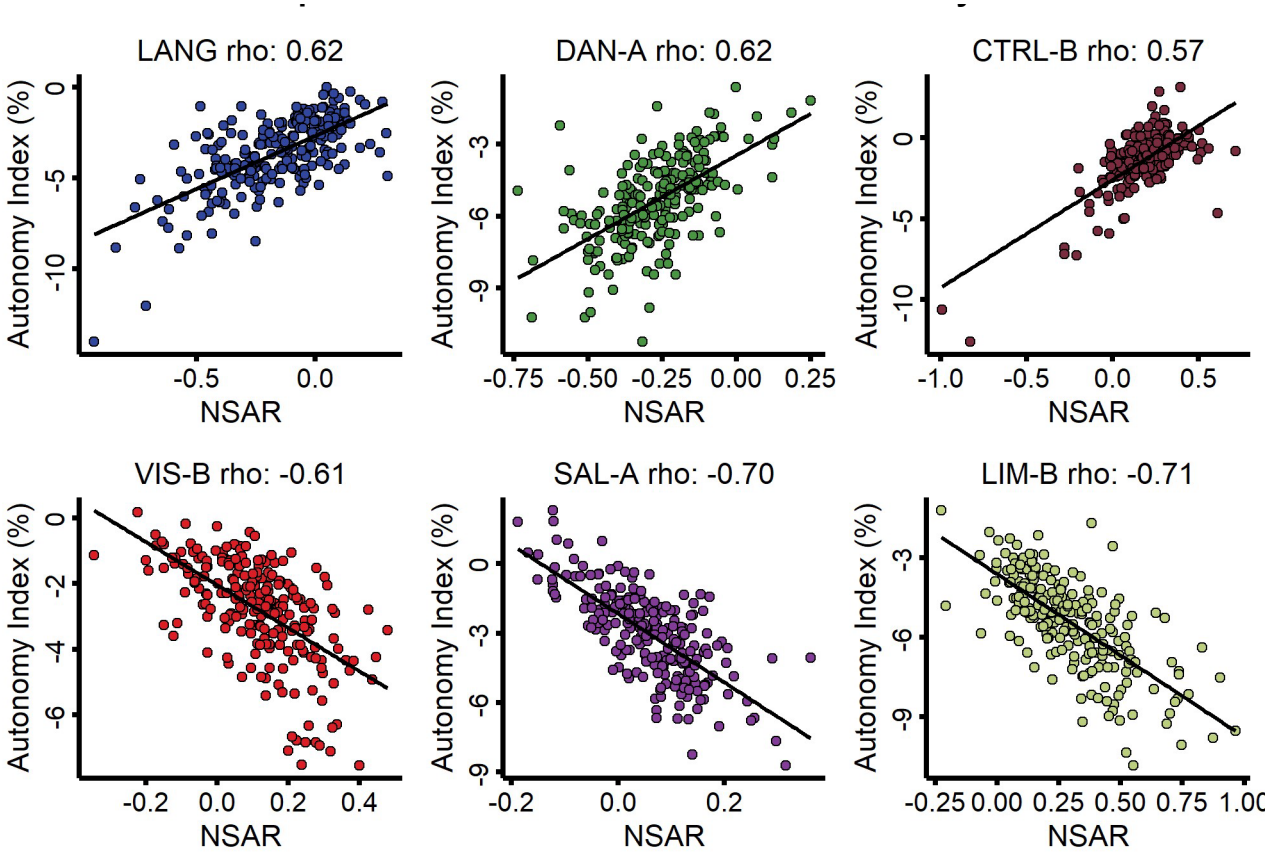

Note. The top row depicts the relationships between the autonomy index and NSAR for three left-lateralized networks (Language, Dorsal Attention-A, and Control-B; Spearman rank correlation r = 0.57-0.62). The bottom row depicts the relationships between the autonomy index and NSAR for three right-lateralized networks (Visual-B, Ventral Attention-A, and Limbic-B; Spearman rank correlation r = -0.61 - -0.71). For each scatterplot, the line of best fit was generated using the *lm* function (no covariates) and each circle represents an individual.

NSAR as a Reliable Measure of Specialization

Stable Estimate Analysis

To address the question of how much data is needed in order to obtain a stable estimate of NSAR values, combinations of five-minute increments (5, 10, 15…30 minutes) were compared against 30 independent minutes of data in a subset of HCP subjects. The intraclass correlations indicate that only five minutes of data are needed to obtain moderate to good intraclass correlations for the majority of subjects (see Figure 5 Panel A). Of note, poor and excellent interclass correlations were observed for some subjects. The stable estimate analysis was also approached from a network basis (as opposed to the subject basis presented in Figure 5 Panel A). Networks with the lowest intraclass correlations included the Limbic-A and Control-A networks, while networks with the greatest intraclass correlations included Visual-A, Limbic-B, and Default-A (for overall distributions, see Figure 5 Panel B; for specific network intraclass correlation coefficients, see Supplementary Figure S2). Interestingly, not all networks improved in reliability with additional data, including the Limbic-A and Control-A networks. This is likely a reflection of a poor signal-to-noise ratio. For parcellation label overlap estimates, see Supplementary Figure S3.

Figure 5

Evidence for Reliable Estimates of NSAR in the HCP Dataset

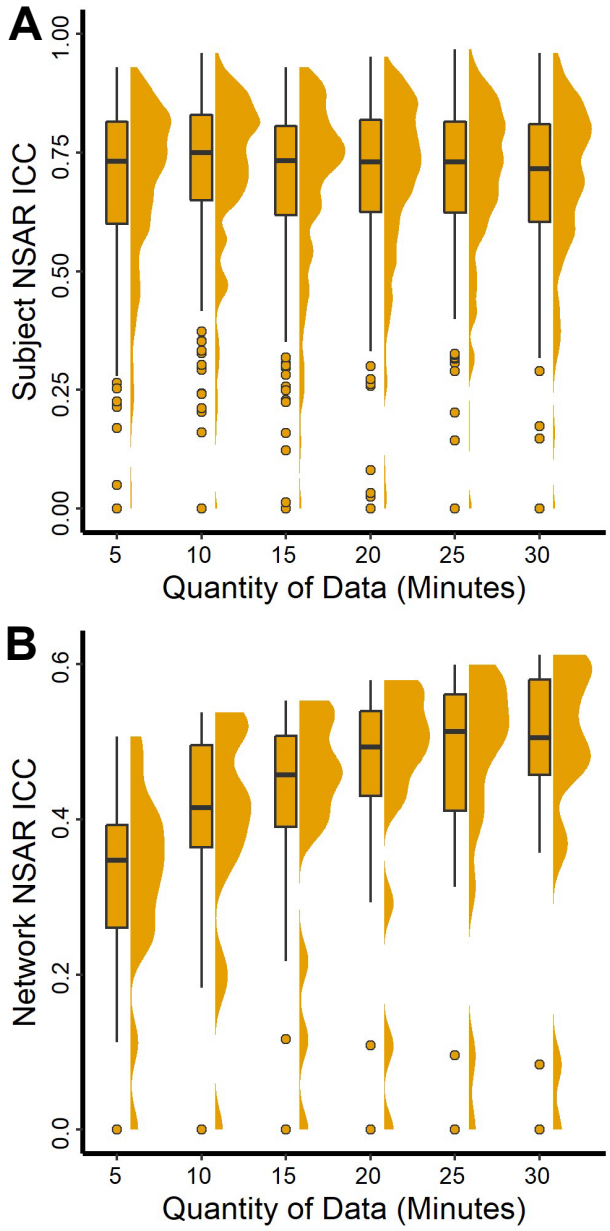

Note. Panel A depicts the intraclass correlation coefficient calculated for each subject's 17 NSAR values for each time increment (5, 10, 15 … 30 minutes) and the subject's 17 NSAR values from 30 independent minutes of data. Panel B depicts the intraclass correlation coefficient calculated for each network's mean NSAR value between the 30 independent minutes of data

and each increment of data. Specific network intraclass correlation coefficients are displayed in Supplementary Figure S2.

Test-Retest Reliability Analysis

Using HCP subjects with all four resting-state runs available post-preprocessing (N = 232), test-retest reliability was assessed for three left-specialized networks (Language, Dorsal Attention-A, and Control-B) and three right-specialized networks (Limbic-B, Visual-B, and Salience/Ventral Attention-A) determined *a priori*. For the left-lateralized networks, intraclass correlations were within the moderate range, from 0.56 to 0.63, with the lowest being the Dorsal Attention-A network (ICC = 0.56, $F(231, 231) = 3.6$, $p < .001$, 95% CI [0.47, 0.64]; see Figure 6). For the right-lateralized networks, intraclass correlations remained in the moderate range, between 0.58 to 0.71, with the Visual-B network exhibiting the lowest reliability (ICC = 0.58, $F(231, 231) = 3.7$, $p < .001$, 95% CI [0.48, 0.66]).

Figure 6

Test-Retest Reliability of NSAR Values for Left- and Right-Specialized Networks in 232 HCP Subjects

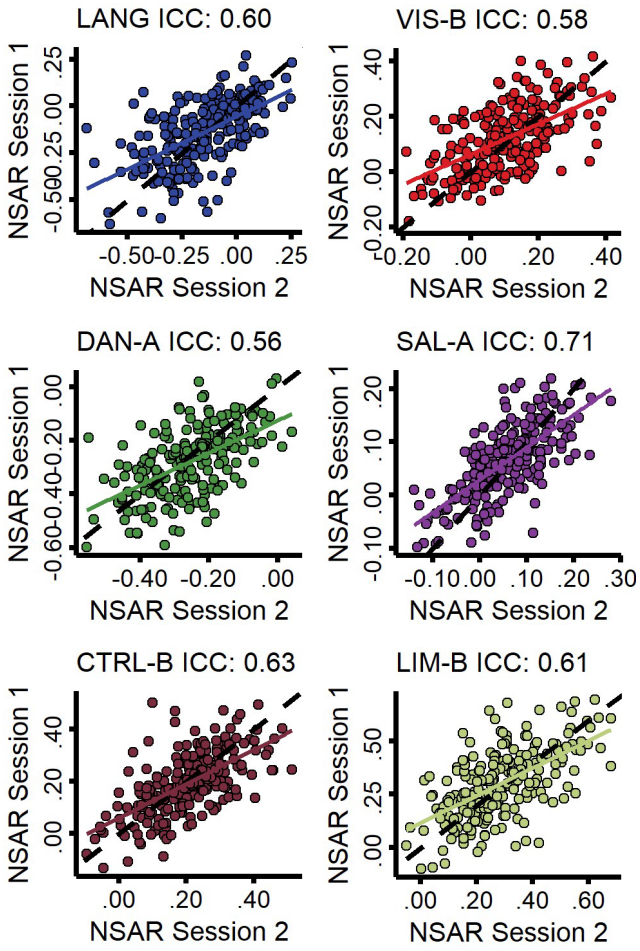

Note. Left-specialized networks (left column) included Language, Dorsal Attention-A, and Control-B. Right-specialized networks (right column) included Visual-B, Salience/Ventral Attention-A, and Limbic-B. In each plot, a circle represents a subject.

Task Effects on Individual Parcellations and NSAR

Using the NSD dataset ($N = 8$) to compare potential differences between resting-state and task fMRI on individual parcellations and NSAR estimates, we found differences between the

within-task comparisons and between task comparisons for both the parcellation dice coefficients and NSAR intraclass correlations (see Figure 7). Wilcoxon signed rank comparisons revealed a difference in within-task (Task-Task and Rest-Rest) dice coefficients for even versus odd numbered runs ($V = 36$, $p = .008$), but no difference for the first half versus the second half of runs ($V = 29$, $p = .15$) or the random selection of runs ($V = 31$, $p = .08$). Regardless of how the data were split, a task effect in dice coefficient was found between within-task (Task-Task) and between-task (Task-Rest) dice coefficients for even versus odd numbered runs ($V = 36$, $p = .008$), the first half versus the second half of runs ($V = 36$, $p = .008$), and the random selection of runs ($V = 36$, $p = .008$).

Similarly, with the NSAR intraclass coefficients, no significant difference was found for within-task (Task-Task and Rest-Rest) reliability across the even versus odd numbered runs ($V = 31$, $p = .08$) and the first half versus the second half of runs ($V = 19$, $p = .95$), but not for the random selection of runs ($V = 35$, $p = .02$). However, a significant difference was not found between within-task (Task-Task) and between-task (Task-Rest) intraclass correlation coefficients across the even versus odd numbered runs ($V = 31$, $p = .08$), the first half versus the second half of runs ($V = 31$, $p = .08$), but for the random selection of runs ($V = 34$, $p = .02$).

Figure 7

Task Dependency of Individual Parcellations and NSAR in the NSD Dataset

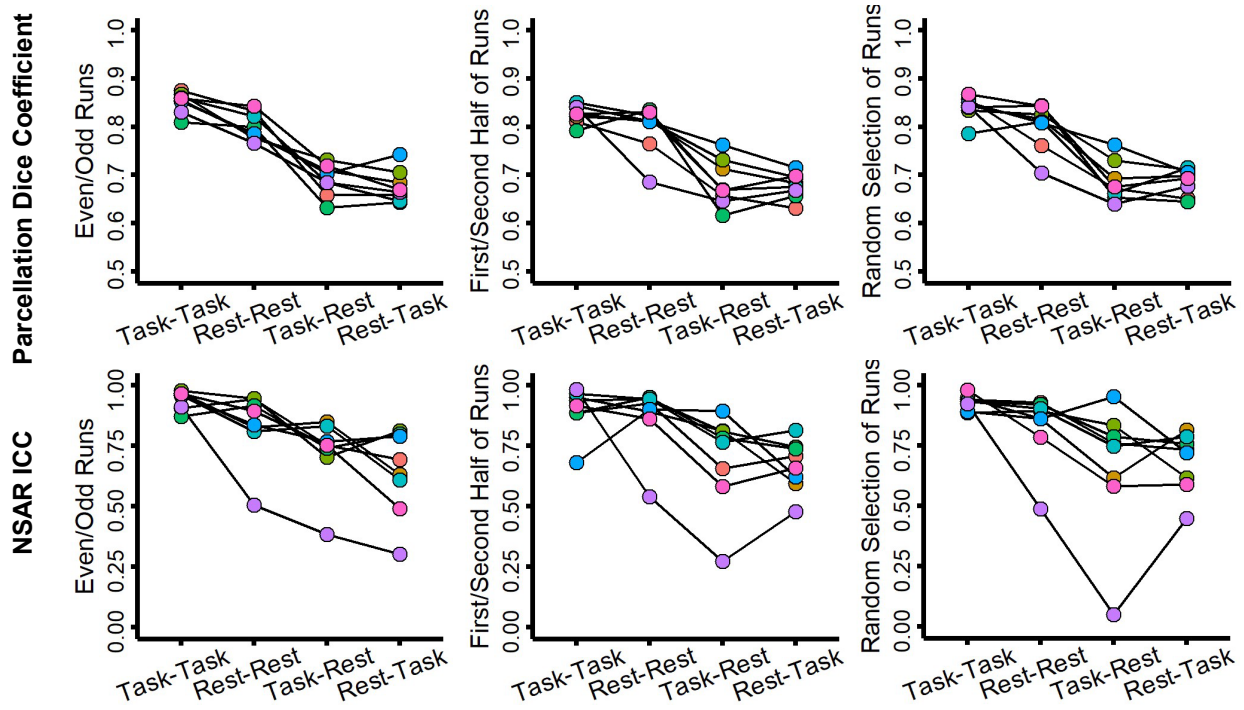

Note. Depicted in the top row are the dice coefficients for the individual parcellations between 30-minute increments of resting-state or task fMRI data. Regardless of how the data were split (even- versus odd-numbered runs, the first half versus the second half, or a random selection without replacement), a task effect was found. Depicted in the second row are the NSAR intraclass correlation coefficients computed in individuals across networks. In each plot, circles connected by a line represent an individual.

Networks with the Greatest Specialization

A series of multiple regressions were used to identify if any of the 17 networks were specialized, first in the HCP-Discovery dataset and then in the HCP-Replication and HCPD datasets. Networks with significant specialization ($p < .003$) in the same direction (e.g., right or

left lateralization) across all three datasets included the following eight networks: Visual-B, Language, Dorsal Attention-A, Salience/Ventral Attention-A, Control-A, Control-B, Control-C, Default-C, and Limbic-B (see Supplementary Table 1). However, given the very low reliability of the Control-A network (mean ICC = 0.12; see Supplementary Figure S2), this network was not considered further. None of the covariates were reliably significant for a given network across all three datasets. See Figure 8 for model-adjusted NSAR values for each of the 17 networks and see Figure 9 for the percentage of surface area occupied by the eight most specialized networks.

Following the identification of eight specialized networks, a series of multiple regressions were used to compare networks with the same direction of specialization two at a time in order to identify the networks with the greatest specialization. Models included a binary network variable and the covariates of mean-centered age, sex, handedness, and mean-centered mean framewise displacement. Of the left-lateralized networks, the Dorsal Attention-A network was the most lateralized compared with the Language and Default-C networks, and this pattern was replicated across the HCP-Discovery, HCP-Replication, and HCPD datasets (see Supplementary Table 2). Of the right-lateralized networks, the Limbic-B network was the most specialized, followed by the Control-B network, Visual-B and Control-C networks (not significantly different), and the Salience/Ventral Attention-A network. This pattern was replicated across the three datasets as well (see Supplementary Table 3).

Figure 8

Specialization for 17 Networks across the HCP-Discovery, HCP-Replication, and HCPD Datasets

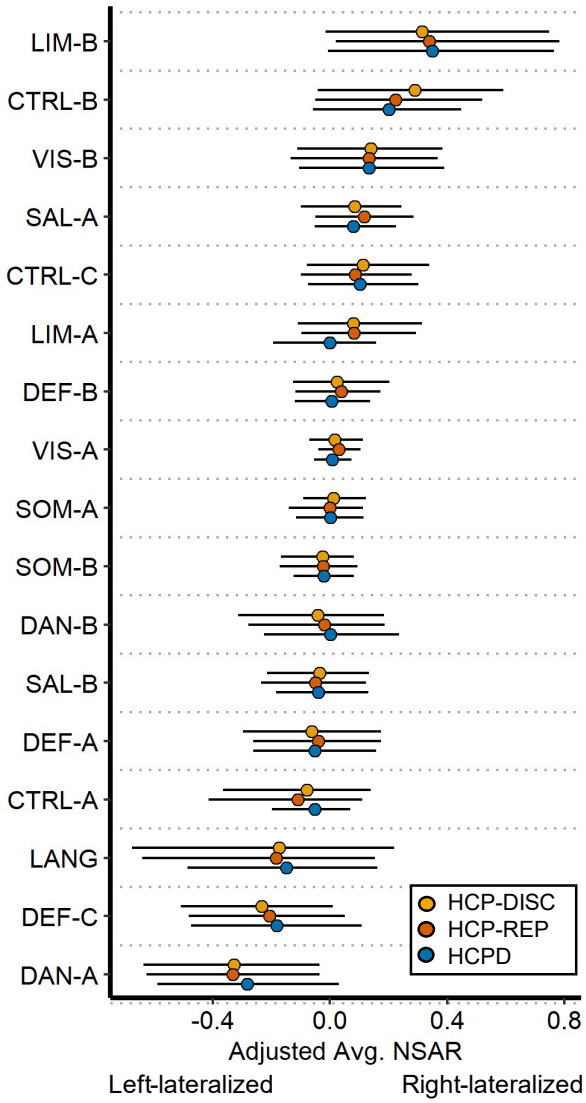

Note. On the y-axis are the 17 networks and on the x-axis are the adjusted NSAR values, with negative values representing left hemisphere lateralization and positive values representing right hemisphere lateralization. Bars represent the 2.5 and 97.5 percentiles. NSAR values were adjusted by regressing out the effects of mean-centered age, mean-centered mean framewise displacement, and sex using the following formula: $NSAR_{adjusted} = NSAR_{raw} — [\beta_1(mean-$

centered age_{raw} - mean of mean-centered age_{raw}) + β_2(mean-centered FD_{raw} - mean of mean-centered FD_{raw}) + β_3(sex_{raw} – mean sex_{raw}) + β_4($handedness_{raw}$ – mean $handedness_{raw}$)]. NSAR adjustment occurred separately for each network within each dataset.

Lines represent the standard error. Across the three datasets, eight networks were reliably and significantly specialized (Visual-B, Language, Dorsal Attention-A, Salience/Ventral Attention-A, Control-B, Control-C, Default-C, and Limbic-B).

Figure 9

Percent Surface Area for 17 Networks Across the HCP-Discovery, HCP-Replication, and HCPD Datasets

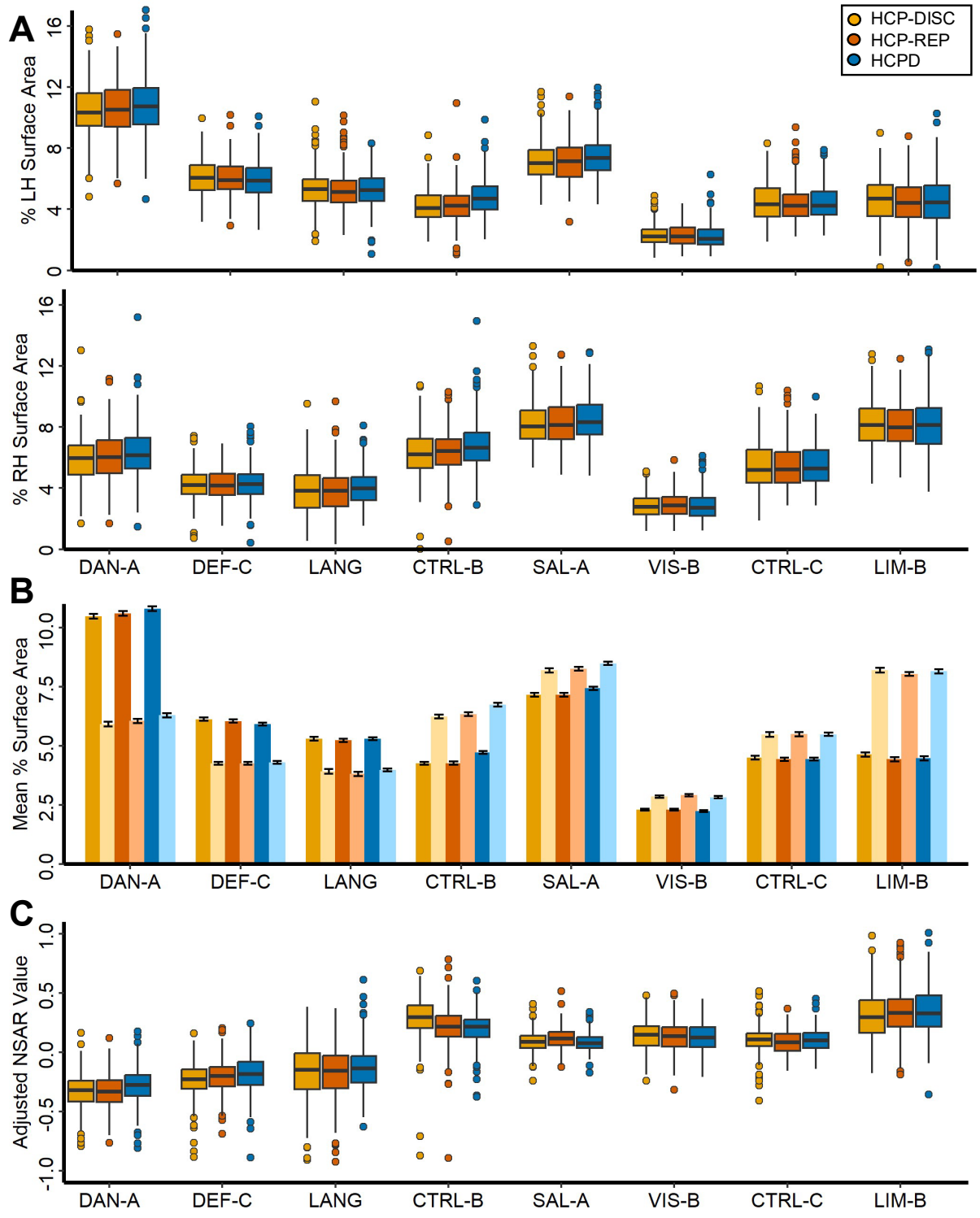

Note. Depicted in the top of Panel A is the percentage of the left hemisphere surface area occupied by a given specialized network. Depicted in the bottom portion of Panel A is the percentage of the right hemisphere surface area occupied by a given network. Points represent individual outliers. Depicted in Panel B is the mean percentage of surface area occupied by a specialized network, with standard error bars. The left and right hemisphere estimates are displayed side-by-side for each dataset. In Panel C, the adjusted NSAR values for each network are shown, with points representing individual outliers.

Relationships between Networks' Specialization

Our hypothesis regarding network relationships was assessed through both correlation matrices and exploratory factor analyses conducted in triplicate across the HCP-Discovery, HCP-Replication, and HCPD datasets. Correlation matrices of the model-adjusted NSAR values from the eight specialized networks evidenced moderate negative relationships between the left- and right-specialized networks (see Figure 10). In the HCP-Discovery dataset, negative relationships were found between the Limbic-B and Dorsal Attention-A networks (r = -0.45; see Figure 11 Panel A), the Limbic-B and Default-C networks (r = -0.42; see Figure 11 Panel B), the Default-C and Visual-B networks (r = -0.16), the Default-C and Control-B networks (r = -0.27), the Default-C and Control-C networks (r = -0.17), the Control-B and Language networks (r = -0.31), and the Control-B and Salience/Ventral Attention-A networks (r = -0.3). Interestingly, a negative relationship was also found between two left-lateralized networks: Dorsal Attention-A and Language (r = -0.23; see Figure 11 Panel C). Each negative relationship was replicated across the HCP-Replication and HCPD datasets (see Figure 10).

Figure 10

Relationships Between Specialized Networks Across the HCP-Discovery, HCP-Replication, and HCPD Datasets

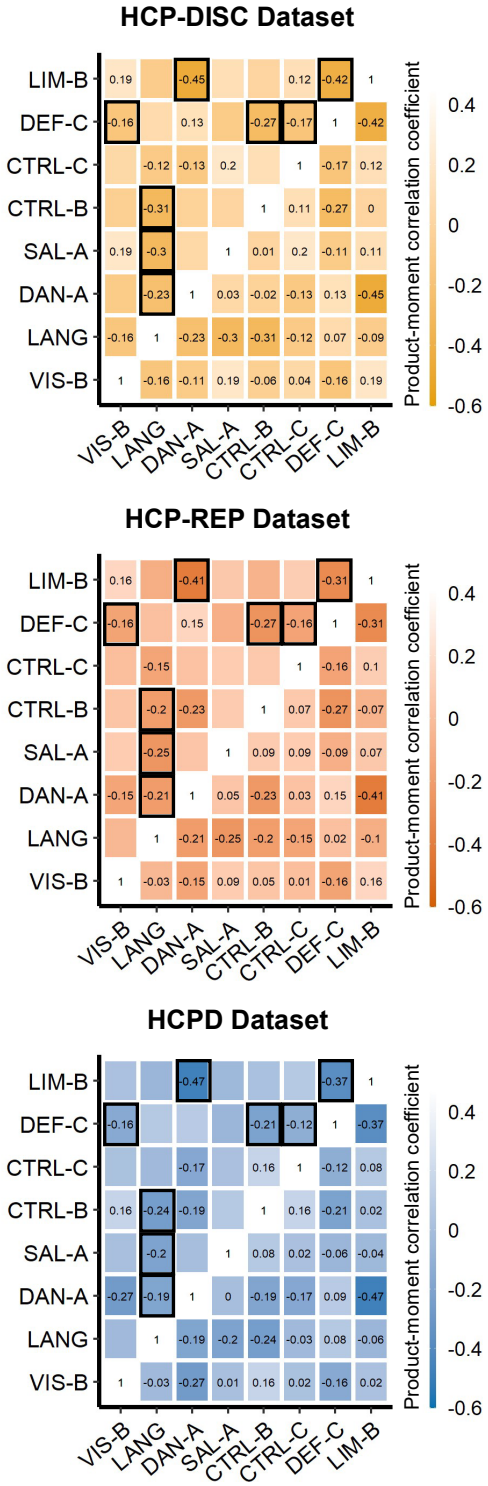

Note. Correlation matrices were created from the model-adjusted NSAR values from the eight specialized networks (Visual-B, Language, Dorsal Attention-A, Salience/Ventral Attention-A, Control-B, Control-C, Default-C, and Limbic-B), controlling for sex, mean-centered age, mean-centered framewise displacement, and handedness. Correlation values thresholded at $p = .05$ are displayed in the upper triangles, and consistent relationships have been highlighted with black boxes.

Figure 11

Negative Correlations Between Highly Left- and Right-Specialized Networks Across the HCP-Discovery, HCP-Replication, and HCPD Datasets

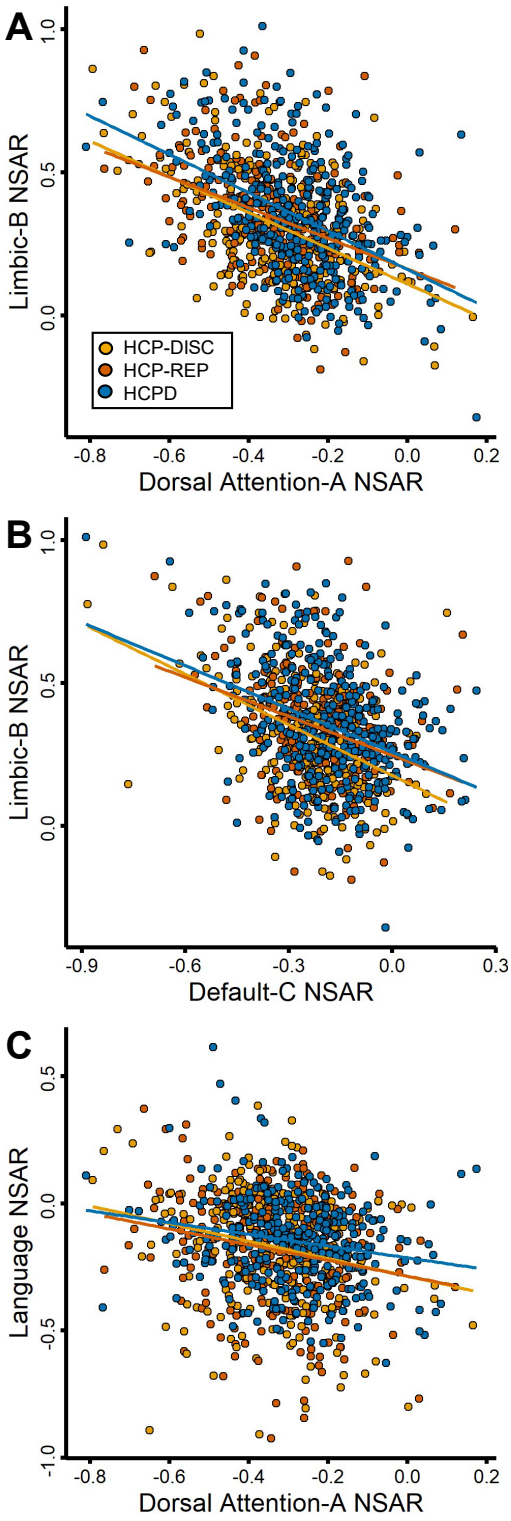

Note. Panel A depicts the negative relationship between the Limbic-B and Dorsal Attention-A networks. Panel B depicts the negative relationship between the right-lateralized Limbic-B and left-lateralized Default-C networks. Panel C depicts the negative relationship between the left-lateralized Dorsal Attention-A and left-lateralized Language networks. In each panel, a circle represents a single participant's model-adjusted NSAR value, which was adjusted for mean-centered age, sex, handedness, and mean-centered mean framewise displacement.

EFA in the HCP-Discovery Dataset

In preparation for the EFA in the HCP-Discovery dataset ($N = 276$; no missing data), linearity and heteroskedasticity of adjusted NSAR values from the eight specialized networks were evaluated in pairwise plots, which were followed by the Doornik-Hansen multivariate test for normality (*DH.test* function from the mvnTest package; $DH = 202.89$, $p = 0$; Doornik & Hansen, 2008; Pya et al., 2016). The NSAR values were then evaluated for multicollinearity, and no items had Variance Inflation Factor values greater than 1.65 (*vif* function from the psych package; Revelle, 2023). Additional assumptions testing included Bartlett's test of sphericity and the Kaiser-Meyer-Olkin (KMO) Measure of Sampling Adequacy. For the test of sphericity, we rejected the null hypothesis that there is no correlation among the items ($\chi^2(28) = 293.43$, $p < .001$). Additionally, the KMO test was .46, revealing that the extracted factors will account for an unacceptable amount of common variance.

To examine network relationships, a principal factors analysis in the HCP-Discovery dataset was performed. Using the correlation matrix from eight specialized networks, two factors were extracted. This first factor had an eigenvalue of 1.38 (explaining 57% of the variance; see Table 1 for factor loadings) and the second factor had an eigenvalue of 1.02 (explaining 43% of

the variance). Of note, the left-lateralized networks load negatively onto the first extracted factor while right-lateralized networks load positively, suggesting that this factor encompasses right-hemisphere lateralization, with the opposite in the second extracted factor.

Table 1

Summary of Exploratory Factor Analysis Results for the NSAR Scores Using Iterated Principal Factors in the HCP-Discovery Dataset (N = 276)

Network	Factor 1 Loadings	Factor 2 Loadings
Visual-B	0.29	
Language	-0.38	**-0.75**
Dorsal Attention-A	-0.37	**0.48**
Salience/VenAttn-A	0.28	0.26
Control-B	0.22	0.23
Control-C	0.28	
Default-C	**-0.51**	
Limbic-B	**0.73**	-0.32
Eigenvalues	1.38	1.02
Proportion of variance explained	0.57	0.43

Note: Factor loadings over .40 appear in bold.

EFA in the HCP-Replication Dataset

In preparation for the EFA in the HCP-Replication dataset ($N = 277$; no missing data), linearity and heteroskedasticity of adjusted NSAR values were evaluated in pairwise plots, which were followed by the Doornik-Hansen multivariate test for normality ($DH = 215.73$, $p = 0$; Doornik & Hansen, 2008; Pya et al., 2016). The NSAR values were then evaluated for

multicollinearity, and no items had Variance Inflation Factor values greater than 1.53 Additional assumptions testing included Bartlett's test of sphericity and the Kaiser-Meyer-Olkin (KMO) Measure of Sampling Adequacy. For the test of sphericity, we rejected the null hypothesis that there is no correlation among the items ($\chi^2(28) = 325.12$, $p < .001$). Additionally, the KMO test was .4, revealing that the extracted factors will account for an unacceptable amount of common variance.

To examine network relationships and potentially replicate the HCP EFA, a principal factors analysis in the HCP-Replication dataset was performed. Using the correlation matrix from eight specialized networks, a single factor was extracted. This factor had an eigenvalue of 1.06 (explaining 13% of variance; see Table 2 for factor loadings). Interestingly, this factor analysis does appear to support the EFA in the HCP-Discovery dataset, with a negative loading from the left-lateralized Dorsal Attention-A and Default-C networks and a positive loading from the Limbic-B network.

Table 2

Summary of Exploratory Factor Analysis Results for the NSAR Scores Using Iterated Principal Factors in the HCP-Replication Dataset (N = 277)

Network	Factor 1 Loadings
Visual-B	0.29
Language	
Dorsal Attention-A	**-0.46**
Salience/VenAttn-A	0.15
Control-B	0.27
Control-C	0.18

Default-C	**-0.54**
Limbic-B	**0.58**
Eigenvalues	1.06
Proportion of variance explained	0.13

Note: Factor loadings over .40 appear in bold.

EFA in the HCPD Dataset

In preparation for the EFA in the HCPD dataset ($N = 343$; no missing data), linearity and heteroskedasticity of adjusted NSAR values were evaluated in pairwise plots, which were followed by the Doornik-Hansen multivariate test for normality ($DH = 67.12$, $p < .001$; Doornik & Hansen, 2008; Pya et al., 2016). The NSAR values were then evaluated for multicollinearity, and no items had Variance Inflation Factor values greater than 1.64. Additional assumptions testing included Bartlett's test of sphericity and the Kaiser-Meyer-Olkin (KMO) Measure of Sampling Adequacy. For the test of sphericity, we rejected the null hypothesis that there is no correlation among the items ($\chi^2(28) = 323.75$, $p < .001$). Additionally, the KMO test was .39, revealing that the extracted factors will account for an unacceptable amount of common variance.

To examine network relationships, a principal factors analysis in the HCPD dataset was performed. Using the correlation matrix from eight specialized networks, one factor was extracted. This factor had an eigenvalue of 1.17 (explaining 15% of the variance; see Table 3 for factor loadings). Once more, right-lateralized networks (such as Limbic-B) loaded positively onto this single factor while left-lateralized networks (including Dorsal Attention-A and Default-C) loaded negatively.

Table 3

Summary of Exploratory Factor Analysis Results for the NSAR Scores Using Iterated Principal Factors in the HCPD Dataset (N = 343)

Network	Factor 1 Loadings
Visual-B	0.28
Language	
Dorsal Attention-A	**-0.64**
Salience/VenAttn-A	
Control-B	0.29
Control-C	0.24
Default-C	**-0.43**
Limbic-B	**0.61**
Eigenvalues	1.17
Proportion of variance explained	0.15

Note: Factor loadings over .40 appear in bold.

Discussion

As a key to understanding brain organization and development (Toga & Thompson, 2003), individual differences (Perez et al., 2023), human-defining cognitive processes (Hartwigsen et al., 2021), and neurodevelopmental conditions (Eyler et al., 2012; X.-Z. Kong et al., 2022), hemispheric specialization is a crucial area of investigation. Previously, functional specialization has been assessed through a variety of approaches dependent on intrinsic connectivity primarily at the group level. However, recent evidence suggests that group-based approaches can obfuscate the idiosyncratic anatomy of individuals and blur potentially meaningful and clinically useful variability (Lynch et al., 2020; Salvo et al., 2021). For example,

the language network has high spatial variability across individuals (Braga et al., 2020; Fedorenko, Duncan, et al., 2012), holding ramifications for the accurate assessment of specialization for this and other variable networks. In light of these findings, we implemented a measure of specialization based upon high-resolution individual network parcellations (NSAR). Using NSAR, we identified eight networks that were reliably specialized across three independent datasets. Furthermore, we examined potential relationships between networks' NSAR values and found evidence for a covariation hypothesis of specialization.

Evidence for the Validity and Reliability of NSAR

In this study, we examined functional specialization using a novel surface area-based index. This measure was developed methodologically through the examination of ecological and convergent validity, as well as a stable estimate analysis, test-retest reliability, and potential task effects. Notably, group parcellation boundaries appear to align moderately well with those from a language task atlas, indicating that the parcellations are likely biologically relevant (in addition to being behaviorally relevant; Kong et al., 2019). Furthermore, estimates from this surface area approach to specialization appear to converge with a different functional connectivity-based method. This result supports the idea that NSAR is approaching specialization in a way that is valid while being distinct from the autonomy index. However, unlike the autonomy index, the formula for NSAR does not normalize for brain size or deal in the minutiae of individual connections, rendering NSAR clearly interpretable and accessible to lay audiences.

Reliability analyses indicated that NSAR is stable within individuals, even after just five minutes of resting-state fMRI data. Interestingly, networks with the greatest reliabilities included the visual and somatomotor networks. This is in keeping with Kong et al. (2019), who found that sensorimotor networks exhibited lower inter-subject functional connectivity variability than

association networks. Since NSAR is indirectly based on an individual's functional connectivity profiles, this result is unexpected.

In addition to the quantity of data available per participant, we also examined the effect of data type (task versus rest) on NSAR estimates within individuals. While within-task type reliability was high, we found that there was indeed a task effect such that resting-state fMRI and task fMRI did not yield identical parcellations and NSAR estimates within individuals. This finding supports the hypothesis that resting-state fMRI can be thought of as another arbitrary task state (Buckner et al., 2013). Yet, the "task" of resting-state fMRI results in greater variability in functional connectivity compared with that resulting from task fMRI, perhaps resulting from mind wandering (Elton & Gao, 2015). And when predicting individual traits, task-based models outperform rest-based models, with this difference likely reflecting the "unconstrained nature" of the resting state (Greene et al., 2018). Since NSAR estimates are derived from individual parcellations which are in turn generated from individual functional connectivity profiles, it stands to reason that connectivity differences resulting from task type could trickle down to differences in NSAR estimates.

The Identification of Eight Reliably Specialized Networks

Following the methodological development of NSAR, we reliably identified eight specialized networks across three datasets: Visual-B, Language, Dorsal Attention-A, Salience/Ventral Attention-A, Control-B, Control-C, Default-C, and Limbic-B. While a ninth specialized network was reliably identified (Control-A), this network was discarded from further analysis due to very poor reliability. Previously, several of these networks have been established as lateralized, particularly those associated with language and visuospatial attention processing.

The Dorsal Attention-A Network Exhibited the Greatest Left-Lateralization

Previously, left-lateralized networks have included the language, frontoparietal control, and default networks. More specifically, evidence for the lateralization of the language network has been derived from a variety of methods including the Wada test (Desmond et al., 1995; Wada & Rasmussen, 1960), lesion cases (Broca, 1861; Wernicke, 1995), task fMRI (Elin et al., 2022; Fedorenko, Duncan, et al., 2012; Fedorenko et al., 2010, 2011; Fedorenko, McDermott, et al., 2012; Lipkin et al., 2022; Malik-Moraleda et al., 2022; Olulade et al., 2020; Scott et al., 2017; Wilson et al., 2017), and resting-state fMRI (Braga et al., 2020; Labache et al., 2020; Zhu et al., 2014), among others. Using NSAR, we also identified the language network as being strongly left-lateralized. However, unlike a prior comparative study (Braga et al., 2020), which examined lateralization in the language, salience, default, and frontoparietal networks, we failed to find that the language network was the most left-lateralized network. Instead, we identified the Dorsal Attention-A network as being the most left-lateralized. Unlike the ventral attention network, the dorsal attention network has been previously identified as a bilateral network (Fox et al., 2006; for review see Mengotti et al., 2020). This was the case for the Dorsal Attention-B network, which was not a significantly specialized network across the three datasets. However, there is evidence for a left-lateralized dorsal attention network across both left- and right-handed individuals, stemming from a within-individual network variants approach (see Figure 7 Panel C of Perez et al., 2023). Additionally, it could be that a finer-grained parcellation deconstructs the dorsal attention network into one bilateral and one specialized network, similar to previous within-individual work on the default network (Braga & Buckner, 2017; DiNicola et al., 2020).

Replication of Right-Lateralized Attention, Control, and Limbic Networks

This is not the first study to identify the ventral attention, control, and limbic networks as being specialized. Abundant evidence exists for the right-lateralization of visuospatial/ventral

attention, stemming from task fMRI (Beume et al., 2015; Cai et al., 2013; Jansen et al., 2004; Shulman et al., 2010; Siman-Tov et al., 2007; Umarova et al., 2010; J. Wang et al., 2016; Zago et al., 2016, 2017), resting-state fMRI (Braga et al., 2020; Wang et al., 2014), hemispatial neglect cases (Corbetta & Shulman, 2011), and others (for review, see Mengotti et al., 2020). Interestingly, we identified the Salience/Ventral Attention-A but not the Salience/Ventral Attention-B network as being right-lateralized. Once more, this may be due to the network resolution selected ($k = 17$), which may have split the canonical ventral attention network into a bilateral and right-lateralized networks.

While this study successfully replicated right-lateralized control networks (Control-B and Control-C), a left-lateralized control network was not identified. Previously, Wang et al. (2014) found evidence for a dually specialized frontoparietal control network using the autonomy index. It was suggested that this control network acted as a coupler between the two hemispheres to increase efficiency while simultaneously supporting within-hemisphere processes. This was also evidenced by Spreng et al. (2013), which found that the frontoparietal control network exhibits distinct connectivity patterns with the default and attention networks in response to varying task requirements. Similarly, using a seed-based analysis, Braga et al. (2020) confirmed the presence of both left-lateralized and right-lateralized frontoparietal control networks. Collectively, these results point to control networks differentially executing cognitive processes within the left and right hemispheres.

Finally, the most right-lateralized network identified using NSAR was the Limbic-B network, a network that occupies cortical real estate associated with emotion (Olson et al., 2007; Pehrs et al., 2017; Sonkusare et al., 2020). Historically, emotion has been identified as being specialized, perhaps beginning with lesion cases (Gainotti, 2019; Hughlings-Jackson, 1878;

Luys, 1879). Later work suggested that specific aspects of emotion were specialized, including the right-lateralization of emotion recognition, the right-lateralization of emotional control and expression, the right-lateralization of negative emotions, and the left-lateralization of positive emotions (Silberman & Weingartner, 1986). Contemporarily, it has been suggested that a hemispheric functional-equivalence hypothesis would better explain emotion neuroimaging results, such that emotion results from networks that are interrelated and may have different patterns of lateralization (for review, see Palomero-Gallagher & Amunts, 2022). This perspective emphasizes the intricate and interconnected nature of emotion-related neural processes, particularly those patterns of lateralization that emerge from inter-network relationships. Interestingly, the Limbic-B network appears to be at the center of our main results regarding specialization relationships between networks.

Support for the Covariation Hypothesis of Network Specialization

Beyond identifying networks with the greatest specialization, we sought to understand how network specialization was related between networks. We proposed three hypotheses: covariation, compensation, and independence. Using correlation matrices, we found support for the covariation hypothesis in networks specialized to contralateral hemispheres. The covariation hypothesis posits that having a highly specialized network corresponds with increased specialization in other networks within an individual. For example, a negative relationship was found between the right-lateralized Limbic-B network and the left-lateralized Dorsal Attention-A network, and between the Limbic-B network and the left-lateralized Default-C network across each of three datasets. These negative relationships suggest that as the Limbic-B network increases in specialization, the Dorsal Attention-A and Default-C networks also increase in specialization, covarying. Additionally, evidence for the compensation hypothesis was found

between networks specialized to the same hemisphere, such as between the left-lateralized Language and Dorsal Attention-A networks. This finding is expected given that NSAR is derived from surface area, which is zero-sum, so networks specialized to the same hemisphere may be in competition with one another for cortical real estate.

Additional support for the covariation hypothesis was found with the EFA structures across the three datasets. While we did not replicate the four-factor model from Liu et al. (2009), we did extract a single factor for both the HCP-Replication and HCPD datasets, and two factors for the HCP-Discovery dataset. Across these factor analyses, significant positive and negative loadings were found within each factor structure, suggesting that left- and right-lateralized networks work within a system level higher than the network.

Limitations and Future Directions

One limitation to this work is that while functional connectivity may be constrained in part by anatomical connectivity, it is not necessarily dictated by anatomical connectivity. Several pieces of evidence point to this conclusion: functional connectivity is modulated by task (Shirer et al., 2012), recent experience (Lewis et al., 2009), caffeine (Laumann et al., 2015), and sleepiness (Tagliazucchi & Laufs, 2014); and is dynamic within a person over time (Hutchison et al., 2013). Furthermore, underlying brain geometry models of spontaneous neural activity appear to be more accurate and parsimonious than those derived from anatomical connectivity (Pang et al., 2023). Hence, NSAR as a connectivity and surface area-based measure is more reflective of functional rather than anatomical specialization.

In this study, individual parcellations were generated using the Kong et al. (2019) MS-HBM algorithm. However, improved versions of this algorithm have since been published (Kong et al., 2021; Yan et al., 2023), which account for parcel distributions, spatial contiguity, local

gradients, and homotopy (or the lack thereof in Schaefer parcels). Thus, future investigations using NSAR might consider implementing an updated individual parcellation algorithm. Moreover, it would be valuable for future studies to explore specialization in developmental and clinical populations to address questions regarding the developmental timeline of network specialization and the potential disruptions in network specialization observed in specific neurodevelopmental conditions.

Conclusions

The present study investigated hemispheric specialization in the human brain, focusing on 17 functional networks. This was accomplished by implementing a surface area-based metric of specialization, for which validity and reliability were examined. Following methodological development, we addressed two main questions: (1) which networks exhibit the greatest hemispheric specialization, and (2) how does specialization in one network relate to the specialization of other networks? We found that the Language, Dorsal Attention-A, and Default-C networks were significantly left-lateralized while the Visual-B, Salience/Ventral Attention-A, Control-B, Control-C, and Limbic-B networks were significantly right-lateralized. Additionally, using EFA to understand how network specialization is related between networks, we found general support for a relationship between left- and right-lateralized networks. This suggests that network specialization follows a covariation paradigm. Further work is needed to understand how these findings may differ in developmental and clinical populations.

Acknowledgements

Data were provided in part by the Human Connectome Project, WU-Minn Consortium (principal Investigators: David Van Essen and Kamil Ugurbil; 1U54MH091657) funded by the 16 NIH Institutes and Centers that support the NIH Blueprint for Neuroscience Research; and by

the McDonnell Center for Systems Neuroscience at Washington University. HCPD data reported in this publication were supported by the National Institute of Mental Health of the National Institutes of Health under Award Number U01MH109589 and by funds provided by the McDonnell Center for Systems Neuroscience at Washington University in St. Louis. The HCP-Development 2.0 Release data used in this report came from DOI: 10.15154/1520708. Collection of the NSD dataset was supported by NSF IIS-1822683 and NSF IIS-1822929. Furthermore, we acknowledge the support of the Office of Research Computing at Brigham Young University.

References

Allen, E. J., St-Yves, G., Wu, Y., Breedlove, J. L., Prince, J. S., Dowdle, L. T., Nau, M., Caron, B., Pestilli, F., Charest, I., Hutchinson, J. B., Naselaris, T., & Kay, K. (2022). A massive 7T fMRI dataset to bridge cognitive neuroscience and artificial intelligence. *Nature Neuroscience*, *25*(1), Art. 1. https://doi.org/10.1038/s41593-021-00962-x

Anticevic, A., Dierker, D. L., Gillespie, S. K., Repovs, G., Csernansky, J. G., Van Essen, D. C., & Barch, D. M. (2008). Comparing surface-based and volume-based analyses of functional neuroimaging data in patients with schizophrenia. *NeuroImage*, *41*(3), 835–848. https://doi.org/10.1016/j.neuroimage.2008.02.052

Argall, B. D., Saad, Z. S., & Beauchamp, M. S. (2006). Simplified intersubject averaging on the cortical surface using SUMA. *Human Brain Mapping*, *27*(1), 14–27.

Beume, L.-A., Kaller, C. P., Hoeren, M., Klöppel, S., Kuemmerer, D., Glauche, V., Köstering, L., Mader, I., Rijntjes, M., Weiller, C., & Umarova, R. (2015). Processing of bilateral versus unilateral conditions: Evidence for the functional contribution of the ventral attention network. *Cortex*, *66*, 91–102. https://doi.org/10.1016/j.cortex.2015.02.018

Binder, J. R., Swanson, S. J., Hammeke, T. A., Morris, G. L., Mueller, W. M., Fischer, M., Benbadis, S., Frost, J. A., Rao, S. M., & Haughton, V. M. (1996). Determination of language dominance using functional MRI: A comparison with the Wada test. *Neurology*, *46*(4), 978–984. https://doi.org/10.1212/WNL.46.4.978

Braga, R. M., & Buckner, R. L. (2017). Parallel interdigitated distributed networks within the individual estimated by intrinsic functional connectivity. *Neuron*, *95*(2), 457-471.e5. https://doi.org/10.1016/j.neuron.2017.06.038

Braga, R. M., DiNicola, L. M., Becker, H. C., & Buckner, R. L. (2020). Situating the left-lateralized language network in the broader organization of multiple specialized large-scale distributed networks. *Journal of Neurophysiology*, *124*(5), Art. 5. https://doi.org/10.1152/jn.00753.2019

Breier, J. I., Simos, P. G., Zouridakis, G., & Papanicolaou, A. C. (2000). Lateralization of activity associated with language function using magnetoencephalography: A reliability study. *Journal of Clinical Neurophysiology*, *17*(5), 503–510.

Broca, P. (1861). Remarques sur le siège de la faculté du langage articulé, suivies d'une observation d'aphémie (perte de la parole). *Bulletin et Memoires de La Societe Anatomique de Paris*, *6*, 330–357.

Buckner, R. L., Krienen, F. M., & Yeo, B. T. T. (2013). Opportunities and limitations of intrinsic functional connectivity MRI. *Nature Neuroscience*, *16*(7), Art. 7. https://doi.org/10.1038/nn.3423

Cai, Q., Van der Haegen, L., & Brysbaert, M. (2013). Complementary hemispheric specialization for language production and visuospatial attention. *Proceedings of the National Academy of Sciences*, *110*(4), E322–E330. https://doi.org/10.1073/pnas.1212956110

Corballis, M. C. (2003). From mouth to hand: Gesture, speech, and the evolution of right-handedness. *Behavioral and Brain Sciences*, *26*(2), 199–208. https://doi.org/10.1017/S0140525X03000062

Corbetta, M., & Shulman, G. L. (2002). Control of goal-directed and stimulus-driven attention in the brain. *Nature Reviews Neuroscience*, *3*(3), 201–215.

Corbetta, M., & Shulman, G. L. (2011). Spatial Neglect and Attention Networks. *Annual Review of Neuroscience*, *34*(1), 569–599. https://doi.org/10.1146/annurev-neuro-061010-113731

Dale, A. M., Fischl, B., & Sereno, M. I. (1999). Cortical surface-based analysis: I. Segmentation and surface reconstruction. *NeuroImage*, *9*(2), 179–194. https://doi.org/10.1006/nimg.1998.0395

Desai, R., Liebenthal, E., Possing, E. T., Waldron, E., & Binder, J. R. (2005). Volumetric vs. Surface-based alignment for localization of auditory cortex activation. *NeuroImage*, *26*(4), 1019–1029. https://doi.org/10.1016/j.neuroimage.2005.03.024

Desmond, J. E., Sum, J. M., Wagner, A. D., Demb, J. B., Shear, P. K., Glover, G. H., Gabrieli, J., & Morrell, M. (1995). Functional MRI measurement of language lateralization in Wada-tested patients. *Brain*, *118*(6), 1411–1419.

DiNicola, L. M., Braga, R. M., & Buckner, R. L. (2020). Parallel distributed networks dissociate episodic and social functions within the individual. *Journal of Neurophysiology*, *123*(3), Art. 3. https://doi.org/10.1152/jn.00529.2019

Doornik, J. A., & Hansen, H. (2008). An omnibus test for univariate and multivariate normality. *Oxford Bulletin of Economics and Statistics*, *70*, 927–939.

Dosenbach, N. U. F., Koller, J. M., Earl, E. A., Miranda-Dominguez, O., Klein, R. L., Van, A. N., Snyder, A. Z., Nagel, B. J., Nigg, J. T., Nguyen, A. L., Wesevich, V., Greene, D. J., & Fair, D. A. (2017). Real-time motion analytics during brain MRI improve data quality and reduce costs. *NeuroImage*, *161*, 80–93. https://doi.org/10.1016/j.neuroimage.2017.08.025

Elin, K., Malyutina, S., Bronov, O., Stupina, E., Marinets, A., Zhuravleva, A., & Dragoy, O. (2022). A new functional magnetic resonance imaging localizer for preoperative

language mapping using a sentence completion task: Validity, choice of baseline condition, and test–retest reliability. *Frontiers in Human Neuroscience*, *16*, 791577. https://doi.org/10.3389/fnhum.2022.791577

Elton, A., & Gao, W. (2015). Task-related modulation of functional connectivity variability and its behavioral correlations. *Human Brain Mapping*, *36*(8), 3260–3272.

Eyler, L. T., Pierce, K., & Courchesne, E. (2012). A failure of left temporal cortex to specialize for language is an early emerging and fundamental property of autism. *Brain*, *135*(3), 949–960.

Fedorenko, E. (2021). The early origins and the growing popularity of the individual-subject analytic approach in human neuroscience. *Current Opinion in Behavioral Sciences*, *40*, 105–112. https://doi.org/10.1016/j.cobeha.2021.02.023

Fedorenko, E., Behr, M. K., & Kanwisher, N. (2011). Functional specificity for high-level linguistic processing in the human brain. *Proceedings of the National Academy of Sciences*, *108*(39), 16428–16433. https://doi.org/10.1073/pnas.1112937108

Fedorenko, E., Duncan, J., & Kanwisher, N. (2012). Language-selective and domain-general regions lie side by side within Broca's area. *Current Biology*, *22*(21), 2059–2062. https://doi.org/10.1016/j.cub.2012.09.011

Fedorenko, E., Hsieh, P.-J., Nieto-Castañón, A., Whitfield-Gabrieli, S., & Kanwisher, N. (2010). New method for fMRI investigations of language: Defining ROIs functionally in individual subjects. *Journal of Neurophysiology*, *104*(2), 1177–1194. https://doi.org/10.1152/jn.00032.2010

Fedorenko, E., McDermott, J. H., Norman-Haignere, S., & Kanwisher, N. (2012). Sensitivity to musical structure in the human brain. *Journal of Neurophysiology*, *108*(12), 3289–3300. https://doi.org/10.1152/jn.00209.2012

Fedorenko, E., & Thompson-Schill, S. L. (2014). Reworking the language network. *Trends in Cognitive Sciences*, *18*(3), 120–126. https://doi.org/10.1016/j.tics.2013.12.006

Fischl, B., Sereno, M. I., Tootell, R. B. H., & Dale, A. M. (1999). High-resolution intersubject averaging and a coordinate system for the cortical surface. *Human Brain Mapping*, *8*(4), 272–284. https://doi.org/10.1002/(SICI)1097-0193(1999)8:4<272::AID-HBM10>3.0.CO;2-4

Fox, M. D., Corbetta, M., Snyder, A. Z., Vincent, J. L., & Raichle, M. E. (2006). Spontaneous neuronal activity distinguishes human dorsal and ventral attention systems. *Proceedings of the National Academy of Sciences*, *103*(26), 10046–10051. https://doi.org/10.1073/pnas.0604187103

Friedrich, P., Patil, K. R., Mochalski, L. N., Li, X., Camilleri, J. A., Kröll, J.-P., Wiersch, L., Eickhoff, S. B., & Weis, S. (2022). Is it left or is it right? A classification approach for investigating hemispheric differences in low and high dimensionality. *Brain Structure and Function*, *227*(2), 425–440. https://doi.org/10.1007/s00429-021-02418-1

Gainotti, G. (2019). A historical review of investigations on laterality of emotions in the human brain. *Journal of the History of the Neurosciences*, *28*(1), 23–41. https://doi.org/10.1080/0964704X.2018.1524683

Gazzaniga, M. S. (2000). Cerebral specialization and interhemispheric communication: Does the corpus callosum enable the human condition? *Brain*, *123*(7), 1293–1326. https://doi.org/10.1093/brain/123.7.1293

Glasser, M. F., & Essen, D. C. V. (2011). Mapping human cortical areas in vivo based on myelin content as revealed by T1- and T2-weighted MRI. *Journal of Neuroscience*, *31*(32), 11597–11616. https://doi.org/10.1523/JNEUROSCI.2180-11.2011

Glasser, M. F., Smith, S. M., Marcus, D. S., Andersson, J. L. R., Auerbach, E. J., Behrens, T. E. J., Coalson, T. S., Harms, M. P., Jenkinson, M., Moeller, S., Robinson, E. C., Sotiropoulos, S. N., Xu, J., Yacoub, E., Ugurbil, K., & Van Essen, D. C. (2016). The Human Connectome Project's neuroimaging approach. *Nature Neuroscience*, *19*(9), Art. 9. https://doi.org/10.1038/nn.4361

Glasser, M. F., Sotiropoulos, S. N., Wilson, J. A., Coalson, T. S., Fischl, B., Andersson, J. L., Xu, J., Jbabdi, S., Webster, M., Polimeni, J. R., Van Essen, D. C., & Jenkinson, M. (2013). The minimal preprocessing pipelines for the Human Connectome Project. *NeuroImage*, *80*, 105–124. https://doi.org/10.1016/j.neuroimage.2013.04.127

Gordon, E. M., Laumann, T. O., Adeyemo, B., Huckins, J. F., Kelley, W. M., & Petersen, S. E. (2016). Generation and evaluation of a cortical area parcellation from resting-state correlations. *Cerebral Cortex*, *26*(1), 288–303. https://doi.org/10.1093/cercor/bhu239

Gotts, S. J., Jo, H. J., Wallace, G. L., Saad, Z. S., Cox, R. W., & Martin, A. (2013). Two distinct forms of functional lateralization in the human brain. *Proceedings of the National Academy of Sciences*, *110*(36), E3435–E3444.

Gratton, C., Nelson, S. M., & Gordon, E. M. (2022). Brain-behavior correlations: Two paths toward reliability. *Neuron*, *110*(9), 1446–1449. https://doi.org/10.1016/j.neuron.2022.04.018

Greene, A. S., Gao, S., Scheinost, D., & Constable, R. T. (2018). Task-induced brain state manipulation improves prediction of individual traits. *Nature Communications*, *9*(1), Art. 1. https://doi.org/10.1038/s41467-018-04920-3

Greve, D. N., & Fischl, B. (2009). Accurate and robust brain image alignment using boundary-based registration. *NeuroImage*, *48*(1), 63–72. https://doi.org/10.1016/j.neuroimage.2009.06.060

Harms, M. P., Somerville, L. H., Ances, B. M., Andersson, J., Barch, D. M., Bastiani, M., Bookheimer, S. Y., Brown, T. B., Buckner, R. L., Burgess, G. C., Coalson, T. S., Chappell, M. A., Dapretto, M., Douaud, G., Fischl, B., Glasser, M. F., Greve, D. N., Hodge, C., Jamison, K. W., … Yacoub, E. (2018). Extending the Human Connectome Project across ages: Imaging protocols for the Lifespan Development and Aging projects. *NeuroImage*, *183*, 972–984. https://doi.org/10.1016/j.neuroimage.2018.09.060

Hartwigsen, G., Bengio, Y., & Bzdok, D. (2021). How does hemispheric specialization contribute to human-defining cognition? *Neuron*, *109*(13), 2075–2090. https://doi.org/10.1016/j.neuron.2021.04.024

Hervé, P.-Y., Zago, L., Petit, L., Mazoyer, B., & Tzourio-Mazoyer, N. (2013). Revisiting human hemispheric specialization with neuroimaging. *Trends in Cognitive Sciences*, *17*(2), 69–80. https://doi.org/10.1016/j.tics.2012.12.004

Ho, D., Imai, K., King, G., Stuart, E., Whitworth, A., & Greifer, N. (2023). *MatchIt: Nonparametric Preprocessing for Parametric Causal Inference* (4.5.4). https://cran.r-project.org/web/packages/MatchIt/index.html

Holmes, A. J., Hollinshead, M. O., O'Keefe, T. M., Petrov, V. I., Fariello, G. R., Wald, L. L., Fischl, B., Rosen, B. R., Mair, R. W., Roffman, J. L., Smoller, J. W., & Buckner, R. L.

(2015). Brain Genomics Superstruct Project initial data release with structural, functional, and behavioral measures. *Scientific Data*, *2*(1), Art. 1. https://doi.org/10.1038/sdata.2015.31

Hughlings-Jackson, J. (1878). On affections of speech from disease of the brain. *Brain*, *1*(3), 304–330.

Hutchison, R. M., Womelsdorf, T., Gati, J. S., Everling, S., & Menon, R. S. (2013). Resting-state networks show dynamic functional connectivity in awake humans and anesthetized macaques. *Human Brain Mapping*, *34*(9), 2154–2177. https://doi.org/10.1002/hbm.22058

Jansen, A., Flöel, A., Deppe, M., van Randenborgh, J., Dräger, B., Kanowski, M., & Knecht, S. (2004). Determining the hemispheric dominance of spatial attention: A comparison between fTCD and fMRI. *Human Brain Mapping*, *23*(3), 168–180. https://doi.org/10.1002/hbm.20055

Jenkinson, M., Bannister, P., Brady, M., & Smith, S. M. (2002). Improved optimization for the robust and accurate linear registration and motion correction of brain images. *NeuroImage*, *17*(2), 825–841. https://doi.org/10.1006/nimg.2002.1132

Kong, R., Li, J., Orban, C., Sabuncu, M. R., Liu, H., Schaefer, A., Sun, N., Zuo, X.-N., Holmes, A. J., Eickhoff, S. B., & Yeo, B. T. T. (2019). Spatial topography of individual-specific cortical networks predicts human cognition, personality, and emotion. *Cerebral Cortex*, *29*(6), Art. 6. https://doi.org/10.1093/cercor/bhy123

Kong, R., Yang, Q., Gordon, E., Xue, A., Yan, X., Orban, C., Zuo, X.-N., Spreng, N., Ge, T., Holmes, A., Eickhoff, S., & Yeo, B. T. T. (2021). Individual-specific areal-level parcellations improve functional connectivity prediction of behavior. *Cerebral Cortex*, *31*(10), 4477–4500. https://doi.org/10.1093/cercor/bhab101

Kong, X.-Z., Postema, M. C., Guadalupe, T., de Kovel, C., Boedhoe, P. S. W., Hoogman, M., Mathias, S. R., van Rooij, D., Schijven, D., Glahn, D. C., Medland, S. E., Jahanshad, N., Thomopoulos, S. I., Turner, J. A., Buitelaar, J., van Erp, T. G. M., Franke, B., Fisher, S. E., van den Heuvel, O. A., … Francks, C. (2022). Mapping brain asymmetry in health and disease through the ENIGMA consortium. *Human Brain Mapping*, *43*(1), 167–181. https://doi.org/10.1002/hbm.25033

Koo, T. K., & Li, M. Y. (2016). A guideline of selecting and reporting intraclass correlation coefficients for reliability research. *Journal of Chiropractic Medicine*, *15*(2), 155–163. https://doi.org/10.1016/j.jcm.2016.02.012

Kwong, K. K. (2012). Record of a single fMRI experiment in May of 1991. *NeuroImage*, *62*(2), 610–612. https://doi.org/10.1016/j.neuroimage.2011.07.089

Labache, L., Mazoyer, B., Joliot, M., Crivello, F., Hesling, I., & Tzourio-Mazoyer, N. (2020). Typical and atypical language brain organization based on intrinsic connectivity and multitask functional asymmetries. *ELife*, *9*, e58722. https://doi.org/10.7554/eLife.58722

Laumann, T. O., Gordon, E. M., Adeyemo, B., Snyder, A. Z., Joo, S. J., Chen, M.-Y., Gilmore, A. W., McDermott, K. B., Nelson, S. M., Dosenbach, N. U. F., Schlaggar, B. L., Mumford, J. A., Poldrack, R. A., & Petersen, S. E. (2015). Functional system and areal organization of a highly sampled individual human brain. *Neuron*, *87*(3), 657–670. https://doi.org/10.1016/j.neuron.2015.06.037

Lewis, C. M., Baldassarre, A., Committeri, G., Romani, G. L., & Corbetta, M. (2009). Learning sculpts the spontaneous activity of the resting human brain. *Proceedings of the National Academy of Sciences*, *106*(41), 17558–17563. https://doi.org/10.1073/pnas.0902455106

Li, J., Kong, R., Liégeois, R., Orban, C., Tan, Y., Sun, N., Holmes, A. J., Sabuncu, M. R., Ge, T., & Yeo, B. T. T. (2019). Global signal regression strengthens association between resting-state functional connectivity and behavior. *NeuroImage*, *196*, 126–141. https://doi.org/10.1016/j.neuroimage.2019.04.016

Lin, T.-Y., Maire, M., Belongie, S., Hays, J., Perona, P., Ramanan, D., Dollár, P., & Zitnick, C. L. (2014). Microsoft COCO: Common Objects in Context. In D. Fleet, T. Pajdla, B. Schiele, & T. Tuytelaars (Eds.), *Computer Vision – ECCV 2014* (pp. 740–755). Springer International Publishing. https://doi.org/10.1007/978-3-319-10602-1_48

Lipkin, B., Tuckute, G., Affourtit, J., Small, H., Mineroff, Z., Kean, H., ... & Fedorenko, E. (2022). Probabilistic atlas for the language network based on precision fMRI data from > 800 individuals. *Scientific Data*, *9*(1), 529. https://doi.org/10.1038/s41597-022-01645-3

Liu, H., Stufflebeam, S. M., Sepulcre, J., Hedden, T., & Buckner, R. L. (2009). Evidence from intrinsic activity that asymmetry of the human brain is controlled by multiple factors. *Proceedings of the National Academy of Sciences*, *106*(48), 20499–20503.

Luys, J. (1879). Etude sur le dédoublement des opérations cérébrales et sur le rôle isolé de chaque hémisphère dans lès phénomènes de la pathologie mentale. *Rev Philos Fr étrang, 8*(1879), 105-106.

Lynch, C. J., Power, J. D., Scult, M. A., Dubin, M., Gunning, F. M., & Liston, C. (2020). Rapid precision functional mapping of individuals using multi-echo fMRI. *Cell Reports*, *33*(12), 108540. https://doi.org/10.1016/j.celrep.2020.108540

Mahowald, K., & Fedorenko, E. (2016). Reliable individual-level neural markers of high-level language processing: A necessary precursor for relating neural variability to behavioral

and genetic variability. *NeuroImage*, *139*, 74–93. https://doi.org/10.1016/j.neuroimage.2016.05.073

Malik-Moraleda, S., Ayyash, D., Gallée, J., Affourtit, J., Hoffmann, M., Mineroff, Z., ... & Fedorenko, E. (2022). An investigation across 45 languages and 12 language families reveals a universal language network. *Nature Neuroscience*, *25*(8), 1014-1019. https://doi.org/10.1038/s41593-022-01114-5

Marcus, D. S., Harms, M. P., Snyder, A. Z., Jenkinson, M., Wilson, J. A., Glasser, M. F., Barch, D. M., Archie, K. A., Burgess, G. C., Ramaratnam, M., Hodge, M., Horton, W., Herrick, R., Olsen, T., McKay, M., House, M., Hileman, M., Reid, E., Harwell, J., … Van Essen, D. C. (2013). Human Connectome Project informatics: Quality control, database services, and data visualization. *NeuroImage*, *80*, 202–219. https://doi.org/10.1016/j.neuroimage.2013.05.077

Marek, S., Tervo-Clemmens, B., Calabro, F. J., Montez, D. F., Kay, B. P., Hatoum, A. S., Donohue, M. R., Foran, W., Miller, R. L., Hendrickson, T. J., Malone, S. M., Kandala, S., Feczko, E., Miranda-Dominguez, O., Graham, A. M., Earl, E. A., Perrone, A. J., Cordova, M., Doyle, O., … Dosenbach, N. U. F. (2022). Reproducible brain-wide association studies require thousands of individuals. *Nature*, *603*(7902), Art. 7902. https://doi.org/10.1038/s41586-022-04492-9

MATLAB. (2018). *9.5.0.944444 (R2018b)*. The MathWorks Inc.

Mengotti, P., Käsbauer, A.-S., Fink, G. R., & Vossel, S. (2020). Lateralization, functional specialization, and dysfunction of attentional networks. *Cortex*, *132*, 206–222. https://doi.org/10.1016/j.cortex.2020.08.022

Milner, B. (1971). Interhemispheric differences in the localization of psychological processes in man. *British Medical Bulletin*, *27*, 272–277.

Mueller, S., Wang, D., Pan, R., Holt, D. J., & Liu, H. (2015). Abnormalities in hemispheric specialization of caudate nucleus connectivity in schizophrenia. *JAMA Psychiatry*, *72*(6), 552–560. https://doi.org/10.1001/jamapsychiatry.2014.3176

Nielsen, J. A., Zielinski, B. A., Ferguson, M. A., Lainhart, J. E., & Anderson, J. S. (2013). An evaluation of the left-brain vs. right-brain hypothesis with resting state functional connectivity magnetic resonance imaging. *PLoS ONE*, *8*(8), Art. 8. https://doi.org/10.1371/journal.pone.0071275

Oldfield, R. (1971). The assessment and analysis of handedness: The Edinburgh inventory. *Neuropsychologia*, *9*(1), 97-113.

Olson, I. R., Plotzker, A., & Ezzyat, Y. (2007). The enigmatic temporal pole: A review of findings on social and emotional processing. *Brain*, *130*(7), 1718–1731. https://doi.org/10.1093/brain/awm052

Olulade, O. A., Seydell-Greenwald, A., Chambers, C. E., Turkeltaub, P. E., Dromerick, A. W., Berl, M. M., Gaillard, W. D., & Newport, E. L. (2020). The neural basis of language development: Changes in lateralization over age. *Proceedings of the National Academy of Sciences*, *117*(38), 23477–23483. https://doi.org/10.1073/pnas.1905590117

Palomero-Gallagher, N., & Amunts, K. (2022). A short review on emotion processing: A lateralized network of neuronal networks. *Brain Structure and Function*, *227*(2), 673–684. https://doi.org/10.1007/s00429-021-02331-7

Pang, J. C., Aquino, K. M., Oldehinkel, M., Robinson, P. A., Fulcher, B. D., Breakspear, M., & Fornito, A. (2023). Geometric constraints on human brain function. *Nature*, 1–9. https://doi.org/10.1038/s41586-023-06098-1

Pehrs, C., Zaki, J., Schlochtermeier, L. H., Jacobs, A. M., Kuchinke, L., & Koelsch, S. (2017). The temporal pole top-down modulates the ventral visual stream during social cognition. *Cerebral Cortex*, *27*(1), 777–792. https://doi.org/10.1093/cercor/bhv226

Penfield, W., & Jasper, H. (1954). *Epilepsy and the functional anatomy of the human brain.* Little, Brown.

Perez, D. C., Dworetsky, A., Braga, R. M., Beeman, M., & Gratton, C. (2023). Hemispheric asymmetries of individual differences in functional connectivity. *Journal of Cognitive Neuroscience*, *35*(2), 200–225. https://doi.org/10.1162/jocn_a_01945

Petersen, S. E., & Sporns, O. (2015). Brain networks and cognitive architectures. *Neuron*, *88*(1), 207–219. https://doi.org/10.1016/j.neuron.2015.09.027

Pya, N., Voinov, V., Makarov, R., & Voinov, Y. (2016). *mvnTest: Goodness of Fit Tests for Multivariate Normality* (1.1-0). https://cran.r-project.org/web/packages/mvnTest/index.html

R Core Team. (2011). *Wilcoxon rank sum and signed rank tests*. R Documentation.[Online]. Available: http://stat. ethz. ch/R-manual/R ….

R Core Team. (2022). *R: A Language and Environment for Statistical Computing*. R Foundation for Statistical Computing. https://www.R-project.org/

Rasmussen, T., & Milner, B. (1977). The role of early left-brain injury in determining lateralization of cerebral speech functions. *Annals of the New York Academy of Sciences*, *299*, 355–369.

Revelle, W. (2023). *psych: Procedures for Psychological, Psychometric, and Personality Research* (2.3.3). https://cran.r-project.org/web/packages/psych/index.html

Reynolds, J. E., Long, X., Grohs, M. N., Dewey, D., & Lebel, C. (2019). Structural and functional asymmetry of the language network emerge in early childhood. *Developmental Cognitive Neuroscience*, *39*, 100682. https://doi.org/10.1016/j.dcn.2019.100682

Salvo, J. J., Holubecki, A. M., & Braga, R. M. (2021). Correspondence between functional connectivity and task-related activity patterns within the individual. *Current Opinion in Behavioral Sciences*, *40*, 178–188. https://doi.org/10.1016/j.cobeha.2021.05.003

Scott, T. L., Gallée, J., & Fedorenko, E. (2017). A new fun and robust version of an fMRI localizer for the frontotemporal language system. *Cognitive Neuroscience*, *8*(3), 167–176. https://doi.org/10.1080/17588928.2016.1201466

Shirer, W. R., Ryali, S., Rykhlevskaia, E., Menon, V., & Greicius, M. D. (2012). Decoding subject-driven cognitive states with whole-brain connectivity patterns. *Cerebral Cortex*, *22*(1), 158–165.

Shulman, G. L., Pope, D. L., Astafiev, S. V., McAvoy, M. P., Snyder, A. Z., & Corbetta, M. (2010). Right hemisphere dominance during spatial selective attention and target detection occurs outside the dorsal frontoparietal network. *Journal of Neuroscience*, *30*(10), 3640–3651.

Silberman, E. K., & Weingartner, H. (1986). Hemispheric lateralization of functions related to emotion. *Brain and Cognition*, *5*(3), 322–353. https://doi.org/10.1016/0278-2626(86)90035-7

Siman-Tov, T., Mendelsohn, A., Schonberg, T., Avidan, G., Podlipsky, I., Pessoa, L., Gadoth, N., Ungerleider, L. G., & Hendler, T. (2007). Bihemispheric leftward bias in a

visuospatial attention-related network. *Journal of Neuroscience*, *27*(42), 11271–11278. https://doi.org/10.1523/JNEUROSCI.0599-07.2007

Smith, S. M., Beckmann, C. F., Andersson, J., Auerbach, E. J., Bijsterbosch, J., Douaud, G., Duff, E., Feinberg, D. A., Griffanti, L., Harms, M. P., Kelly, M., Laumann, T., Miller, K. L., Moeller, S., Petersen, S., Power, J., Salimi-Khorshidi, G., Snyder, A. Z., Vu, A. T., … Glasser, M. F. (2013). Resting-state fMRI in the Human Connectome Project. *NeuroImage*, *80*, 144–168. https://doi.org/10.1016/j.neuroimage.2013.05.039

Smith, S. M., Jenkinson, M., Woolrich, M. W., Beckmann, C. F., Behrens, T. E. J., Johansen-Berg, H., Bannister, P. R., De Luca, M., Drobnjak, I., Flitney, D. E., Niazy, R. K., Saunders, J., Vickers, J., Zhang, Y., De Stefano, N., Brady, J. M., & Matthews, P. M. (2004). Advances in functional and structural MR image analysis and implementation as FSL. *NeuroImage*, *23*, S208–S219. https://doi.org/10.1016/j.neuroimage.2004.07.051

Somerville, L. H., Bookheimer, S. Y., Buckner, R. L., Burgess, G. C., Curtiss, S. W., Dapretto, M., Elam, J. S., Gaffrey, M. S., Harms, M. P., Hodge, C., Kandala, S., Kastman, E. K., Nichols, T. E., Schlaggar, B. L., Smith, S. M., Thomas, K. M., Yacoub, E., Van Essen, D. C., & Barch, D. M. (2018). The Lifespan Human Connectome Project in Development: A large-scale study of brain connectivity development in 5–21 year olds. *NeuroImage*, *183*, 456–468. https://doi.org/10.1016/j.neuroimage.2018.08.050

Sonkusare, S., Nguyen, V. T., Moran, R., van der Meer, J., Ren, Y., Koussis, N., Dionisio, S., Breakspear, M., & Guo, C. (2020). Intracranial-EEG evidence for medial temporal pole driving amygdala activity induced by multi-modal emotional stimuli. *Cortex*, *130*, 32–48. https://doi.org/10.1016/j.cortex.2020.05.018

Spreng, R. N., Sepulcre, J., Turner, G. R., Stevens, W. D., & Schacter, D. L. (2013). Intrinsic architecture underlying the relations among the default, dorsal attention, and frontoparietal control networks of the human brain. *Journal of Cognitive Neuroscience*, *25*(1), 74–86. https://doi.org/10.1162/jocn_a_00281

Stippich, C., Mohammed, J., Kress, B., Hähnel, S., Günther, J., Konrad, F., & Sartor, K. (2003). Robust localization and lateralization of human language function: An optimized clinical functional magnetic resonance imaging protocol. *Neuroscience Letters*, *346*(1), 109–113. https://doi.org/10.1016/S0304-3940(03)00561-5

Sun, J., Gao, X., Hua, Q., Du, R., Liu, P., Liu, T., Yang, J., Qiu, B., Ji, G.-J., Hu, P., & Wang, K. (2022). Brain functional specialization and cooperation in Parkinson's disease. *Brain Imaging and Behavior*, *16*(2), 565–573. https://doi.org/10.1007/s11682-021-00526-4

Tagliazucchi, E., & Laufs, H. (2014). Decoding wakefulness levels from typical fMRI resting-state data reveals reliable drifts between wakefulness and sleep. *Neuron*, *82*(3), 695–708. https://doi.org/10.1016/j.neuron.2014.03.020

Toga, A. W., & Thompson, P. M. (2003). Mapping brain asymmetry. *Nature Reviews Neuroscience*, *4*(1), Art. 1. https://doi.org/10.1038/nrn1009

Uğurbil, K., Xu, J., Auerbach, E. J., Moeller, S., Vu, A. T., Duarte-Carvajalino, J. M., Lenglet, C., Wu, X., Schmitter, S., Van de Moortele, P. F., Strupp, J., Sapiro, G., De Martino, F., Wang, D., Harel, N., Garwood, M., Chen, L., Feinberg, D. A., Smith, S. M., … Yacoub, E. (2013). Pushing spatial and temporal resolution for functional and diffusion MRI in the Human Connectome Project. *NeuroImage*, *80*, 80–104. https://doi.org/10.1016/j.neuroimage.2013.05.012

Umarova, R. M., Saur, D., Schnell, S., Kaller, C. P., Vry, M.-S., Glauche, V., Rijntjes, M., Hennig, J., Kiselev, V., & Weiller, C. (2010). Structural connectivity for visuospatial attention: Significance of Ventral Pathways. *Cerebral Cortex*, *20*(1), 121–129. https://doi.org/10.1093/cercor/bhp086

van der Kouwe, A. J. W., Benner, T., Salat, D. H., & Fischl, B. (2008). Brain morphometry with multiecho MPRAGE. *NeuroImage*, *40*(2), 559–569. https://doi.org/10.1016/j.neuroimage.2007.12.025

Van Essen, D. C. (2005). A Population-Average, Landmark- and Surface-based (PALS) atlas of human cerebral cortex. *NeuroImage*, *28*(3), 635–662. https://doi.org/10.1016/j.neuroimage.2005.06.058

Van Essen, D. C., Smith, S. M., Barch, D. M., Behrens, T. E. J., Yacoub, E., & Ugurbil, K. (2013). The WU-Minn Human Connectome Project: An overview. *NeuroImage*, *80*, 62–79. https://doi.org/10.1016/j.neuroimage.2013.05.041

Van Essen, D. C., Ugurbil, K., Auerbach, E., Barch, D., Behrens, T. E. J., Bucholz, R., Chang, A., Chen, L., Corbetta, M., Curtiss, S. W., Della Penna, S., Feinberg, D., Glasser, M. F., Harel, N., Heath, A. C., Larson-Prior, L., Marcus, D., Michalareas, G., Moeller, S., … Yacoub, E. (2012). The Human Connectome Project: A data acquisition perspective. *NeuroImage*, *62*(4), 2222–2231. https://doi.org/10.1016/j.neuroimage.2012.02.018

Wada, J., & Rasmussen, T. (1960). Intracarotid injection of sodium amytal for the lateralization of cerebral speech dominance: Experimental and clinical observations. *Journal of Neurosurgery*, *17*(2), 266–282.

Wang, D., Buckner, R. L., & Liu, H. (2014). Functional specialization in the human brain estimated by intrinsic hemispheric interaction. *Journal of Neuroscience*, *34*(37), Art. 37. https://doi.org/10.1523/JNEUROSCI.0787-14.2014

Wang, J., Tian, Y., Wang, M., Cao, L., Wu, H., Zhang, Y., Wang, K., & Jiang, T. (2016). A lateralized top-down network for visuospatial attention and neglect. *Brain Imaging and Behavior*, *10*(4), 1029–1037. https://doi.org/10.1007/s11682-015-9460-y

Wernicke, K. (1995). The aphasia symptom-complex: A psychological study on an anatomical basis (1875). *Reader in the History of Aphasia: From (Franz Gall To)*, *4*, 69–89.

Wilcoxon, F. (1945). Individual comparisons by ranking methods. *Biometrics Bulletin*, *1*(6), 80–83. https://doi.org/10.2307/3001968

Wilson, S. M., Bautista, A., Yen, M., Lauderdale, S., & Eriksson, D. K. (2017). Validity and reliability of four language mapping paradigms. *NeuroImage: Clinical*, *16*, 399–408. https://doi.org/10.1016/j.nicl.2016.03.015

Yan, X., Kong, R., Xue, A., Yang, Q., Orban, C., An, L., Holmes, A. J., Qian, X., Chen, J., Zuo, X.-N., Zhou, J. H., Fortier, M. V., Tan, A. P., Gluckman, P., Chong, Y. S., Meaney, M. J., Bzdok, D., Eickhoff, S. B., & Yeo, B. T. T. (2023). Homotopic local-global parcellation of the human cerebral cortex from resting-state functional connectivity. *NeuroImage*, *273*, 120010. https://doi.org/10.1016/j.neuroimage.2023.120010

Yeo, B. T. T., Krienen, F. M., Sepulcre, J., Sabuncu, M. R., Lashkari, D., Hollinshead, M., Roffman, J. L., Smoller, J. W., Zöllei, L., Polimeni, J. R., Fischl, B., Liu, H., & Buckner, R. L. (2011). The organization of the human cerebral cortex estimated by intrinsic functional connectivity. *Journal of Neurophysiology*, *106*(3), 1125–1165. https://doi.org/10.1152/jn.00338.2011

Zago, L., Petit, L., Jobard, G., Hay, J., Mazoyer, B., Tzourio-Mazoyer, N., Karnath, H.-O., & Mellet, E. (2017). Pseudoneglect in line bisection judgement is associated with a modulation of right hemispheric spatial attention dominance in right-handers. *Neuropsychologia*, *94*, 75–83. https://doi.org/10.1016/j.neuropsychologia.2016.11.024

Zago, L., Petit, L., Mellet, E., Jobard, G., Crivello, F., Joliot, M., Mazoyer, B., & Tzourio-Mazoyer, N. (2016). The association between hemispheric specialization for language production and for spatial attention depends on left-hand preference strength. *Neuropsychologia*, *93*, 394–406. https://doi.org/10.1016/j.neuropsychologia.2015.11.018

Zhu, L., Fan, Y., Zou, Q., Wang, J., Gao, J.-H., & Niu, Z. (2014). Temporal reliability and lateralization of the resting-state language network. *PLOS ONE*, *9*(1), e85880. https://doi.org/10.1371/journal.pone.0085880

Study 1 Supplementary Materials

Figure S1

Data Quality for the NSD Dataset

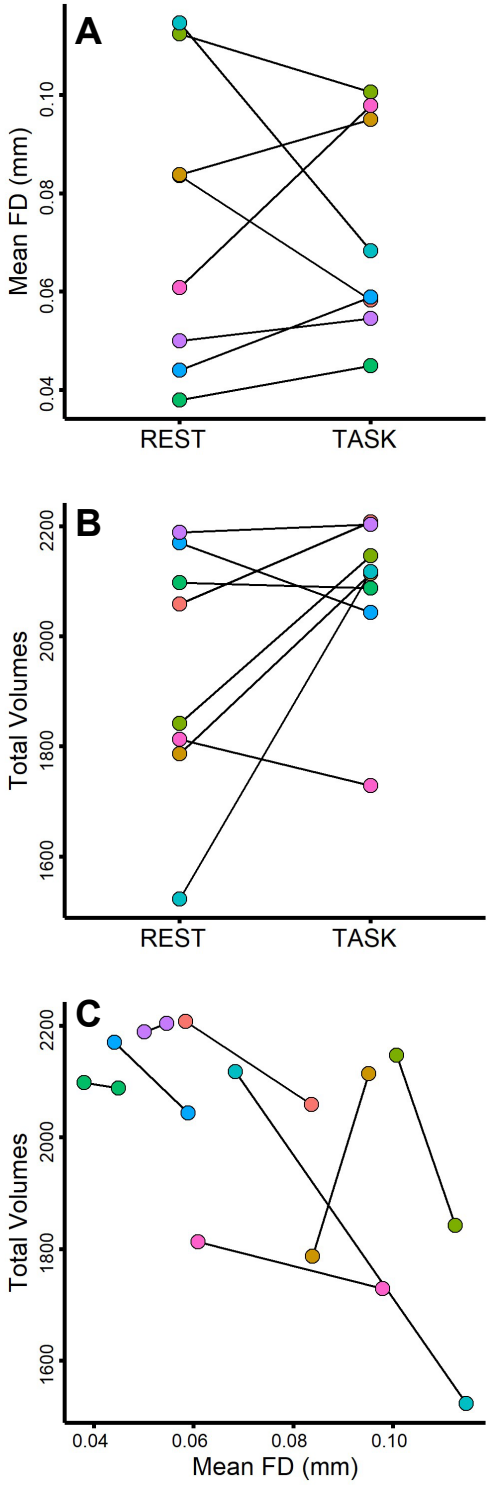

Note. Panel A depicts the mean framewise displacement across both resting-state and task fMRI data (12 runs each). Panel B depicts the total number of volumes post-motion correction available per participant for both resting-state and task fMRI data. Panel C depicts the total number of volumes available post-motion correction per participant by the mean framewise displacement. In each panel, a colored circle connected by a line to another colored circle represents the same individual.

Figure S2

NSAR Network Reliability

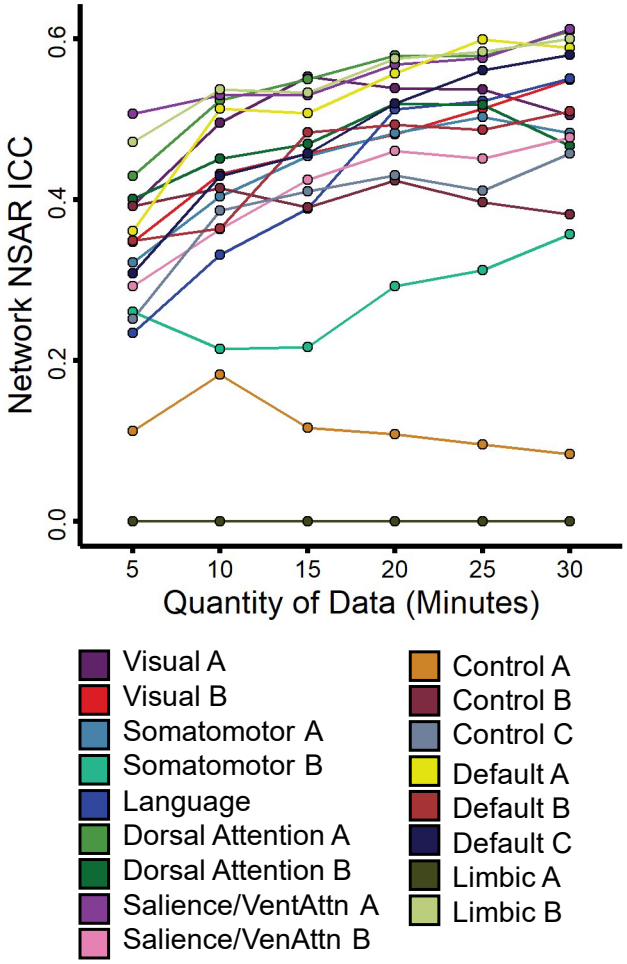

Note. Depicted is the intraclass correlation coefficient calculated for each network's mean NSAR value between the 30 independent minutes of data and each increment of data.

Figure S3

Parcellation Overlap Estimates in a Subset of Participants From the HCP Dataset (N = 232)

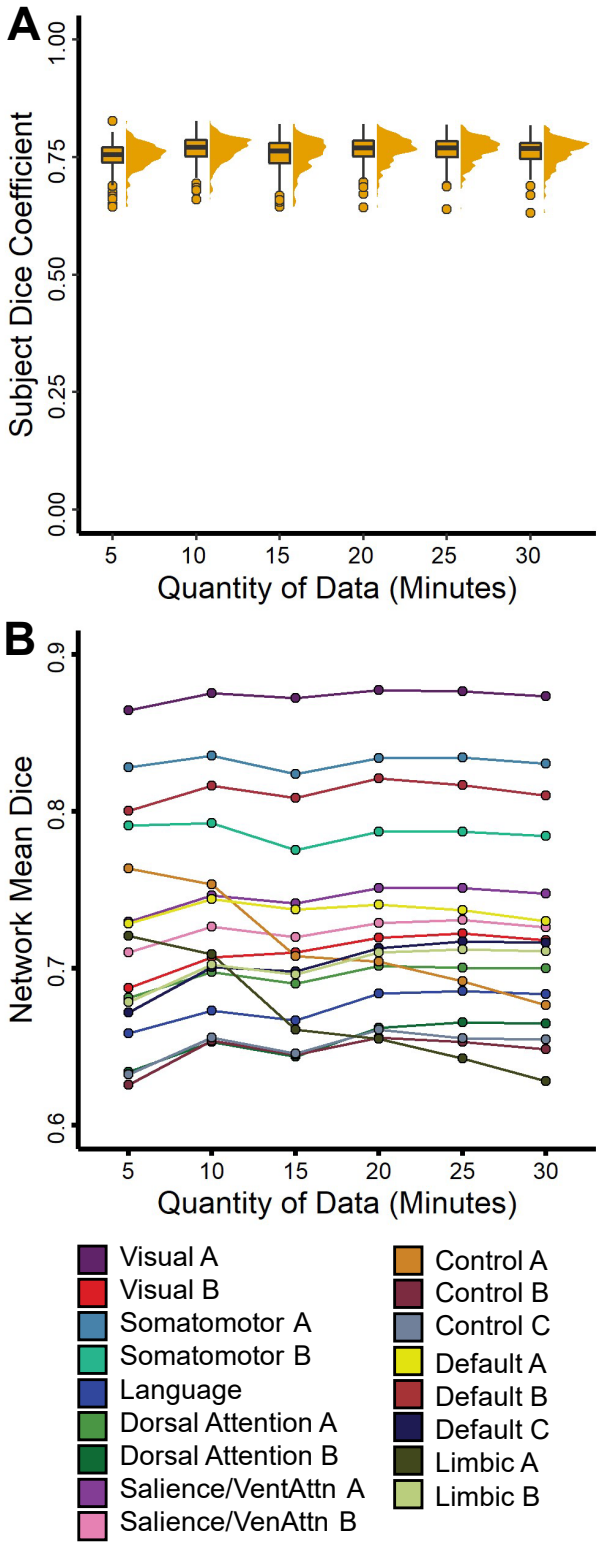

Note. Panel A depicts the subject dice coefficients calculated for the individual parcellations between each increment of data (5, 10, 15, … 30 minutes) and 30 independent minutes of data. Dice coefficient calculations are detailed in the Supplementary Methods. Comparable subject-level network assignment overlap analyses were conducted in the Midnight Scan Club dataset (see (Gordon et al., 2017) Figure 2 Panel B), finding that dice coefficients began at ~0.4 - 0.6 and plateaued at ~0.6 - 0.8. Panel B depicts the subject dice coefficients calculated for the individual parcellations between each increment of data (5, 10, 15, … 30 minutes) and 30 independent minutes of data averaged within each network. Comparable test-retest findings for parcellation overlap were described in Kong et al. (2019) Figures S10 Panel C and S11 Panel C, for which the somatomotor and visual networks exhibited the greatest intra-subject reproducibility.

Supplementary Table 1

Identifying Specialized Networks Using Multiple Regressions in the HCP-Discovery (N = 276), HCP-Replication (N = 277), and HCPD (N = 343) Datasets

Network Intercept	Dataset	β	*SE*	*t*	*p*
Visual-A					
	HCP-DISC	0.02	0.01	3.63	< .001
	HCP-REP	0.01	0.01	2.79	.006
	HCPD	0.01	0.00	1.54	.13
Visual-B					
	HCP-DISC	0.07	0.02	3.95	< .001
	HCP-REP	0.11	0.02	6.26	< .001
	HCPD	0.11	0.01	8.18	< .001
Somatomotor-A					
	HCP-DISC	0.02	0.01	2.92	.004
	HCP-REP	0.01	0.01	1.41	.16
	HCPD	0.01	0.01	1.22	.22
Somatomotor-B					
	HCP-DISC	-0.03	0.01	-3.35	< .001
	HCP-REP	-0.03	0.01	-2.85	.005
	HCPD	-0.01	0.01	-3.42	< .001

Language					
	HCP-DISC	-0.15	0.03	-4.71	< .001
	HCP-REP	-0.12	0.03	-4.13	< .001
	HCPD	-0.19	0.02	-8.11	< .001
Dorsal Attention-A					
	HCP-DISC	-0.25	0.02	-12.05	< .001
	HCP-REP	-0.31	0.02	-15.37	< .001
	HCPD	-0.22	0.02	-13.74	< .001
Dorsal Attention-B					
	HCP-DISC	-0.02	0.02	-1.24	.21
	HCP-REP	-0.03	0.02	-1.47	.14
	HCPD	0.01	0.01	0.87	.38
Salience/VenAttn-A					
	HCP-DISC	0.05	0.01	4.48	< .001
	HCP-REP	0.07	0.01	6.05	< .001
	HCPD	0.05	0.01	6.35	< .001
Salience/VenAttn-B					
	HCP-DISC	-0.02	0.01	-1.59	.11
	HCP-REP	-0.03	0.01	-2.56	.01
	HCPD	-0.03	0.01	-3.52	< .001
Control-A					
	HCP-DISC	-0.07	0.02	-3.7	< .001
	HCP-REP	-0.11	0.02	-6.51	< .001
	HCPD	-0.05	0.01	-6.52	< .001
Control-B					
	HCP-DISC	0.19	0.02	7.95	< .001
	HCP-REP	0.18	0.02	8.09	< .001
	HCPD	0.14	0.01	9.93	< .001
Control-C					
	HCP-DISC	0.09	0.02	6.11	< .001
	HCP-REP	0.09	0.01	7.16	< .001
	HCPD	0.09	0.01	9.53	< .001
Default-A					
	HCP-DISC	-0.02	0.02	-1.01	.31
	HCP-REP	-0.02	0.02	-1.52	.13
	HCPD	-0.01	0.01	-1.04	.3
Default-B					
	HCP-DISC	0.01	0.01	1.04	.29
	HCP-REP	0.02	0.01	2.13	.03
	HCPD	0.01	0.01	0.87	.39
Default-C					
	HCP-DISC	-0.21	0.02	-10.56	< .001
	HCP-REP	-0.17	0.02	-9.37	< .001
	HCPD	-0.15	0.02	-8.83	< .001
Limbic-A					
	HCP-DISC	0.06	0.01	4.4	< .001

	HCP-REP	0.09	0.01	6.3	< .001
	HCPD	0.01	0.01	0.91	.37
Limbic-B					
	HCP-DISC	0.25	0.03	8.93	< .001
	HCP-REP	0.32	0.03	11.89	< .001
	HCPD	0.28	0.02	12.21	< .001

Note. Coefficients and *p*-values for the intercept are shown. None of the covariates (mean-centered age, mean-centered framewise displacement, handedness, and sex) were consistently significant across the three datasets for any of the networks. Networks with reliably significant (Bonferroni-corrected alpha level of .003) intercepts are bolded.

Supplementary Table 2

Left-lateralized Network Comparisons

Network Comparison	Dataset	β	*SE*	*t*	*p*
Language					
Dorsal Attention-A					
	HCP-DISC	-0.11	0.02	-6.98	< .001
	HCP-REP	-0.11	0.02	-6.73	< .001
	HCPD	-0.12	0.01	-9.69	< .001
Default-C					
	HCP-DISC	0.09	0.01	7.94	< .001
	HCP-REP	0.1	0.01	8.63	< .001
	HCPD	0.11	0.01	9.09	< .001
Dorsal Attention-A					
Default-C					
	HCP-DISC	-0.01	0.02	-0.93	.36
	HCP-REP	-0.00	0.02	-0.31	.76
	HCPD	-.02	0.01	-1.29	.19

Note. Comparisons consist of multiple regressions, which included a network variable with two levels (the two networks under comparison), mean-centered age, sex, handedness, and mean-centered mean framewise displacement.

Supplementary Table 3

Right-lateralized Network Comparisons

Network Comparison	Dataset	*β*	*SE*	*t*	*p*
Visual-B					
Salience/VenAttn-A					
	HCP-DISC	-0.04	0.01	-4.56	< .001
	HCP-REP	-0.05	0.01	-5.04	< .001
	HCPD	-0.05	0.01	-6.69	< .001
Control-B					
	HCP-DISC	0.09	0.02	5.69	< .001
	HCP-REP	0.08	0.01	6.19	< .001
	HCPD	0.05	0.01	5.47	< .001
Control-C					
	HCP-DISC	-0.01	0.01	-1.03	.3
	HCP-REP	-0.01	0.01	-1.27	.2
	HCPD	-0.01	0.01	-1.56	.12
Limbic-B					
	HCP-DISC	0.08	0.02	4.21	< .001
	HCP-REP	0.18	0.01	12.89	< .001
	HCPD	0.18	0.01	13.46	< .001
Salience/VenAttn-A					
Control-B					
	HCP-DISC	0.06	0.01	4.32	< .001
	HCP-REP	0.12	0.01	11.18	< .001
	HCPD	0.11	0.01	13.1	< .001
Control-C					
	HCP-DISC	0.03	0.01	3.71	< .001
	HCP-REP	0.03	0.01	4.29	< .001
	HCPD	0.04	0.07	6.04	< .001
Limbic-B					
	HCP-DISC	0.21	0.01	16.23	< .001
	HCP-REP	0.22	0.01	17.81	< .001
	HCPD	0.23	0.01	19.23	< .001
Control-B					
Control-C					
	HCP-DISC	-0.09	0.01	-6.97	< .001
	HCP-REP	-0.09	0.01	-7.78	< .001
	HCPD	-0.07	0.01	-7.59	< .001
Limbic-B					
	HCP-DISC	0.09	0.02	5.89	< .001
	HCP-REP	0.1	0.02	6.74	< .001
	HCPD	0.12	0.01	9.32	< .001
Control-C					
Limbic-B					

HCP-DISC	0.18	0.01	13.04	< .001
HCP-REP	0.19	0.01	14.69	< .001
HCPD	0.19	0.01	15.35	< .001

Note. Comparisons consist of multiple regressions, which included a network variable with two levels (the two networks under comparison), mean-centered age, sex, handedness, and mean-centered mean framewise displacement.

Supplementary Methods

This section provides additional information on estimating the quantity of data needed to generate stable individual parcellation labels, similar to the in-text analysis performed with NSAR values.

Stable Estimate Analysis for Individual Parcellation Labels

A dice coefficient (Dice, 1945; Sorenson, 1948) was calculated in order to identify parcellation label overlap between the parcellations resulting from iteration (5, 10, 15, etc. minutes) and the parcellation resulting from the independent 30 minutes of data. The dice coefficient is calculated as follows:

$$\text{Dice} = \frac{2|X \cap Y|}{|X|+|Y|}$$

where $X \cap Y$ represents the number of vertices with the same network labels in the same positions across the iteration parcellation and the independent 30 minutes parcellation. The denominator represents the total number of vertices with a given network label across both the iteration parcellation and the independent 30 minutes parcellation. Dice coefficients were also estimated for each network within each participant between each increment of data and the 30 independent minutes of data, and then an average dice coefficient for each network was computed for each increment of data.

When a single dice coefficient was calculated within individuals, only five minutes of data were needed obtain a mean dice coefficient of 0.75 (*SD* = 0.03), which was highly similar to the 0.76 mean (*SD* = 0.03) dice coefficient obtained with 30 minutes of data (see Supplementary Figure S2 Panel A). Networks with the highest mean dice coefficients include those related to sensory and somatomotor functions such as the Visual-A, Visual-B, Somatomotor-A, and Somatomotor-B networks (see Supplementary Figure S2 Panel B).

References

Dice, L. R. (1945). Measures of the Amount of Ecologic Association Between Species. *Ecology*, *26*(3), 297–302. https://doi.org/10.2307/1932409

Gordon, E. M., Laumann, T. O., Gilmore, A. W., Newbold, D. J., Greene, D. J., Berg, J. J., Ortega, M., Hoyt-Drazen, C., Gratton, C., Sun, H., Hampton, J. M., Coalson, R. S., Nguyen, A. L., McDermott, K. B., Shimony, J. S., Snyder, A. Z., Schlaggar, B. L., Petersen, S. E., Nelson, S. M., & Dosenbach, N. U. F. (2017). Precision functional mapping of individual human brains. *Neuron*, *95*(4), Art. 4. https://doi.org/10.1016/j.neuron.2017.07.011

Kong, R., Li, J., Orban, C., Sabuncu, M. R., Liu, H., Schaefer, A., Sun, N., Zuo, X.-N., Holmes, A. J., Eickhoff, S. B., & Yeo, B. T. T. (2019). Spatial topography of individual-specific cortical networks predicts human cognition, personality, and emotion. *Cerebral Cortex*, *29*(6), Art. 6. https://doi.org/10.1093/cercor/bhy123

Sorenson, T. (1948). A method of establishing groups of equal amplitude in plant sociology based on similarity of species content, and its application to analyses of the vegetation on Danish commons. *K Dan Vidensk Selsk Biol Skr*, *5*, 1–34.

Study 2: Estimating Brain Network Specialization in Autistic and Neurotypical Individuals

Abstract

Autism spectrum disorder has been characterized by disruptions in hemispheric lateralization which may be localized to language-relevant regions or be distributed pervasively. In the present study, we estimated hemispheric specialization in autism using an individual-level approach and explored potential relationships between language specialization and behavioral phenotypes including verbal ability, language delay, and autism symptom severity. We hypothesized that disruptions to hemispheric specialization in autism would be limited to the language network. We tested this and other hypotheses by employing a cross-sectional dataset of 121 individuals (48 autistic, 73 neurotypical). Using multi-echo resting-state fMRI scans, we generated individual network parcellations and estimated network specialization using a surface area-based approach. A series of multiple regressions were then used to compare network specialization for each of 17 networks between groups. Contrary to our hypothesis, we found significant group differences in specialization for the Language, Salience/Ventral Attention-A, and Control-B networks. Furthermore, we found that language delay stratified language specialization, with group differences in language specialization occurring solely between autistic individuals with language delay and neurotypical individuals. These results evidence the pervasive disruption hypothesis of atypical functional asymmetry in autism, with a differential relationship between language asymmetry and specific symptom profiles (namely, language delay) of autism.

Keywords: lateralization, specialization, asymmetry, brain networks, network specialization, neuroimaging, MRI, fMRI, autism spectrum disorder, autism, ASD, neurodevelopmental conditions

Introduction

Autism spectrum disorder (ASD) is a heterogenous neurodevelopmental condition characterized by challenges in social communication and the presence of restricted repetitive behaviors (Diagnostic and Statistical Manual-5; *Diagnostic and Statistic Manual of Mental Disorders*, 2013). As a neurodevelopmental condition, ASD is linked to atypical timelines of social, cognitive, and physiological development. Of particular historical and ongoing interest is the role that disrupted specialization may play in the development of autism.

Hemispheric specialization refers to a characteristic of brain organization in which specific functions draw on one hemisphere more than another. The resulting asymmetries reflect a dynamic trade-off between decreases in redundancy (Levy, 1969), processing speed (Ringo et al., 1994), and interhemispheric conflict in function initiation (Andrew et al., 1982; Corballis, 1991), and the loss of system redundancies and inter-hemispheric connections. When considering neurodevelopmental conditions such as ASD, the consequences of hemispheric specialization or a lack thereof become particularly relevant.

Autism research is not new to the investigation of specialization, and has historically approached specialization with a variety of methods. A dichotic listening task paradigm identified a reversal or reduction of lateralization for speech in ASD (Prior & Bradshaw, 1979). Later evidence from electroencephalography studies arrived at a similar conclusion (Cantor et al., 1986; Dawson et al., 1982, 1986, 1989). Despite evidence from these and additional studies, it is unknown if disruptions in hemispheric lateralization in autism are localized to language-relevant regions, as posited in the left hemisphere dysfunction theory of autism (McCann, 1982), or if they are more pervasive.

Current evidence surrounding this specialization debate is consistent, with findings for generally increased activity in the right hemisphere in autism (Anderson et al., 2010; Knaus et al., 2008; Takeuchi et al., 2004; Tesink et al., 2009; Wang et al., 2006), generally decreased activity in the left hemisphere (Eyler et al., 2012; Harris et al., 2006; Müller et al., 2003), both increased activity in the right hemisphere and decreased activity in the left hemisphere (Boddaert et al., 2003; Kleinhans et al., 2008; Redcay & Courchesne, 2008), and generally decreased connectivity across both hemispheres in autism (Cardinale et al., 2013). Conversely, recent evidence for specific disruptions in lateralization for regions involved in language processing in autism is compelling. For example, in a functional connectivity-based study that employed a graph analytic approach, a reduction in left lateralization was observed for several connections involving left-lateralized hubs, particularly those related to language and the default network (Nielsen et al., 2014). This was examined once more by Jouravlev et al. (2020) with a functional language task on an individual level. Within the language network, autistic participants showed less lateralized responses due to greater right hemisphere activity (Jouravlev et al., 2020). Interestingly, there was no strong difference in lateralization for the theory of mind and multiple demand networks between autistic and neurotypical (NT) participants, suggesting that differences in lateralization are constrained to language regions (Jouravlev et al., 2020).

Adding another layer to this debate is the potential role that language delay might play in stratifying disruptions in specialization in autism. Using normative modeling, one team found that language delay explained the most variance in extreme rightward deviations of laterality in autism (Floris et al., 2021). This is a promising direction, as it appears language delay is capable of parsing the heterogeneity of atypical specialization patterns in autism. Furthermore, this result points to the behavioral relevance of atypical lateralization patterns to language development in

autism. However, it is unclear as to if atypical language lateralization specifically or global alterations of lateralization are contributing to the observed language deficits (Khundrakpam et al., 2021).

The aim of the present study is to address this ongoing debate regarding the specificity of atypical lateralization patterns to language-relevant regions in autism. This was undertaken by approaching both brain network parcellations and network specialization from an individual level. The use of these individualized elements is non-trivial, since functional networks vary more by stable group and individual factors than cognitive or daily variation (Gratton et al., 2018). Furthermore, group averaging can obscure individual differences and blur functional and anatomical details—details which are potentially clinically useful (Lynch et al., 2020; Salvo et al., 2021). Thus, through the use of this individual approach, we are better positioned to capture idiosyncratic functional and anatomical details relevant to network specialization.

The present study explored four main hypotheses. First, it was hypothesized that ASD individuals would show reduced hemispheric specialization only in areas associated with language (e.g., the Language network) compared with neurotypical individuals. Second, we examined the relationships between language specialization and three behavioral phenotypes: verbal ability, autism symptom severity, and language delay. More specifically, we hypothesized a positive relationship between language specialization and verbal ability, and a negative relationship between language specialization and autism symptom severity. Finally, we hypothesized that language delay would stratify language specialization, with the greatest expected differences in specialization to occur between autistic individuals with language delay and neurotypical individuals.

Methods

Participants

A previously collected dataset was used to address these hypotheses regarding network specialization in ASD. This dataset was originally developed to understand ASD from a longitudinal perspective, and further information on participant recruitment and diagnosis can be found elsewhere (Alexander et al., 2007; Prigge et al., 2013, 2018; Zielinski et al., 2014). All data were obtained with assent and informed consent according to the University of Utah's Institutional Review Board. For the purposes of this analysis, data from collection wave five were exclusively used due to the availability of multi-echo fMRI data, which were solely acquired during this particular wave. Participants underwent two 15-minute resting-state multi-echo fMRI scans and were instructed to simply rest with their eyes open while letting their thoughts wander (King et al., 2018). Exclusion criteria for the Utah dataset included removing participants without fMRI data from wave five, participants without age data, participants older than 50 years, female participants, participants with less than 50% of volumes remaining after motion censoring, and participants with a mean framewise displacement greater than 0.2 mm and mean DVARS greater than 50. The exclusion criterion of age greater than 50 was selected due to the lack of matched controls for participants older than 50. Female participants were excluded from the analyses due to their limited representation ($N = 3$). Additional demographic information can be found in Table 1. In summary, ASD mean age was 27.22 years, range 14.67–46.42 years; NT mean age was 28.42 years, range 16.33–46.92 years; overall mean age was 27.95 years.

Table 1

Demographics

	Autism, *N* = 48		**Neurotypical, *N* = 73**		**Group Comparison**	
	Mean (SD)	Range	Mean (SD)	Range	*t*	*p*
Age at Time 5 Scan (Years)	27.22 (7.71)	14.67 – 46.42	28.42 (7.59)	16.33 – 46.92	-0.84	.4
Mean Framewise Displacement	0.09 (0.03)	0.04 – 0.19	0.08 (0.03)	0.04 – 0.16	2.26	.03
Percent Volumes Available	76.79 (15.49)	50.17 – 98.98	83.56 (12.22)	55.38 – 100	-2.55	.01
Mean Performance IQ[a]	100.07 (17.34)	65 – 131.33	116.32 (15.26)	77 – 136.33	-4.24	< .001
Mean Verbal IQ[b]	97.11 (20.64)	64.67 – 132.8	115.61 (13.73)	84 – 146.33	-4.57	< .001
Mean Full-scale IQ[c]	99.36 (16.89)	61.8 – 132.33	118.24 (14.39)	78 – 142.5	-5.14	< .001
ADOS CSS at Entry[d]	7.91 (1.89)	2 - 10	-	-	-	-
ADI-R[e]	28.2 (7.32)	12-40	-	-	-	-

Note. NT = Neurotypical

[a]Mean Performance IQ: Autism $N = 45$, Neurotypical $N=29$.

[b]Mean Verbal IQ: Autism $N = 43$, Neurotypical $N = 29$.

[c]Full-scale IQ: Autism $N = 45$, Neurotypical $N = 29$.

[d]ADOS CSS at Entry: Autism $N = 47$. ADOS CSS scores at time 5 were introduced when a participant did not have an ADOS CSS at Entry score.

[e]ADI-R: Autism $N = 44$.

Autistic participants and neurotypical participants did not significantly differ in mean age ($t(99.55) = -0.84$, $p = .4$). However, the two groups did differ in data quality ($t(93.95) = 2.26$, p

= .03) and quantity ($t(84.15) = -2.55$, $p = .01$). Furthermore, there was a significant difference between groups on available intelligence quotient (IQ) measures ($p < .001$), which were averaged within each participant if scores from multiple timepoints were available. Details regarding IQ measures in this dataset have been previously reported (Prigge et al., 2013; Zielinski et al., 2014). Using an average full-scale IQ score of 79 or lower as the criterion for low verbal and cognitive performance (Gabrielsen et al., 2018), there were five autistic participants and one neurotypical participant who met this criterion. Additionally, 40 scans came from autistic participants with high verbal and cognitive performance and 28 scans came from neurotypical participants with high verbal and cognitive performance.

Table 1 also presents the Autism Diagnostic Observation Schedule (ADOS) calibrated severity scores (CSS) at entry. The ADOS was administered by trained clinicians or research-reliable senior study staff as detailed previously (Prigge et al., 2013; Zielinski et al., 2014). The ADOS CSS scores were then calculated based on ADOS module and participant age (Gotham et al., 2009). However, ADOS CSS scores taken at time five were used when ADOS CSS at entry scores were not available, which is the case for some participants who were clinical patients of one of the senior study staff members. The ASD diagnosis of these select participants was confirmed prior to study enrollment, so the ADOS was not administered. Autism Diagnostic Interview-Revised (ADI-R) scores are also reported, and these scores act as a summary of autism severity during childhood.

Since one aim of this study is to examine the potential stratification of language specialization by language delay in autism, characteristics of autistic participants with and without language delay can be found in Table 2. In accordance with prior work (Floris et al., 2016, 2021), language delay was operationalized as having the onset of first words later than 24

months and/or having onset of first phrases later than 33 months as assessed via the ADI. These ADI items were available for 42/48 autistic participants, of which 27 met the threshold for language delay.

Table 2

Language Delay Demographics

	No Language Delay *N* = 15		**Language Delay *N* = 27**		**Group Comparison**	
	Mean (SD)	Range	Mean (SD)	Range	*t*	*p*
Age at Time 5 Scan (Years)	29.34 (7.34)	19.5 – 46.42	26.54 (8.25)	15.33 – 45.42	-1.13	.27
Mean Framewise Displacement	0.09 (0.03)	0.04 – 0.14	0.09 (0.03)	0.06 – 0.19	-0.46	.65
Percent Volumes Available	72.03 (16.23)	50.17 – 98.98	79.57 (14.38)	50.59 – 97.01	1.5	.15
Mean Performance IQ	100.09 (16.27)	73 - 128	99.65 (18.91)	65 – 131.33	-0.08	.94
Mean Verbal IQ[a]	105.93 (20.65)	63.5 – 132.8	92.29 (20.47)	54.57 – 129	-2.03	.05
Mean Full-scale IQ	104.05 (17.62)	71.67 – 132.33	86.64 (17.14)	61.8 – 130	-1.32	.19
ADOS CSS at Entry[b]	8.07 (1.71)	5 – 10	8.08 (1.62)	3 – 10	0.02	.99
ADI-R	25.47 (7.81)	12 – 38	29.63 (6.89)	15 – 40	1.72	.09

[a]Mean Verbal IQ: No Language Delay $N = 15$, Language Delay $N = 25$.

[b]ADOS CSS at Entry: No Language Delay $N = 15$, Language Delay $N = 26$. ADOS CSS scores at time 5 were introduced when a participant did not have an ADOS CSS at Entry score.

MRI Acquisition Parameters

The Utah dataset was acquired at the Utah Center for Advanced Imaging Research using a Siemens Prisma 3T MRI scanner (80 mT/m gradients) with the vendor's 64-channel head coil (see King et al., 2018; Siemens, Erlangen, Germany). Structural images were acquired with a MP2RAGE sequence with isotropic 1-mm resolution (TR = 5000 milliseconds, TE = 2.91 milliseconds, and inversion time = 700 milliseconds). Resting-state functional images were acquired with a multiband, multi-echo, echo-planar sequence (TR = 1553 milliseconds; flip angle = 65°; inplane acceleration factor = 2; fields of view = 208 mm; 72 axial slices; resolution = 2.0 mm isotropic; multiband acceleration factor = 4; partial Fourier = 6/8; bandwidth = 1850 Hz; 3 echoes with TEs of 12.4 milliseconds, 34.28 milliseconds, and 56.16 milliseconds; and effective TE spacing = 22 milliseconds).

fMRI Preprocessing

Preprocessing took place on raw NIFTI files for the resting-state fMRI runs using a pipeline developed by the Computational Brain Imaging Group (CBIG2016; Kong et al., 2019; Li et al., 2019). Briefly, preprocessing steps included surface reconstruction (using FreeSurfer 6.0.1; Dale et al., 1999), removal of the first four frames (using FSL; Jenkinson et al., 2002; Smith et al., 2004), multi-echo integration and denoising (using *tedana*; DuPre et al., 2021), structural and functional alignment using boundary-based registration (using FsFast; Greve & Fischl, 2009), linear regression using multiple nuisance regressors (using a combination of CBIG in-house scripts and the FSL MCFLIRT tool; Jenkinson et al., 2002), projection to FreeSurfer fsaverage6 surface space (using FreeSurfer's *mri_vol2surf* function), and smoothing with a 6 mm full-width half-maximum kernel (using FreeSurfer's *mri_surf2surf* function; Fischl et al., 1999). To take full advantage of the multi-echo EPI scans in this dataset, the parameters of the CBIG2016 preprocessing pipeline included *tedana* (DuPre et al., 2021). Multi-echo data are

acquired by taking three or more images per volume at echo times spanning tens of milliseconds (Posse, 2012; Posse et al., 1999). This provides two specific benefits: 1) Echoes can be integrated into a single time-series with improved BOLD contrast and less susceptibility artifact via weighted averaging, and 2) the way in which signals decay across echoes can be used to inform denoising (Lynch et al., 2021). Therefore, to take advantage of these properties, *tedana* creates a weighted sum of individual echoes and then denoises the data using a multi-echo ICA-based denoising method (DuPre et al., 2021). Additionally, as suggested by Kundu et al. (2017), bandpass filtering was not included as a preprocessing step for the multi-echo data.

Individual Network Parcellation

After the implementation of multi-echo preprocessing, network parcellations were computed using a multi-session hierarchical Bayesian modeling (MS-HBM) pipeline (Kong et al., 2019). The MS-HBM pipeline was implemented as described in Study 1 in MATLAB R2018b (MATLAB, 2018). In summary, the pipeline estimates group-level priors from a training dataset (40 Brain Genomics Superstruct Project subjects; Holmes et al., 2015; Kong et al., 2019) and applies those to estimate individual-specific parcellations. A *k* of 17 networks was selected for all subjects, following the 17-network solution found in Yeo et al. (2011). A Hungarian matching algorithm was then used to match the parcellation labels with the Yeo et al. (2011) 17-network group parcellation labels.

Network Surface Area Ratio

Following the generation of individual network parcellations, specialization was estimated using the network surface area ratio (NSAR) calculated in Connectome Workbench *wb_command* v1.5.0 (Marcus et al., 2013). This measure was previously examined for validity and reliability in Study 1 and is calculated on an individual basis for each of 17 networks. NSAR

values range from -1.0 to +1.0, with negative values indicating left hemisphere specialization for a given network while positive values indicate right hemisphere specialization. NSAR values closer to zero indicate less specialization (e.g., hemispheric symmetry).

Statistical Analysis

Group Differences Network Specialization

To verify that the NT individuals from the Utah dataset were a good reference group and could replicate previous network specialization findings using NSAR, we implemented a series of multiple regressions in the NT subset of the Utah dataset. Models consisted of NSAR values as the dependent variable with the covariates of mean-centered age and mean-centered framewise displacement. Next, to test our first hypothesis and compare hemispheric specialization between autistic and neurotypical individuals, a series of multiple regressions were used. Models consisted of NSAR values as the dependent variable, group (ASD and NT) as the independent variable, and the following covariates: mean-centered age and mean-centered mean framewise displacement. Sex was not included as a covariate since females ($N = 3$) were excluded from the analysis. Findings meeting a Bonferroni-corrected alpha level of .003 were considered significant. Effect sizes (Cohen's *d*) for any potential group differences were calculated on contrasts extracted from the corresponding multiple regression model (Nakagawa & Cuthill, 2007).

Network Specialization and Behavioral Phenotypes

To address the second hypothesis and examine the relationship between language network lateralization and verbal IQ across ASD and NT individuals, a multiple regression was used. Since the dataset examined here comes from a single wave of a longitudinal study and multiple assessments of IQ are available for many participants, available verbal IQ scores were

averaged within each participant. Covariates included mean-centered age and mean-centered mean framewise displacement. A similar analysis including language lateralization as a predictor of autism symptom severity (measured via ADOS CSS scores) was also performed.

Lastly, the potential relationship between language delay and language lateralization in ASD was investigated. For these analyses, language lateralization measured via NSAR was the dependent variable while the predictor was group (NT, ASD with language delay, and ASD without language delay), and covariates included mean-centered age and mean-centered mean framewise displacement. All statistical analyses took place in R 4.2.0 (R Core Team, 2022).

Results

Group Differences in Network Specialization

In order to validate the neurotypical group as a reference group for the group analysis, multiple regressions were used to identify significantly specialized networks, and ten networks were identified as being specialized: Visual-A, Visual-B, Language, Dorsal Attention-A, Salience/Ventral Attention-A, Control-B, Control-C, Default-A, Default-C, and Limbic-B (see Supplementary Table 1 and Supplementary Figure S1). With the exception of two networks (Visual-A and Default-A), this result aligns with that in Study 1, validating the neurotypical group as a reference group. Interestingly, the Visual-A network was also identified as being specialized across the HCP-Discovery and HCP-Replication datasets in Study 1 (see Study 1 Supplementary Table 1). Differences in results between the present neurotypical group and the results in Study 1 may stem from a variety of factors, including the type of fMRI data collected (multi-echo versus single-echo), selected covariates (handedness data were not available for the present dataset), and the quantity of available data per individual.

Next, multiple regressions were used to examine potential differences between the ASD and NT groups in specialization. No age effects on specialization were identified for any of the 17 networks. However, a significant group effect on specialization was found for three networks at the Bonferroni-corrected alpha level of 0.003: Language ($t(117) = -3.85$, $p < .001$), Salience/Ventral Attention-A ($t(117) = 3.33$, $p = .001$), and Control-B ($t(117) = 3.05$, $p = .003$). Medium effect sizes, measured via Cohen's *d,* were found for the Language ($d = -0.73$), Salience/Ventral Attention-A ($d = 0.63$), and Control-B ($d = 0.58$) networks. Network surface areas adjusted for mean-centered age and mean-centered mean framewise displacement are depicted in Figure 1, and group differences in network specialization are depicted in Figure 2.

Figure 1

Percent Surface Area for 17 Networks in ASD and NT Individuals

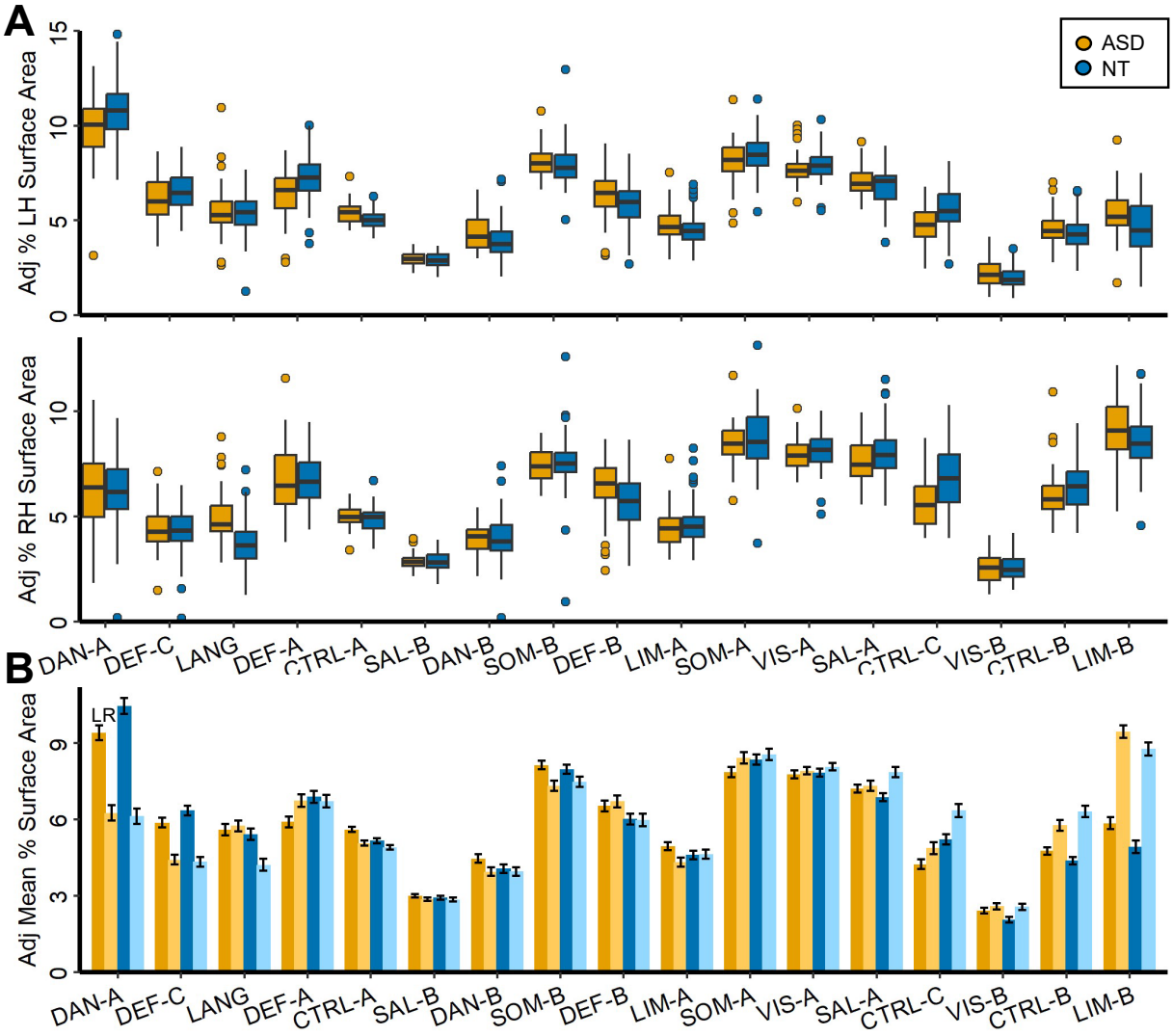

Note. Depicted in the top of Panel A is the model-adjusted percentage of the left hemisphere surface area occupied by a given specialized network. Percent surface area was adjusted using the following formula: Surface $area_{adjusted}$ = Surface $area_{raw}$ - [β_1(mean-centered age_{raw} - mean of mean-centered age_{raw}) + β_2(mean-centered FD_{raw} - mean of mean-centered FD_{raw}) + β_3($group_{raw}$ - mean $group_{raw}$)]. Depicted in the bottom portion of Panel A is the model-adjusted percentage of the right hemisphere surface area occupied by a given network. Points represent individual

outliers. Depicted in Panel B is the mean percentage of surface area occupied by a specialized network, with 95% confidence intervals. The left and right hemisphere estimates are displayed side-by-side.

Figure 2

Specialization for 17 Networks

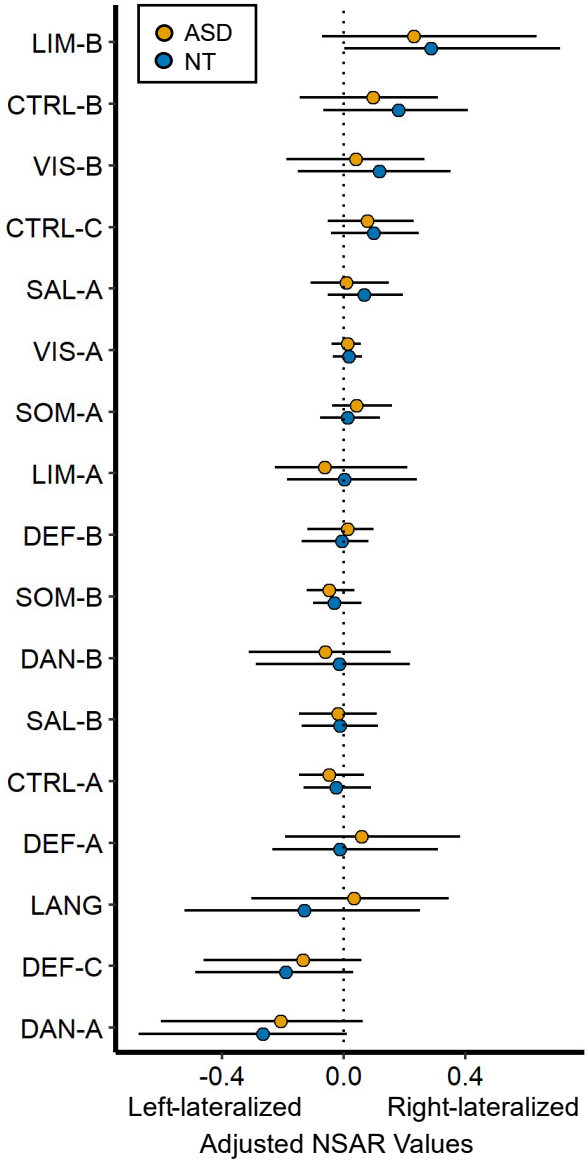

Note. On the y-axis are the 17 networks and on the x-axis are model-adjusted NSAR values, with negative values representing left hemisphere lateralization and positive values representing right

hemisphere lateralization. NSAR values were adjusted by regressing out the effects of mean-centered age and mean-centered mean framewise displacement using the following formula: $NSAR_{adjusted} = NSAR_{raw} - [\beta_1(\text{mean-centered age}_{raw} - \text{mean of mean-centered age}_{raw}) + \beta_2(\text{mean-centered FD}_{raw} - \text{mean of mean-centered FD}_{raw}) + \beta_3(\text{group}_{raw} - \text{mean group}_{raw})]$. NSAR adjustment occurred separately for each network and each group. A significant group effect on specialization was found for three networks at the Bonferroni-corrected alpha level of 0.003: Language ($t(117) = -3.85$, $p < .001$), Salience/Ventral Attention-A ($t(117) = 3.33$, $p = .001$), and Control-B ($t(117) = 3.05$, $p = .003$). Each point represents the group mean NSAR value and bars represent the 2.5 and 97.5 percentiles.

Verbal Ability, ASD Symptom Severity and Language Specialization

To examine the potential relationship between verbal ability (measured via verbal IQ and Language network specialization, a multiple regression with the covariates of mean-centered age and mean-centered mean framewise displacement was used ($N = 74$; ASD = 45, NT = 29). Language specialization was not a significant predictor of mean verbal IQ ($t(67) = .23$, $p = .82$).

Next, the relationship between language specialization and autism symptom severity (measured via ADOS CSS scores, $N = 47$ ASD) was examined using a multiple regression with the covariates of mean-centered age and mean-centered mean framewise displacement. Language specialization was not a significant predictor of ADOS CSS scores ($t(43) = 0.27$, $p = .79$).

Language Delay and Language Specialization

The potential relationship between language delay and language specialization was investigated using a multiple regression with the covariates of mean-centered age and mean-

centered mean framewise displacement. A significant group difference was found between the ASD with Language Delay and NT groups ($t(110) = 3.69$, $p < .001$, Cohen's $d = 0.79$). However, no a significant group difference was found between the ASD without Language Delay and NT groups ($t(110) = 1.78$, $p = .08$; see Figure 3). When the ASD without Language Delay was set as the reference group, no significant group difference between ASD without Language Delay and ASD with Language was found ($t(110) = 1.03$, $p = .3$).

Figure 3

Language Specialization is Stratified by Language Delay

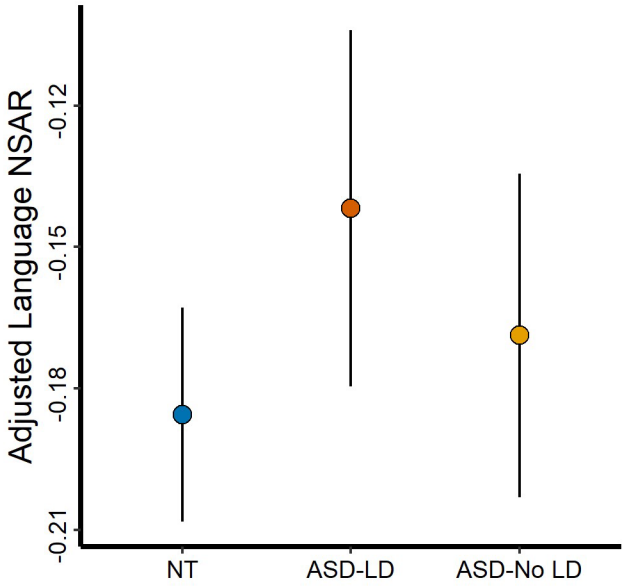

Note. Participants were binned into NT ($N = 73$), ASD with Language Delay ($N = 27$), and ASD without Language Delay ($N = 15$), with six participants missing language delay data. On the y-axis are model-adjusted NSAR values for the language network, with negative values representing left hemisphere lateralization and positive values representing right hemisphere lateralization. NSAR values were adjusted by regressing out the effects of mean-centered age and mean-centered mean framewise displacement using the following formula: $NSAR_{adjusted} =$

$NSAR_{raw}$ - [β_1(mean-centered age_{raw} - mean of mean-centered age_{raw}) + β_2(mean-centered FD_{raw} - mean of mean-centered FD_{raw}) + β_3(group$_{raw}$ - mean group$_{raw}$)]. NSAR adjustment occurred separately for each group. A significant group effect on language specialization was found between the NT and ASD Language Delay groups ($t(110) = 3.69$, $p < .001$). Circles represent group mean adjusted NSAR values while bars represent the standard error of the mean.

Discussion

In this study, we examined network specialization in autistic and neurotypical individuals using a network surface area-based approach. Inconsistent with our first hypothesis that group differences would be constrained to areas associated with language, we found group differences in specialization for the Language, Salience/Ventral Attention-A, and Control-B networks. Next, in our investigation of the relationship between behavioral phenotypes and language specialization, no significant relationships were found for verbal ability or autism symptom severity. However, language delay was a stratification marker of language specialization between the ASD with Language Delay and NT groups. This result suggests that the difference in language specialization between the ASD and NT groups identified for the first hypothesis was predominantly driven by ASD individuals with language delay. Taken as a whole, these results provide further evidence for disruptions in functional specialization in ASD, which appear to be behaviorally and clinically relevant in the case of language specialization and language delay.

Evidence for Pervasive Disruptions in Functional Specialization in ASD

Here, we identified three networks for which specialization differs between ASD and NT individuals: Language, Salience/Ventral Attention-A, and Control-B. Previously, language

regions have been identified as potential areas for disruptions in connectivity and asymmetry, leading to the postulation of the left hemisphere dysfunction theory of autism (McCann, 1982). Interestingly, the direction of group differences indicates that the language network in ASD is less asymmetrical than in NT individuals. Specifically, the mean ASD specialization value adjusted for covariates was right-lateralized (see Figure 2). This appears to be driven by an increase in language network surface area in the right hemisphere compared with the NT group (see Figure 1). Other functional work has similarly identified a rightward shift in asymmetry in autism (Anderson et al., 2010; Knaus et al., 2008; Takeuchi et al., 2004; Tesink et al., 2009; Wang et al., 2006).

Perhaps, as suggested by the expansion-fractionation-specialization hypothesis, disruptions to the fractionation or specialization of the interdigitated theory of mind and language networks may contribute to the development of autism symptoms (DiNicola & Buckner, 2021). This hypothesis suggests that as the cerebral cortex expands, certain core organizing areas act as anchors, while areas farther from these anchors self-organize into association cortex (Buckner & Krienen, 2013). These untethered association regions may exhibit a proto-organization at birth, which then fractionates and specializes through processes including competition and inherent connectivity differences. Any disruptions in the processes of expansion or fractionation may impact network specialization. Considering the interdigitated nature of functional networks, disturbances in the expansion or fractionation of one core area are likely to impact multiple networks both directly and indirectly. In the present study, we identified multiple differences in specialization across various networks in autism, which aligns with this hypothesis.

The present study also identified a decrease in specialization in the Control-B network in ASD. A mapping between resting-state functional connectivity and task activation has identified an executive control network as being associated with action–inhibition, emotion, and perception–somesthesis–pain (Smith et al., 2009). This has since been disentangled into two functional distinct control networks, which are linked to initiating and adapting control and the stable maintenance of goal-directed behavior (Dosenbach et al., 2007). In ASD specifically, prior evidence has supported disruptions in control network structure (de Lacy et al., 2017), as well as increased right-lateralization in frontoparietal network components (Cardinale et al., 2013). However, because there is no standardized network taxonomy (Uddin et al., 2023), we cannot definitively determine if the previous findings in control and frontoparietal networks directly relate to the observed specialization differences in the Control-B network in the present study.

Unexpectedly, our research revealed a decrease in lateralization within the Salience/Ventral Attention-A network in ASD compared with NT individuals. Although this outcome was surprising, it could be partly attributed to the sensitive individualized approach taken in the present study. Regardless, the salience network is thought to identify relevant stimuli from internal and external inputs in order to direct behavior and is distinct from executive control networks (Menon & Uddin, 2010; Seeley et al., 2007). Complementary in function to the salience network, the ventral attention network is involved in spatial selective attention (Corbetta & Shulman, 2011; Shulman et al., 2010). Our finding is intriguing considering that disruptions in attention are among the most frequently reported cognitive deficits in ASD (Allen & Courchesne, 2001). Neuroimaging studies have also supported this observation. Of note, Farrant & Uddin (2016) reported hyperconnectivity in the ventral and dorsal attention networks in children with ASD, while hypo-connectivity was observed in the dorsal attention network in

adults. However, the present study specifically identified decreased lateralization in the ventral attention network in ASD. Regardless, a salience network dysfunction theory of ASD has been proposed, suggesting that deviations in the salience network and anterior insula in particular may contribute to social communication and theory of mind deficits in ASD (Toyomaki & Murohashi, 2013; Uddin & Menon, 2009).

Language Delay as a Stratification Marker for ASD

The present study identified a significant difference in language specialization between NT and ASD with Language Delay individuals, similar to a previous study which found that language delay explained the most variance in extreme rightward deviations of laterality in autism (Floris et al., 2021). This finding is particularly remarkable considering the disparities in datasets and modeling techniques between this study and that of Floris et al. (2021). In the prior study, gray matter voxels were the subject of laterality, as opposed to functional connectivity-derived language network surface area. Additionally, significant group differences were identified using individual deviations from a normative pattern of brain laterality across development rather than from group mean comparisons. Another challenge, highlighted by Marek et al. (2022) and Liu et al. (2023), is the difficulty of establishing connections between scanner-derived data (such as functional connectivity) and out-of-scanner behavioral measures. This is of particular concern with the use of the ADI for determining language delay, since this measure is retrospective and susceptible to memory errors such as telescoping (Hus et al., 2011). Thus, there is a clear need for prospective investigations of the relationship between language delay and language specialization.

Regardless of these challenges, the causal direction and origins of the relationship between language delay in ASD and language specialization remain unknown. Bishop (2013)

proposed several explanations for these disruptions. It was suggested that genetic risk may lead to language impairment, subsequently resulting in weak laterality (the neuroplasticity model). Alternatively, genetic risk might independently cause weak laterality and language impairment (the pleiotropy model), or weak laterality caused by genetic risk could subsequently lead to language impairment (the endophenotype model). Evidence from Nielsen et al. (2014) suggests that deficits in language development may result in the abnormal language lateralization observed in ASD. This is supported by several pieces of evidence observed in the present study as well as in Studies 1 and 3. Notably, no consistent age-related effects on specialization were found in Studies 1 and 3, and the present study evidenced no direct relationship between language specialization and verbal ability. However, language delay was found to act as a stratification marker for language specialization. Together, this suggests that disruptions in language specialization occurring early in development (likely *in utero* or shortly after birth), could underlie the differences in language specialization observed in autism.

Limitations and Future Directions

Network specialization in this study was examined through the use of NSAR, which has previously been established as a reliable measure (see Study 1). However, this measure is derived by generating individual parcellations using functional connectivity, and then calculating the ratio of left and right hemisphere surface areas for each network. Thus, rather than using a language localizer task to determine network boundaries (unavailable with this dataset), this measure is indirectly reliant upon functional connectivity. This is an important limitation since functional connectivity is not necessarily reflective of underlying anatomical connectivity, and may instead better reflect brain geometry (Pang et al., 2023). Furthermore, NSAR is one of many

available measures of functional asymmetry, and it is unknown if the present results can be reproduced using other measures.

Moreover, it should be noted that the dataset chosen for this study has certain characteristics which restrict the generalizability of our findings. First, the participant sample consisted entirely of males, which restricts the applicability of our results to females with ASD and may overlook potential sex differences. Additionally, the relatively small sample size and the overwhelming representation of high verbal and cognitive performance individuals within the dataset further impact the generalizability of our findings.

Further investigations should focus on replicating these findings in larger and more diverse samples, as well as exploring the longitudinal trajectories of network specialization in individuals with ASD. Additionally, the incorporation of multimodal neuroimaging techniques could provide a more comprehensive understanding of the relationship between language network specialization and language delay in ASD.

Conclusions

In this study, we examined network specialization in ASD and NT individuals using an individual-level approach based on participant network parcellations. Inconsistent with our hypothesis that group differences in specialization would be constrained to language-relevant regions, we identified group differences in specialization for the Language, Salience/Ventral Attention-A, and Control-B networks. Additionally, we hypothesized that language delay would stratify language specialization, such that the greatest group differences would be found between the NT and ASD with Language Delay groups. Support for this hypothesis was found, suggesting that language specialization is behaviorally and clinically relevant to autism.

Acknowledgements

We thank former members of the Utah Autism CPEA for their assistance during the early stages of this project. We sincerely thank the children, adolescents, and adults with autism and the individuals with typical development who participated in this study, and their families. The Utah dataset was collected with support by the National Institute of Mental Health of the National Institutes of Health under Award Numbers R01MH080826 and K08 MH100609. Furthermore, we acknowledge the support of the Office of Research Computing at Brigham Young University.

References

Alexander, A. L., Lee, J. E., Lazar, M., Boudos, R., DuBray, M. B., Oakes, T. R., Miller, J. N., Lu, J., Jeong, E.-K., McMahon, W. M., Bigler, E. D., & Lainhart, J. E. (2007). Diffusion tensor imaging of the corpus callosum in autism. *NeuroImage*, *34*(1), 61–73. https://doi.org/10.1016/j.neuroimage.2006.08.032

Allen, G., & Courchesne, E. (2001). Attention function and dysfunction in autism. *Frontiers in Bioscience-Landmark*, *6*(3), Art. 3. https://doi.org/10.2741/allen

Anderson, J. S., Lange, N., Froehlich, A., DuBray, M. B., Druzgal, T. J., Froimowitz, M. P., Alexander, A. L., Bigler, E. D., & Lainhart, J. E. (2010). Decreased left posterior insular activity during auditory language in autism. *American Journal of Neuroradiology*, *31*(1), 131–139.

Andrew, R., Mench, J., & Rainey, C. (1982). Right-left asymmetry of response to visual stimuli in the domestic chick. *Analysis of Visual Behaviour*, 197–209.

Bishop, D. V. M. (2013). Cerebral asymmetry and language development: Cause, correlate, or consequence? *Science*, *340*(6138), 1230531. https://doi.org/10.1126/science.1230531

Boddaert, N., Belin, P., Chabane, N., Poline, J.-B., Barthélémy, C., Mouren-Simeoni, M.-C., Brunelle, F., Samson, Y., & Zilbovicius, M. (2003). Perception of complex sounds: Abnormal pattern of cortical activation in autism. *American Journal of Psychiatry*, *160*(11), 2057–2060.

Buckner, R. L., & Krienen, F. M. (2013). The evolution of distributed association networks in the human brain. *Trends in Cognitive Sciences*, *17*(12), 648–665. https://doi.org/10.1016/j.tics.2013.09.017

Cantor, D. S., Thatcher, R. W., Hrybyk, M., & Kaye, H. (1986). Computerized EEG analyses of autistic children. *Journal of Autism and Developmental Disorders*, *16*(2), 169–187. https://doi.org/10.1007/BF01531728

Cardinale, R. C., Shih, P., Fishman, I., Ford, L. M., & Müller, R.-A. (2013). Pervasive rightward asymmetry shifts of functional networks in Autism Spectrum Disorder. *JAMA Psychiatry*, *70*(9), 975–982. https://doi.org/10.1001/jamapsychiatry.2013.382

Corballis, M. C. (1991). *The lopsided ape: Evolution of the generative mind.* (pp. vii, 366). Oxford University Press.

Corbetta, M., & Shulman, G. L. (2011). Spatial neglect and attention networks. *Annual Review of Neuroscience*, *34*(1), 569–599. https://doi.org/10.1146/annurev-neuro-061010-113731

Dale, A. M., Fischl, B., & Sereno, M. I. (1999). Cortical surface-based analysis: I. Segmentation and surface reconstruction. *NeuroImage*, *9*(2), 179–194. https://doi.org/10.1006/nimg.1998.0395

Dawson, G., Finley, C., Phillips, S., & Galpert, L. (1986). Hemispheric specialization and the language abilities of autistic children. *Child Development*, *57*(6), 1440–1453. https://doi.org/10.2307/1130422

Dawson, G., Finley, C., Phillips, S., & Lewy, A. (1989). A comparison of hemispheric asymmetries in speech-related brain potentials of autistic and dysphasic children. *Brain and Language*, *37*(1), 26–41. https://doi.org/10.1016/0093-934X(89)90099-0

Dawson, G., Warrenburg, S., & Fuller, P. (1982). Cerebral lateralization in individuals diagnosed as autistic in early childhood. *Brain and Language*, *15*(2), 353–368. https://doi.org/10.1016/0093-934X(82)90065-7

de Lacy, N., Doherty, D., King, B. H., Rachakonda, S., & Calhoun, V. D. (2017). Disruption to control network function correlates with altered dynamic connectivity in the wider autism spectrum. *NeuroImage: Clinical*, *15*, 513–524. https://doi.org/10.1016/j.nicl.2017.05.024

Diagnostic and Statistic Manual of Mental Disorders (5th ed.). (2013). American Psychiatric Association.

DiNicola, L. M., & Buckner, R. L. (2021). Precision estimates of parallel distributed association networks: Evidence for domain specialization and implications for evolution and development. *Current Opinion in Behavioral Sciences*, *40*, 120–129. https://doi.org/10.1016/j.cobeha.2021.03.029

Dosenbach, N. U. F., Fair, D. A., Miezin, F. M., Cohen, A. L., Wenger, K. K., Dosenbach, R. A. T., Fox, M. D., Snyder, A. Z., Vincent, J. L., Raichle, M. E., Schlaggar, B. L., & Petersen, S. E. (2007). Distinct brain networks for adaptive and stable task control in humans. *Proceedings of the National Academy of Sciences*, *104*(26), 11073–11078. https://doi.org/10.1073/pnas.0704320104

DuPre, E., Salo, T., Ahmed, Z., Bandettini, P. A., Bottenhorn, K. L., Caballero-Gaudes, C., Dowdle, L. T., Gonzalez-Castillo, J., Heunis, S., Kundu, P., Laird, A. R., Markello, R., Markiewicz, C. J., Moia, S., Staden, I., Teves, J. B., Uruñuela, E., Vaziri-Pashkam, M., Whitaker, K., & Handwerker, D. A. (2021). TE-dependent analysis of multi-echo fMRI with tedana. *Journal of Open Source Software*, *6*(66), 3669. https://doi.org/10.21105/joss.03669

Eyler, L. T., Pierce, K., & Courchesne, E. (2012). A failure of left temporal cortex to specialize for language is an early emerging and fundamental property of autism. *Brain*, *135*(3), 949–960.

Farrant, K., & Uddin, L. Q. (2016). Atypical developmental of dorsal and ventral attention networks in autism. *Developmental Science*, *19*(4), 550–563. https://doi.org/10.1111/desc.12359

Fischl, B., Sereno, M. I., Tootell, R. B. H., & Dale, A. M. (1999). High-resolution intersubject averaging and a coordinate system for the cortical surface. *Human Brain Mapping*, *8*(4), 272–284. https://doi.org/10.1002/(SICI)1097-0193(1999)8:4<272::AID-HBM10>3.0.CO;2-4

Floris, D. L., Lai, M.-C., Auer, T., Lombardo, M. V., Ecker, C., Chakrabarti, B., Wheelwright, S. J., Bullmore, E. T., Murphy, D. G. M., Baron-Cohen, S., & Suckling, J. (2016). Atypically rightward cerebral asymmetry in male adults with autism stratifies individuals with and without language delay. *Human Brain Mapping*, *37*(1), 230–253. https://doi.org/10.1002/hbm.23023

Floris, D. L., Wolfers, T., Zabihi, M., Holz, N. E., Zwiers, M. P., Charman, T., Tillmann, J., Ecker, C., Dell'Acqua, F., Banaschewski, T., Moessnang, C., Baron-Cohen, S., Holt, R., Durston, S., Loth, E., Murphy, D. G. M., Marquand, A., Buitelaar, J. K., Beckmann, C. F., … Zwiers, M. P. (2021). Atypical brain asymmetry in autism—A candidate for clinically meaningful stratification. *Biological Psychiatry: Cognitive Neuroscience and Neuroimaging*, *6*(8), 802–812. https://doi.org/10.1016/j.bpsc.2020.08.008

Gabrielsen, T. P., Anderson, J. S., Stephenson, K. G., Beck, J., King, J. B., Kellems, R., Top, D. N., Russell, N. C. C., Anderberg, E., Lundwall, R. A., Hansen, B., & South, M. (2018). Functional MRI connectivity of children with autism and low verbal and cognitive performance. *Molecular Autism*, *9*(1), 67. https://doi.org/10.1186/s13229-018-0248-y

Gotham, K., Pickles, A., & Lord, C. (2009). Standardizing ADOS Scores for a Measure of Severity in Autism Spectrum Disorders. *Journal of Autism and Developmental Disorders*, *39*(5), 693–705. https://doi.org/10.1007/s10803-008-0674-3

Gratton, C., Laumann, T. O., Nielsen, A. N., Greene, D. J., Gordon, E. M., Gilmore, A. W., Nelson, S. M., Coalson, R. S., Snyder, A. Z., Schlaggar, B. L., Dosenbach, N. U. F., & Petersen, S. E. (2018). Functional brain networks are dominated by stable group and individual factors, not cognitive or daily variation. *Neuron*, *98*(2), 439-452.e5. https://doi.org/10.1016/j.neuron.2018.03.035

Greve, D. N., & Fischl, B. (2009). Accurate and robust brain image alignment using boundary-based registration. *NeuroImage*, *48*(1), 63–72. https://doi.org/10.1016/j.neuroimage.2009.06.060

Harris, G. J., Chabris, C. F., Clark, J., Urban, T., Aharon, I., Steele, S., McGrath, L., Condouris, K., & Tager-Flusberg, H. (2006). Brain activation during semantic processing in autism spectrum disorders via functional magnetic resonance imaging. *Brain and Cognition*, *61*(1), 54–68. https://doi.org/10.1016/j.bandc.2005.12.015

Holmes, A. J., Hollinshead, M. O., O'Keefe, T. M., Petrov, V. I., Fariello, G. R., Wald, L. L., Fischl, B., Rosen, B. R., Mair, R. W., Roffman, J. L., Smoller, J. W., & Buckner, R. L. (2015). Brain Genomics Superstruct Project initial data release with structural, functional, and behavioral measures. *Scientific Data*, *2*(1), Art. 1. https://doi.org/10.1038/sdata.2015.31

Hus, V., Taylor, A., & Lord, C. (2011). Telescoping of caregiver report on the Autism Diagnostic Interview – Revised. *Journal of Child Psychology and Psychiatry*, *52*(7), 753–760. https://doi.org/10.1111/j.1469-7610.2011.02398.x

Jenkinson, M., Bannister, P., Brady, M., & Smith, S. M. (2002). Improved optimization for the robust and accurate linear registration and motion correction of brain images. *NeuroImage*, *17*(2), 825–841. https://doi.org/10.1006/nimg.2002.1132

Jouravlev, O., Kell, A. J. E., Mineroff, Z., Haskins, A. J., Ayyash, D., Kanwisher, N., & Fedorenko, E. (2020). Reduced language lateralization in autism and the broader autism phenotype as assessed with robust individual-subjects analyses. *Autism Research*, *13*(10), 1746–1761. https://doi.org/10.1002/aur.2393

Khundrakpam, B., Tuerk, C., & Booij, L. (2021). Understanding heterogeneity in Autism Spectrum Disorder: A methodological shift in neuroimaging research from investigating group differences to individual differences. *Biological Psychiatry: Cognitive Neuroscience and Neuroimaging*, *6*(8), 762–764. https://doi.org/10.1016/j.bpsc.2021.04.004

King, J. B., Prigge, M. B. D., King, C. K., Morgan, J., Dean, D. C., III, Freeman, A., Villaruz, J. A. M., Kane, K. L., Bigler, E. D., Alexander, A. L., Lange, N., Zielinski, B. A., Lainhart, J. E., & Anderson, J. S. (2018). Evaluation of differences in temporal synchrony between brain regions in individuals with autism and typical development. *JAMA Network Open*, *1*(7), e184777. https://doi.org/10.1001/jamanetworkopen.2018.4777

Kleinhans, N. M., Müller, R.-A., Cohen, D. N., & Courchesne, E. (2008). Atypical functional lateralization of language in autism spectrum disorders. *Brain Research*, *1221*, 115–125. https://doi.org/10.1016/j.brainres.2008.04.080

Knaus, T. A., Silver, A. M., Lindgren, K. A., Hadjikhani, N., & Tager-Flusberg, H. (2008). FMRI activation during a language task in adolescents with ASD. *Journal of the*

International Neuropsychological Society, *14*(6), 967–979. https://doi.org/10.1017/S1355617708081216

Kong, R., Li, J., Orban, C., Sabuncu, M. R., Liu, H., Schaefer, A., Sun, N., Zuo, X.-N., Holmes, A. J., Eickhoff, S. B., & Yeo, B. T. T. (2019). Spatial topography of individual-specific cortical networks predicts human cognition, personality, and emotion. *Cerebral Cortex*, *29*(6), Art. 6. https://doi.org/10.1093/cercor/bhy123

Kundu, P., Voon, V., Balchandani, P., Lombardo, M. V., Poser, B. A., & Bandettini, P. A. (2017). Multi-echo fMRI: A review of applications in fMRI denoising and analysis of BOLD signals. *Neuroimage*, *154*, 59–80.

Levy, J. (1969). Possible basis for the evolution of lateral specialization of the human brain. *Nature*, *224*(5219), Art. 5219. https://doi.org/10.1038/224614a0

Li, J., Kong, R., Liégeois, R., Orban, C., Tan, Y., Sun, N., Holmes, A. J., Sabuncu, M. R., Ge, T., & Yeo, B. T. T. (2019). Global signal regression strengthens association between resting-state functional connectivity and behavior. *NeuroImage*, *196*, 126–141. https://doi.org/10.1016/j.neuroimage.2019.04.016

Liu, S., Abdellaoui, A., Verweij, K. J. H., & van Wingen, G. A. (2023). Replicable brain–phenotype associations require large-scale neuroimaging data. *Nature Human Behaviour*, 1–13. https://doi.org/10.1038/s41562-023-01642-5

Lynch, C. J., Elbau, I., & Liston, C. (2021). Improving precision functional mapping routines with multi-echo fMRI. *Current Opinion in Behavioral Sciences*, *40*, 113–119. https://doi.org/10.1016/j.cobeha.2021.03.017

Lynch, C. J., Power, J. D., Scult, M. A., Dubin, M., Gunning, F. M., & Liston, C. (2020). Rapid precision functional mapping of individuals using multi-echo fMRI. *Cell Reports*, *33*(12), 108540. https://doi.org/10.1016/j.celrep.2020.108540

Marcus, D. S., Harms, M. P., Snyder, A. Z., Jenkinson, M., Wilson, J. A., Glasser, M. F., Barch, D. M., Archie, K. A., Burgess, G. C., Ramaratnam, M., Hodge, M., Horton, W., Herrick, R., Olsen, T., McKay, M., House, M., Hileman, M., Reid, E., Harwell, J., … Van Essen, D. C. (2013). Human Connectome Project informatics: Quality control, database services, and data visualization. *NeuroImage*, *80*, 202–219. https://doi.org/10.1016/j.neuroimage.2013.05.077

Marek, S., Tervo-Clemmens, B., Calabro, F. J., Montez, D. F., Kay, B. P., Hatoum, A. S., Donohue, M. R., Foran, W., Miller, R. L., Hendrickson, T. J., Malone, S. M., Kandala, S., Feczko, E., Miranda-Dominguez, O., Graham, A. M., Earl, E. A., Perrone, A. J., Cordova, M., Doyle, O., … Dosenbach, N. U. F. (2022). Reproducible brain-wide association studies require thousands of individuals. *Nature*, *603*(7902), Art. 7902. https://doi.org/10.1038/s41586-022-04492-9

MATLAB. (2018). *9.5.0.944444 (R2018b)*. The MathWorks Inc.

McCann, B. S. (1982). Hemispheric asymmetries and early infantile autism. *Journal of Autism and Developmental Disorders*, *11*(4), 401–411. https://doi.org/10.1007/BF01531615

Menon, V., & Uddin, L. Q. (2010). Saliency, switching, attention and control: A network model of insula function. *Brain Structure and Function*, *214*(5), 655–667. https://doi.org/10.1007/s00429-010-0262-0

Müller, R.-A., Kleinhans, N., Kemmotsu, N., Pierce, K., & Courchesne, E. (2003). Abnormal variability and distribution of functional maps in autism: An fMRI study of visuomotor

learning. *American Journal of Psychiatry*, *160*(10), 1847–1862. https://doi.org/10.1176/appi.ajp.160.10.1847

Nakagawa, S., & Cuthill, I. C. (2007). Effect size, confidence interval and statistical significance: A practical guide for biologists. *Biological Reviews*, *82*(4), 591–605. https://doi.org/10.1111/j.1469-185X.2007.00027.x

Nielsen, J. A., Zielinski, B. A., Fletcher, P. T., Alexander, A. L., Lange, N., Bigler, E. D., Lainhart, J. E., & Anderson, J. S. (2014). Abnormal lateralization of functional connectivity between language and default mode regions in autism. *Molecular Autism*, *5*(1), 8. https://doi.org/10.1186/2040-2392-5-8

Pang, J. C., Aquino, K. M., Oldehinkel, M., Robinson, P. A., Fulcher, B. D., Breakspear, M., & Fornito, A. (2023). Geometric constraints on human brain function. *Nature*, 1–9. https://doi.org/10.1038/s41586-023-06098-1

Posse, S. (2012). Multi-echo acquisition. *NeuroImage*, *62*(2), 665–671. https://doi.org/10.1016/j.neuroimage.2011.10.057

Posse, S., Wiese, S., Gembris, D., Mathiak, K., Kessler, C., Grosse-Ruyken, M.-L., Elghahwagi, B., Richards, T., Dager, S. R., & Kiselev, V. G. (1999). Enhancement of BOLD-contrast sensitivity by single-shot multi-echo functional MR imaging. *Magnetic Resonance in Medicine*, *42*(1), 87–97. https://doi.org/10.1002/(SICI)1522-2594(199907)42:1<87::AID-MRM13>3.0.CO;2-O

Prigge, M. B. D., Bigler, E. D., Fletcher, P. T., Zielinski, B. A., Ravichandran, C., Anderson, J., Froehlich, A., Abildskov, T., Papadopolous, E., Maasberg, K., Nielsen, J. A., Alexander, A. L., Lange, N., & Lainhart, J. (2013). Longitudinal Heschl's gyrus growth during

childhood and adolescence in typical development and autism. *Autism Research*, *6*(2), 78–90. https://doi.org/10.1002/aur.1265

Prigge, M. B. D., Bigler, E. D., Travers, B. G., Froehlich, A., Abildskov, T., Anderson, J. S., Alexander, A. L., Lange, N., Lainhart, J. E., & Zielinski, B. A. (2018). Social Responsiveness Scale (SRS) in relation to longitudinal cortical thickness changes in Autism Spectrum Disorder. *Journal of Autism and Developmental Disorders*, *48*(10), Art. 10. https://doi.org/10.1007/s10803-018-3566-1

Prior, M. R., & Bradshaw, J. L. (1979). Hemisphere functioning in Autistic Children. *Cortex*, *15*(1), 73–81. https://doi.org/10.1016/S0010-9452(79)80008-8

R Core Team. (2022). *R: A Language and Environment for Statistical Computing*. R Foundation for Statistical Computing. https://www.R-project.org/

Redcay, E., & Courchesne, E. (2008). Deviant functional magnetic resonance imaging patterns of brain activity to speech in 2–3-year-old children with autism spectrum disorder. *Biological Psychiatry*, *64*(7), 589–598.

Ringo, J. L., Doty, R. W., Demeter, S., & Simard, P. Y. (1994). Time is of the essence: A conjecture that hemispheric specialization arises from interhemispheric conduction delay. *Cerebral Cortex*, *4*(4), 331–343. https://doi.org/10.1093/cercor/4.4.331

Salvo, J. J., Holubecki, A. M., & Braga, R. M. (2021). Correspondence between functional connectivity and task-related activity patterns within the individual. *Current Opinion in Behavioral Sciences*, *40*, 178–188. https://doi.org/10.1016/j.cobeha.2021.05.003

Seeley, W. W., Menon, V., Schatzberg, A. F., Keller, J., Glover, G. H., Kenna, H., Reiss, A. L., & Greicius, M. D. (2007). Dissociable intrinsic connectivity networks for salience

processing and executive control. *Journal of Neuroscience*, *27*(9), 2349–2356. https://doi.org/10.1523/JNEUROSCI.5587-06.2007

Shulman, G. L., Pope, D. L., Astafiev, S. V., McAvoy, M. P., Snyder, A. Z., & Corbetta, M. (2010). Right hemisphere dominance during spatial selective attention and target detection occurs outside the dorsal frontoparietal network. *Journal of Neuroscience*, *30*(10), 3640–3651.

Smith, S. M., Fox, P. T., Miller, K. L., Glahn, D. C., Fox, P. M., Mackay, C. E., Filippini, N., Watkins, K. E., Toro, R., Laird, A. R., & Beckmann, C. F. (2009). Correspondence of the brain's functional architecture during activation and rest. *Proceedings of the National Academy of Sciences*, *106*(31), 13040–13045. https://doi.org/10.1073/pnas.0905267106

Smith, S. M., Jenkinson, M., Woolrich, M. W., Beckmann, C. F., Behrens, T. E. J., Johansen-Berg, H., Bannister, P. R., De Luca, M., Drobnjak, I., Flitney, D. E., Niazy, R. K., Saunders, J., Vickers, J., Zhang, Y., De Stefano, N., Brady, J. M., & Matthews, P. M. (2004). Advances in functional and structural MR image analysis and implementation as FSL. *NeuroImage*, *23*, S208–S219. https://doi.org/10.1016/j.neuroimage.2004.07.051

Takeuchi, M., Harada, M., Matsuzaki, K., Nishitani, H., & Mori, K. (2004). Difference of signal change by a language task on autistic patients using functional MRI. *The Journal of Medical Investigation*, *51*(1,2), 59–62. https://doi.org/10.2152/jmi.51.59

Tesink, C. M., Buitelaar, J. K., Petersson, K. M., van der Gaag, R. J., Kan, C. C., Tendolkar, I., & Hagoort, P. (2009). Neural correlates of pragmatic language comprehension in autism spectrum disorders. *Brain*, *132*(7), 1941–1952.

Toyomaki, A., & Murohashi, H. (2013). “Salience network” dysfunction hypothesis in autism spectrum disorders. *Japanese Psychological Research*, *55*(2), 175–185. https://doi.org/10.1111/jpr.12012

Uddin, L. Q., Betzel, R. F., Cohen, J. R., Damoiseaux, J. S., De Brigard, F., Eickhoff, S. B., Fornito, A., Gratton, C., Gordon, E. M., Laird, A. R., Larson-Prior, L., McIntosh, A. R., Nickerson, L. D., Pessoa, L., Pinho, A. L., Poldrack, R. A., Razi, A., Sadaghiani, S., Shine, J. M., … Spreng, R. N. (2023). Controversies and progress on standardization of large-scale brain network nomenclature. *Network Neuroscience*, 1–42. https://doi.org/10.1162/netn_a_00323

Uddin, L. Q., & Menon, V. (2009). The anterior insula in autism: Under-connected and under-examined. *Neuroscience & Biobehavioral Reviews*, *33*(8), 1198–1203. https://doi.org/10.1016/j.neubiorev.2009.06.002

Wang, A. T., Lee, S. S., Sigman, M., & Dapretto, M. (2006). Neural basis of irony comprehension in children with autism: The role of prosody and context. *Brain*, *129*(4), 932–943.

Yeo, B. T. T., Krienen, F. M., Sepulcre, J., Sabuncu, M. R., Lashkari, D., Hollinshead, M., Roffman, J. L., Smoller, J. W., Zöllei, L., Polimeni, J. R., Fischl, B., Liu, H., & Buckner, R. L. (2011). The organization of the human cerebral cortex estimated by intrinsic functional connectivity. *Journal of Neurophysiology*, *106*(3), 1125–1165. https://doi.org/10.1152/jn.00338.2011

Zielinski, B. A., Prigge, M. B. D., Nielsen, J. A., Froehlich, A. L., Abildskov, T. J., Anderson, J. S., Fletcher, P. T., Zygmunt, K. M., Travers, B. G., Lange, N., Alexander, A. L., Bigler,

E. D., & Lainhart, J. E. (2014). Longitudinal changes in cortical thickness in autism and typical development. *Brain*, *137*(6), 1799–1812. https://doi.org/10.1093/brain/awu083

Study 2 Supplementary Materials

Supplementary Table 1

Identifying Specialized Networks Using Multiple Regressions in Neurotypical Individuals (N = 73)

Network Intercept	β	*SE*	*t*	*p*
Visual-A	0.02	0.00	5.12	< .001
Visual-B	0.14	0.01	10.19	< .001
Somatomotor-A	0.00	0.01	0.18	.86
Somatomotor-B	-0.03	0.01	-1.99	.05
Language	-0.19	0.02	-7.96	< .001
Dorsal Attention-A	-0.28	0.02	-15.43	< .001
Dorsal Attention-B	0.00	0.02	0.06	.95
Salience/VenAttn-A	0.09	0.01	9.01	< .001
Salience/VenAttn-B	-0.01	0.01	-1.17	.25
Control-A	-0.02	0.01	-2.36	0.02
Control-B	0.21	0.01	14.58	< .001
Control-C	0.10	0.01	9.77	< .001
Default-A	-0.03	0.01	-3.03	.003
Default-B	-0.01	0.01	-2.15	0.04
Default-C	-0.21	0.02	-11.77	< .001
Limbic-A	0.02	0.01	2.12	0.04
Limbic-B	0.31	0.02	15.20	< .001

Note: Coefficients and *p*-values for the intercept are shown. Networks with significant (Bonferroni-corrected alpha level of .003) intercepts are bolded.

Figure S1

Specialized Networks in Neurotypical Individuals

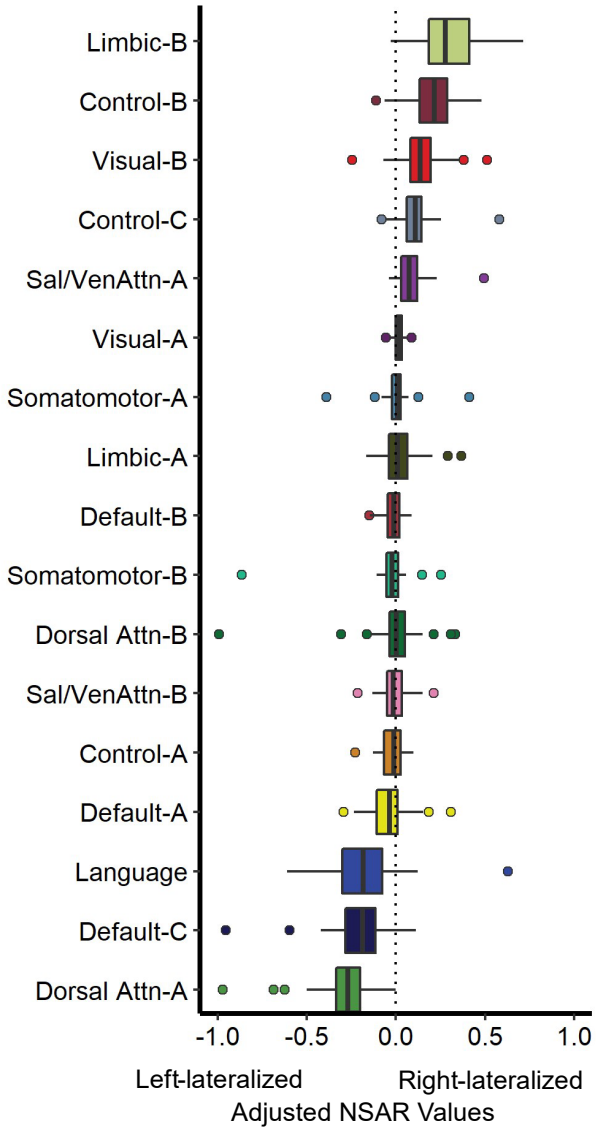

Note. On the y-axis are the 17 networks and on the x-axis are model-adjusted NSAR values, with negative values representing left hemisphere lateralization and positive values representing right hemisphere lateralization. NSAR values were adjusted by regressing out the effects of mean-centered age and mean-centered mean framewise displacement using the following formula: $NSAR_{adjusted} = NSAR_{raw} - [\beta_1(\text{mean-centered age}_{raw} - \text{mean of mean-centered age}_{raw}) + \beta_2(\text{mean-centered FD}_{raw} - \text{mean of mean-centered FD}_{raw})]$. NSAR adjustment occurred separately for each

network. Ten networks were found to be significantly specialized: Visual-A, Visual-B, Language, Dorsal Attention-A, Salience/Ventral Attention-A, Control-B, Control-C, Default-A, Default-C, and Limbic-B.

Study 3: Parsing Brain Network Specialization: A Replication and Expansion of Wang et al. (2014)

Abstract

One organizing principle of brain function is specialization, or the dominance of a specific function in one hemisphere or another. Previously, Wang et al. (2014) identified networks associated with language and visuospatial attention as being specialized to the left and right hemispheres, respectively; and a dual-specialization of the frontoparietal network. However, it remains unknown which networks are specialized when specialization is examined within individuals using a higher resolution parcellation, as well as which connections are contributing the most to a given network's specialization. In the present study, we estimated network specialization across three datasets using the autonomy index and a novel method of deconstructing network specialization. After examining the reliability of these methods as implemented on an individual level, we addressed two hypotheses. First, we hypothesized that the most specialized networks would include those associated with language, visuospatial, and executive control. Second, we hypothesized that within-network contributions to specialization would follow one of three outcomes: a within-between network gradient, a specialization gradient, or a sensorimotor-association gradient. Interestingly, we found that the majority of networks exhibited greater within-hemisphere connectivity than between-hemisphere connectivity. Additionally, we found that the greatest network contributions were within-network, followed by those from specialized networks.

Keywords: lateralization, specialization, asymmetry, autonomy index, brain networks, network specialization, neuroimaging, MRI, fMRI

Introduction

Hemispheric specialization refers to a characteristic of brain organization in which specific functions draw on one hemisphere of the brain more than the other. These functional asymmetries give rise to reductions in redundancy (Levy, 1969), processing speed (Ringo et al., 1994), and interhemispheric conflict in function initiation (Andrew et al., 1982; Corballis, 1991). Importantly, disruptions to hemispheric specialization can have significant clinical implications, particularly in the context of neurodevelopmental and psychiatric conditions (X.-Z. Kong et al., 2022).

Methods of Estimating Hemispheric Specialization

Measures of hemispheric specialization have previously ranged from the examination of split-brain patients (for review, see Gazzaniga, 2000) and brain lesions (Milner, 1971; Rasmussen & Milner, 1977) to the Wada test (Wada & Rasmussen, 1960) and intraoperative brain stimulation mapping (Penfield & Jasper, 1954). With the advent and development of functional neuroimaging, these methods now include many functional connectivity-based metrics. One such measure is the intrinsic laterality index (Liu et al., 2009), which quantifies within- versus between-hemisphere connectivity. Another includes the hemispheric contrast (Gotts et al., 2013), which examines node interactions between the two hemispheres through cl "segregation" (highly within-hemisphere interactions) versus "integration" (highly between-hemisphere interactions). Similarly, the autonomy index (Wang et al., 2014) captures a normalized ratio of within- versus between-hemisphere connectivity on the vertex level. Taking a different approach, a classification metric (Friedrich et al., 2022) identifies the "classifiability" of each hemisphere and determines which areas are necessary to accurately classify the left and right hemispheres. Also of interest, a network variants approach (Perez et al., 2023) was recently

applied to hemispheric specialization, examining inter-individual variability in network organization between the two hemispheres.

Using the autonomy index, Wang et al. (2014) quantified specialization across seven functional networks and found that specialization was not restricted to a single left- or right-specialized network (Wang et al., 2014). Rather, the right frontoparietal network and right ventral and dorsal attention networks, as well as the left default and frontoparietal networks exhibited high degrees of specialization (see Fig. 5; Wang et al., 2014). Interestingly, the dual specialization of the frontoparietal control network evidences a joint coupling of executive control functions with a distinct pattern of networks in either hemisphere (Wang et al., 2014).While this and other studies have made significant contributions, much of what is known regarding hemispheric specialization has been derived from group-level analyses, an approach which is increasingly being exchanged for a within-individual "precision" approach.

The Need for Individual-Level Analyses

Increasing attention has been drawn towards the pitfalls of group-level analytic approaches, which face critiques concerning their validity (Dubois & Adolphs, 2016) and sensitivity and resolution (Fedorenko & Blank, 2020). The major question facing the validity of group-based approaches focuses on if one is indeed comparing functionally homologous regions across subjects (Dubois & Adolphs, 2016). This is a legitimate concern in light of findings pointing to the high interindividual variability of association cortices compared with sensorimotor cortices (Kong et al., 2019; Laumann et al., 2015; Mueller et al., 2013). This issue is particularly problematic since it can result in functional activation maps that fail to align perfectly between individuals (Fedorenko & Blank, 2020; Fischl et al., 2008; Frost & Goebel, 2012; Vázquez-Rodríguez et al., 2019). But beyond questionable validity, group-level analyses

also face issues with sensitivity and resolution. As discussed in Fedorenko and Blank (2020), in task fMRI studies, some activations may not be detectable at the group level despite being clearly present in each individual. Additionally, two regions that are spatially adjacent but distinct functionally on an individual level may be resolved as one region at the group level. This issue of low functional resolution was demonstrated recently as default networks A and B, and the language network previously resolved as overlapping at the group level were disentangled only at the individual level (Braga et al., 2020; Braga & Buckner, 2017; DiNicola et al., 2020). Thus, to counter the issues of validity, sensitivity, and resolution intrinsic to group-level analyses, individual-level approaches appear to be a viable alternative.

A Precision Approach

Individual-level analyses are intertwined with the origins of fMRI research, beginning with a 1991 study featuring a flickering lights paradigm and a single participant (Kwong, 2012). Just over 30 years later, a return to this design is being heralded as a well-powered alternative to the large and costly sample sizes required for cross-sectional group and brain-wide association studies (Gratton et al., 2022; Marek et al., 2022). This method of densely sampling individuals can, as noted by Marek et al. (2022), generate precise brain maps as well as blueprints for reducing MRI artifacts. Moreover, in combination with a functional localizer, individual approaches can have superior sensitivity, functional resolution, and interpretability (Fedorenko, 2021). Despite these many advantages, the questions that can be answered using this method are different from those approached with a traditional group analysis and may be seen as limiting to some researchers. However, this approach has been demonstrated to be effective in examining brain plasticity (Newbold et al., 2020; Newbold & Dosenbach, 2021), disentangling functional networks (Braga et al., 2020; Braga & Buckner, 2017; DiNicola et al., 2020), and identifying

network variants (Gordon et al., 2017; Laumann et al., 2015; Perez et al., 2023) among other outcomes.

Aims and Hypotheses

In line with the precision neuroimaging approach and previous efforts to understand brain network organization and specialization, the present study examines two open questions. First, we explore which networks exhibit the greatest hemispheric specialization. Previously, Wang et al. (2014), identified networks associated with language, visuospatial attention, and executive control as being the most specialized. However, it remains unclear how these estimates might change with a greater number of examined networks, and when implemented in individuals. In line with previous work, we hypothesized that networks associated with language, visuospatial attention, and executive control would show the greatest specialization.

Second, we investigate which connections support specialization in a given network. Although a data-driven approach was implemented to address contributions to network specialization, we anticipated that the pattern of network contributions would follow one of three outcomes: a within-between network gradient, a specialization gradient, or a sensorimotor-association gradient.

Methods

Datasets and Overview

Three independent datasets were used for these analyses: The Human Connectome Project (HCP; split into discovery and replication datasets), the Human Connectome Project-Development (HCPD; Somerville et al., 2018), and the Natural Scenes Dataset (NSD; Allen et al., 2022). Each dataset was selected for its relatively high quantity of low-motion data per participant. See Study 1 for dataset descriptions and accompanying MRI acquisition parameters.

MRI Processing

Processing for BOLD NIFTI files was comprised of the following steps: preprocessing, generation of individual parcellations, implementation of the autonomy index and the deconstructed autonomy index.

Preprocessing

Preprocessing took place on raw NIFTI files for the resting-state fMRI and task fMRI runs using a pipeline developed by the Computational Brain Imaging Group (CBIG; Kong et al., 2019; Li et al., 2019). The implementation of this pipeline was described previously (see Study 1) and is summarized briefly here. Following FreeSurfer surface reconstruction (FreeSurfer 6.0.1, Dale et al., 1999), the pipeline includes the removal of the first four frames and motion correction (using FSL; Jenkinson et al., 2002; Smith et al., 2004), functional and structural image alignment (using FsFast; Greve & Fischl, 2009), linear regression using multiple nuisance regressors (using a combination of CBIG in-house scripts and FSL MCFLIRT; Jenkinson et al., 2002), bandpass filtering (using CBIG in-house scripts), surface project (using FreeSurfer's *mri-vol2surf* function), and surface smoothing using a 6 mm full-width half-maximum kernel (using FreeSurfer's *mri_surf2surf* function; Fischl et al., 1999).

Individual Network Parcellations

Following preprocessing, network parcellations were computed using a multi-session hierarchical Bayesian modeling (MS-HBM) pipeline (Kong et al., 2019) in MATLAB R2018b (MATLAB, 2018). This pipeline generates parcellations for individuals with multiple sessions of fMRI data by using a variational Bayes expectation-maximization algorithm to learn group-level priors from a training dataset and apply those to estimate individual-specific parcellations. The model estimates various parameters, including group-level network connectivity profiles, inter-

subject functional connectivity variability, intra-subject functional connectivity variability, a spatial smoothness prior, and an inter-subject spatial variability prior. A *k* of 17 was selected for all participants (Yeo et al., 2011). Following the generation of individual parcellations, a Hungarian matching algorithm was used to match the parcellation labels with the Yeo et al. (2011) 17-network group parcellation labels.

Autonomy Index

The autonomy index approaches specialization from a functional connectivity perspective and is known to reliably estimate specialization across neurotypical and clinical samples (Mueller et al., 2015; Sun et al., 2022; Wang et al., 2014). First, individual functional connectivity matrices were calculated for each BOLD run and then averaged across runs within an individual at the fsaverage6 resolution in MATLAB R2018b (MATLAB, 2018). From here, the autonomy index was computed. In summary, for each seed vertex obtained from a functional connectivity matrix, the degree of within-hemisphere connectivity and cross-hemisphere connectivity were computed by summing the number of vertices correlated to the seed in the ipsilateral hemisphere and in the contralateral hemisphere. This is then normalized by the total number of vertices in the corresponding hemisphere, thus the accounting for a potential brain size asymmetry between the two hemispheres. Finally, AI is calculated as the difference between normalized within- and cross-hemisphere connectivity as follows:

$$AI = N_i/H_i - N_c/H_c$$

where N_i and N_c are the number of vertices correlated to the seed ROI (using a threshold of |0.25|) in the ipsilateral hemisphere and contralateral hemisphere, respectively. H_i and H_c are the total number of vertices in the ipsilateral and contralateral hemisphere, respectively. To compute

the specialization of each functional network, the AI was averaged within the boundary of each network within each hemisphere on an individual basis.

Deconstructed Autonomy Index

To address the aim of identifying contributions to network specialization, the autonomy index was deconstructed for each network. This was accomplished by first calculating functional connectivity matrices for each BOLD run as previously described. Then, for each target network (1-17) and each seed vertex derived from a functional connectivity matrix, the degree of within- and cross-hemisphere connectivity was computed by summing the number of highly correlated vertices belonging to that target network in each hemisphere. This is normalized by the total number of vertices with a given target network label in each hemisphere. This deconstructed AI is calculated as follows:

$$dAI = \frac{TN_i}{TNH_i} - \frac{TN_c}{TNH_c}$$

where TN_i represents the number of vertices correlated with the seed vertex (using a threshold of |0.25|) that fall within the target network in the ipsilateral hemisphere, TNH_i represents the number vertices with the target network label in the ipsilateral hemisphere, TN_c represents the number of vertices correlated with the seed vertex that fall within the target network in the contralateral hemisphere, and TNH_c represents the number of vertices with a given target network label in the contralateral hemisphere. This results in a matrix of dAI values for each target network for each subject. Then, for each target network matrix, the deconstructed AI is averaged within the boundaries of each network within each subject (1-17; see Figure 1).

Figure 1

The Deconstructed Autonomy Index (dAI)

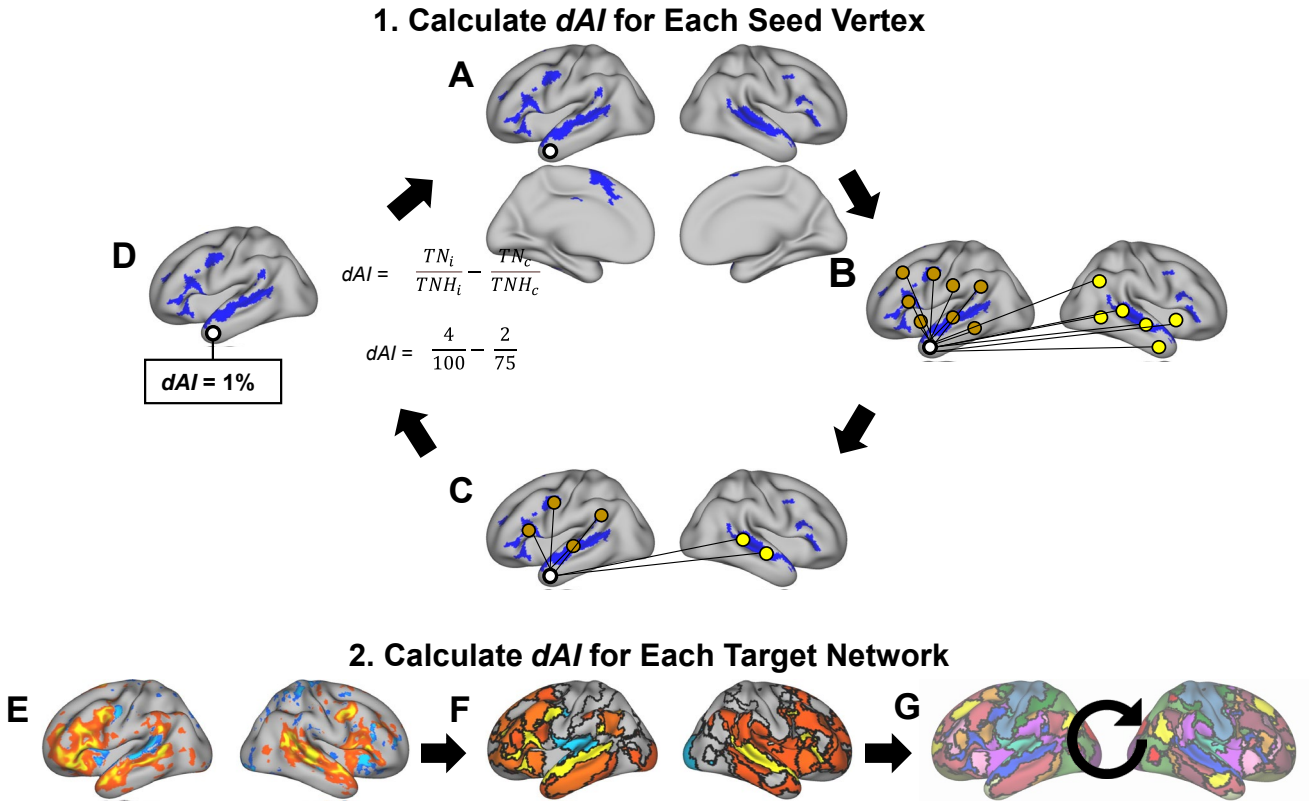

Note. The first step consists of calculating dAI for each vertex. Panel A depicts a seed vertex (white circle) and a target network (highlighted in blue). In Panel B, vertices correlated with the seed vertex in the ipsilateral and contralateral hemispheres are identified. In Panel C, the correlated vertices are filtered to those that fall within the boundaries of the target network. In Panel D, the dAI is calculated for the seed vertex, which is the ratio of connections between the seed vertex and target network above |.25| in the ipsilateral hemisphere divided by the total number of vertices in the target network in the ipsilateral hemisphere and subtract from this the ratio of connections between the seed vertex and target network in the contralateral hemisphere divided by the total number of vertices in the target network in the contralateral hemisphere. This process (Panels A-D) is repeated for each vertex, after which dAI is calculated for each target network. Panel E depicts the dAI values when Language is the target network. Next, in Panel F,

dAI values are averaged within each network. This process is repeated for each target network (1-17; Panel G).

Replications of Wang et al. (2014)

Before expanding on the work of Wang et al. (2014), which was originally performed in Brain Genomics Superstruct Project subjects (Holmes et al., 2015), we first performed a replication in the HCP-Discovery and HCP-Replication datasets. This was accomplished by averaging left hemisphere and right hemisphere autonomy index values within the network boundaries of a seven-network group parcellation produced from 1000 subjects (the parcellation is freely available online: https://surfer.nmr.mgh.harvard.edu/fswiki/CorticalParcellation_Yeo2011; Yeo et al., 2011). Then, to proceed in a step-wise fashion, the same procedure was undertaken with a 17-network group parcellation (Yeo et al., 2011).

Reliability Analyses

Reliability analyses sought to address three questions: 1) What is the test-retest reliability of the autonomy index using individual parcellations, 2) How much data is needed to obtain a stable estimate of the autonomy index, and 3) Is there a task effect on autonomy index estimation?

Test-Retest Reliability

In order to determine the test-retest reliability of the autonomy index, HCP subjects with all four resting-state runs available post-preprocessing were utilized ($N = 232$). Individual parcellations were generated separately for the first two runs and the second two runs. Functional connectivity matrices were also generated separately for the first session and the second session,

and the autonomy index was calculated on both. Next, the autonomy index was averaged within network boundaries for the left and right hemispheres for each session. Outliers were fenced on a network basis to an upper limit of the third quartile plus 1.5 multiplied by the interquartile range, and a lower limit of the first quartile minus 1.5 multiplied by the interquartile range. Finally, an intraclass correlation was calculated for the averaged autonomy index values for the top five most left-lateralized (Language, Dorsal Attention-A, Default-A, Default-C, and Limbic-B) and the top five most right-lateralized networks (Salience/Ventral Attention-A, Control-B, Control-C, Default-C, and Limbic-B). Intraclass correlations were then evaluated using the standard guidelines from Koo & Li (2016), with values less than 0.5 indicating poor reliability, values between 0.5 and 0.75 indicating moderate reliability, values between 0.75 and 0.9 indicating good reliability, and values greater than 0.9 indicating excellent reliability (based on a 95% confidence interval). Spearman rank correlations were then used to examine potential relationships between network test-retest reliability and a network-averaged signal-to-noise ratio.

Stable Estimate Analysis

Given that MRI scanning is costly, rendering it relatively rare to have highly sampled individuals, it is important to understand how much data is needed to reliably estimate specialization. To address this concern, we utilized HCP subjects with all four resting-state runs ($N = 232$) available post-preprocessing. Following preprocessing, the first and third scans from each participant were set aside to compose 30 minutes of independent data. Next, the second and fourth scans were each split into three five-minute segments. Runs were split in MATLAB R2018b (MATLAB, 2018) using native MATLAB functions as well as the FreeSurfer functions *MRIread* and *MRIwrite*. The MS-HBM pipeline was then used to generate separate individual parcellations from 5, 10, 15, 20, 25, and 30 minutes of data from the segmented scans. The MS-

HBM pipeline was also used to separately generate individual parcellations from 30 minutes of independent data from the same subjects. Of note, the reliability of the MS-HBM pipeline has been examined previously through test-retest reliability (see Kong et al. (2019) Figure 2B and supplementary Figure S10C) and a stable estimate analysis (see Study 1). The autonomy index was then calculated for each iteration (5, 10, 15, etc. minutes) and the independent 30 minutes of data. An intraclass correlation between the autonomy index from each iteration parcellation and the independent 30 minutes parcellation were assessed within the right and left hemispheres for each subject. Similarly, an intraclass correlation between the autonomy index from each iteration parcellation and the independent 30 minutes parcellation were assessed within the right and left hemispheres for each network. Intraclass correlations from the stable estimate analysis were also evaluated using the guidelines from Koo & Li (2016).

Task Effects on the Autonomy Index

Following the procedure outlined in Study 1, task effects were also examined for the estimation of the autonomy index within individuals. Briefly, individual parcellations were generated using both task and resting-state fMRI data from the NSD dataset using various combinations of runs within task type: even-numbered runs, odd-numbered runs, the first half of runs, the second half of runs, and two random selections of runs (without replacement). Intraclass correlation coefficients were then used to compare autonomy index overlap within task and between tasks for each hemisphere. Wilcoxon Signed Rank tests were then used to compare the intraclass correlations (R Core Team, 2011; Wilcoxon, 1945).

Identifying Specialized Networks with Individual Parcellations

After establishing the reliability of approaching specialization from an individual-level perspective using the autonomy index, we addressed the first hypothesis of determining whether

any of the 17 networks exhibited specialization, and if so, which exhibited the greatest specialization. The following analyses were first implemented in the HCP-Discovery dataset and then replicated in the HCP-Replication and HCPD datasets using all data available from each participant. First, to determine whether any networks exhibited specialization, multiple regressions were implemented for each of the 17 networks, separately for the left and right hemispheres. Models consisted of the a given network's mean autonomy index value and the covariates of mean-centered age, sex, mean-centered mean framewise displacement, and handedness (measured via the Edinburgh Handedness Inventory, Oldfield, 1971). A network was considered specialized if the model intercept was significant at the Bonferroni-corrected alpha level of 0.001.

Within-Network Contributions

To address our second hypothesis regarding contributions to specialized networks, we implemented the deconstructed autonomy index in the top five left- and right-lateralized networks as determined via the HCP-Discovery dataset. These values were adjusted for mean-centered age, mean-centered framewise displacement, sex, and handedness. Following model-adjustment, potential patterns were visually identified and then assessed quantitatively via matrices of mean dAI values first within the HCP-Discovery dataset and then within the HCP-Replication and HCPD datasets.

Results

Replication of Wang et al. (2014)

Using the Yeo et al. (2011) seven-network group parcellation, we identified the Default and Frontoparietal networks as the most left-lateralized networks, and the Frontoparietal, Dorsal Attention and Ventral Attention networks as the most right-lateralized networks for both the

HCP-Discovery and HCP-Replication datasets (see Supplementary Figure S1). This pattern of specialized networks replicates that found by Wang et al. (2014). Next, using the Yeo et al. (2011) 17-network group parcellation, we identified the Dorsal Attention-A, Language, Default-A, Default-C, and Limbic-B networks as the most left-lateralized across both datasets (see Supplementary Figure S2). The Control-B, Default-C, and Limbic-B networks showed the greatest right- hemisphere lateralization.

Reliability Analyses

The reliability of the autonomy index was examined through the following three analyses: test-retest reliability, a stable estimate analysis, and a task effects analysis.

Test-Retest Reliability

Using HCP subjects with all four resting-state runs available post-preprocessing (N = 232), test-retest reliability was assessed for the top five left- and right-lateralized networks. For the left-lateralized networks, intraclass correlations were within a moderate range, between 0.55 to 0.77, with the lowest being the Limbic-B network (ICC = 0.55, $F(231, 231) = 3.5$, $p < .001$, 95% CI [0.46, 0.63]; see Figure 2). For the right-lateralized networks, the intraclass correlations were also in the moderate range, from 0.55 to 0.72, with the Control-C network exhibiting the lowest reliability (ICC = 0.55, $F(231, 231) = 3.5$, $p < .001$, 95% CI [0.45, 0.63]). Spearman rank correlations identified no relationship between test-retest reliability (intraclass correlation coefficients) and network-averaged temporal signal-to-noise ratios (left hemisphere: $r(15)$ = 0.11, $p = .68$; right hemisphere: $r(15) = .27$, $p = .29$; see Supplementary Figure S3).

Figure 2

Test-Retest Reliability of Autonomy Index Values for Five Left- and Right-Specialized Networks in 232 HCP Subjects

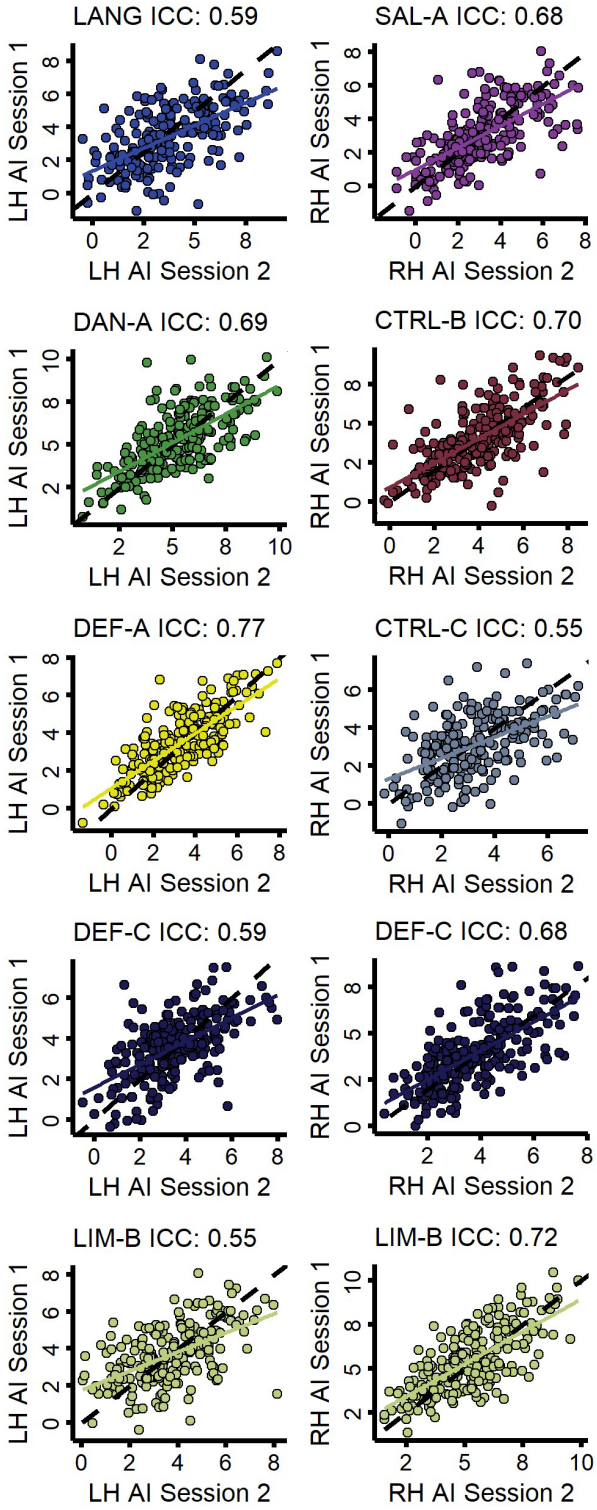

Note. Left-specialized networks (left column) included Language, Dorsal Attention-A, Default-A, Default-C, and Limbic-B. Right-specialized networks (right column) included Salience/Ventral Attention-A, Control-B, Control-C, Default-C, and Limbic-B. In each plot, a circle represents a subject.

Stable Estimate Analysis

To address the question of how much data is needed in order to obtain a stable estimate of autonomy index values, combinations of five-minute increments (5, 10, 15…30 minutes) were compared against 30 independent minutes of data in 232 HCP subjects. The intraclass correlations indicate that approximately 20 minutes of data are needed to obtain moderate to good intraclass correlations for the majority of subjects (see Figure 3 Panel A). The stable estimate analysis was also approached from a network basis (as opposed to the subject basis presented in Figure 3 Panel A). Across both hemispheres, networks with the lowest intraclass correlation were Limbic-A, Control-A, and Somatomotor-B (for the overall distributions, see Figure 3 Panel B; for the individual network intraclass correlations, see Supplementary Figure S4). Notably, the network with the greatest intraclass correlation for the left hemisphere autonomy index was as the Default-A network, while the Control-B network was the right hemisphere counterpart. Most networks improved in reliability with additional data.

Figure 3

Evidence for Reliable Estimates of the Autonomy Index in 232 HCP Subjects

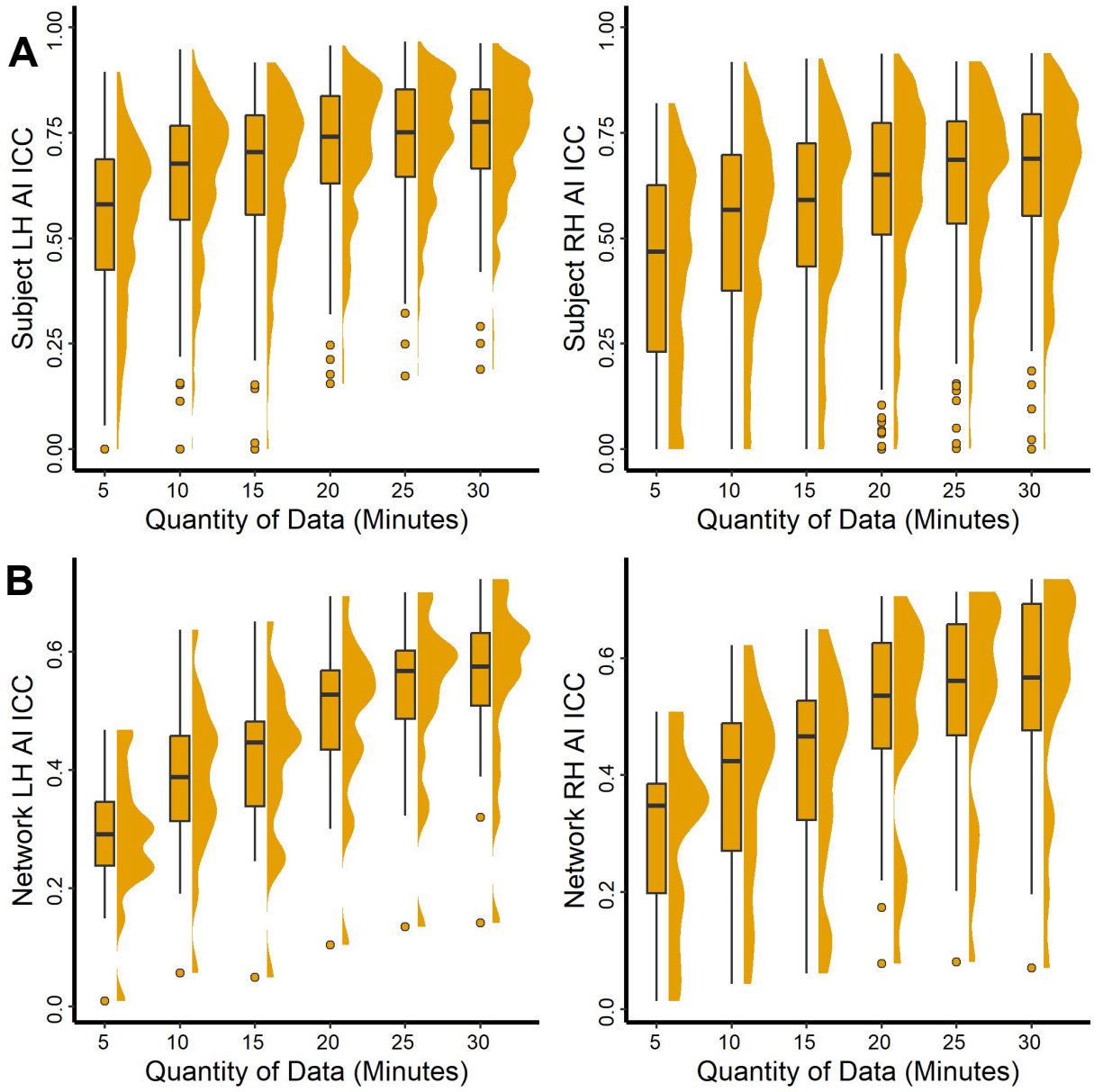

Note. Panel A depicts the intraclass correlation coefficient calculated for each subject's 17 mean autonomy index values for each time increment (5, 10, 15 … 30 minutes) and the subject's 17 mean autonomy index values from 30 independent minutes of data for the left and right hemispheres. Panel B depicts the distribution of intraclass correlations in autonomy index between the 30 independent minutes of data and each increment of data for each network for the

left and right hemispheres. Individual network intraclass correlation coefficients are depicted in Supplementary Figure S4.

Task Effects on the Autonomy Index

Using the NSD dataset ($N = 8$) to compare potential differences between resting-state and task fMRI on autonomy index estimates for the left and right hemispheres, we found differences between the within-task comparisons and between task comparisons for autonomy index intraclass correlation coefficients (see Figure 4). For the left hemisphere autonomy index intraclass correlation coefficients, Wilcoxon signed rank comparisons revealed a difference in within-task (Task-Task and Rest-Rest) intraclass correlation coefficients for even versus odd numbered runs ($V = 33$, $p = .04$) as well as for the first half versus the second half of runs ($V = 34$, $p = .02$), but not for the random selection of runs ($V = 26$, $p = 31$). Regardless of how the data were split, a task effect in intraclass correlation coefficients was found between within-task (Task-Task) and between-task (Task-Rest) intraclass correlation coefficients for even versus odd numbered runs ($V = 36$, $p = .008$), the first half versus the second half of runs ($V = 36$, $p = .008$), and the random selection of runs ($V = 34$, $p = .02$).

Similarly, with the right hemisphere autonomy index intraclass correlation coefficients, a significant difference was found for within-task (Task-Task and Rest-Rest) reliability across the even versus odd numbered runs ($V = 34$, $p = .02$) and the first half versus the second half of runs ($V = 32$, $p = .05$), but not for the random selection of runs ($V = 24$, $p = .46$). Regardless of how the data were split, a significant difference was found between within-task (Task-Task) and between-task intraclass correlation coefficients across the even versus odd numbered runs ($V =$

35, p = .02), the first half versus the second half of runs (V = 36, p = .008), and the random selection of runs (V = 36, p = .008).

Figure 4

Task Dependency of the Autonomy Index in the NSD Dataset

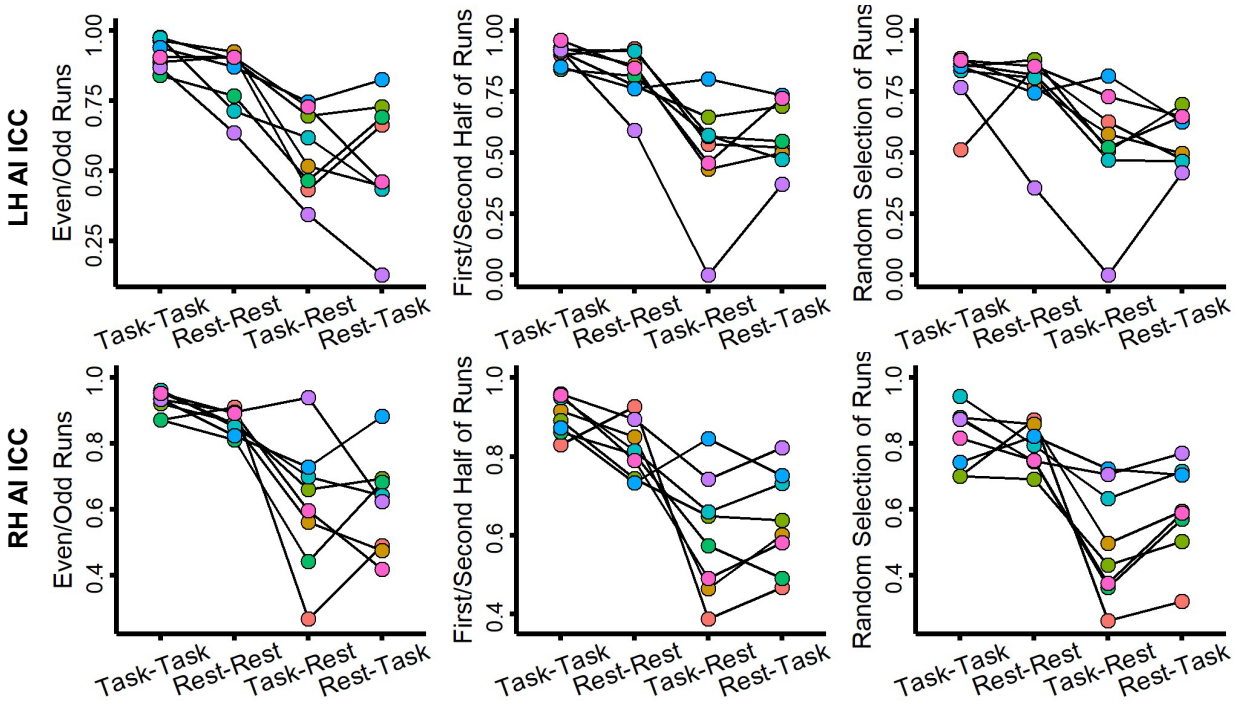

Note. Depicted in the top row are the intraclass correlation coefficients for the left hemisphere autonomy index for each participant. Regardless of how the data were split (even- versus odd-numbered runs, the first half versus the second half, or a random selection without replacement), a task effect was found. Depicted in the second row are the intraclass correlation coefficients for the right hemisphere autonomy index for each participant. In each plot, circles connected by a line represent an individual.

Identifying Specialized Networks with Individual Parcellations

A series of multiple regressions were used to identify if any of the 17 networks were specialized, first in the HCP-Discovery dataset and then in the HCP-Replication and HCPD datasets. Networks with significant left-hemisphere specialization ($p < .001$) across all three datasets included each network except Visual-A and Default-B (see Supplementary Table 1). All 17 networks were found to have significant right-hemisphere specialization ($p < .001$) across all three datasets (see Supplementary Table 2). Of the covariates, only handedness was reliably significant across all three datasets for the left-hemisphere averaged Salience/Ventral Attention-A autonomy index (see Supplementary Figure S5). See Figure 5 for model-adjusted mean autonomy index values for each of the 17 networks for the left hemisphere (Panel A) and the right hemisphere (Panel B). Notably, the Limbic-B and Default-C networks appear to be strongly lateralized to both hemispheres, not unlike what has previously been observed with the frontoparietal control network (Wang et al., 2014).

Figure 5

Specialization for 17 Networks Across the HCP-Discovery, HCP-Replication, and HCPD Datasets

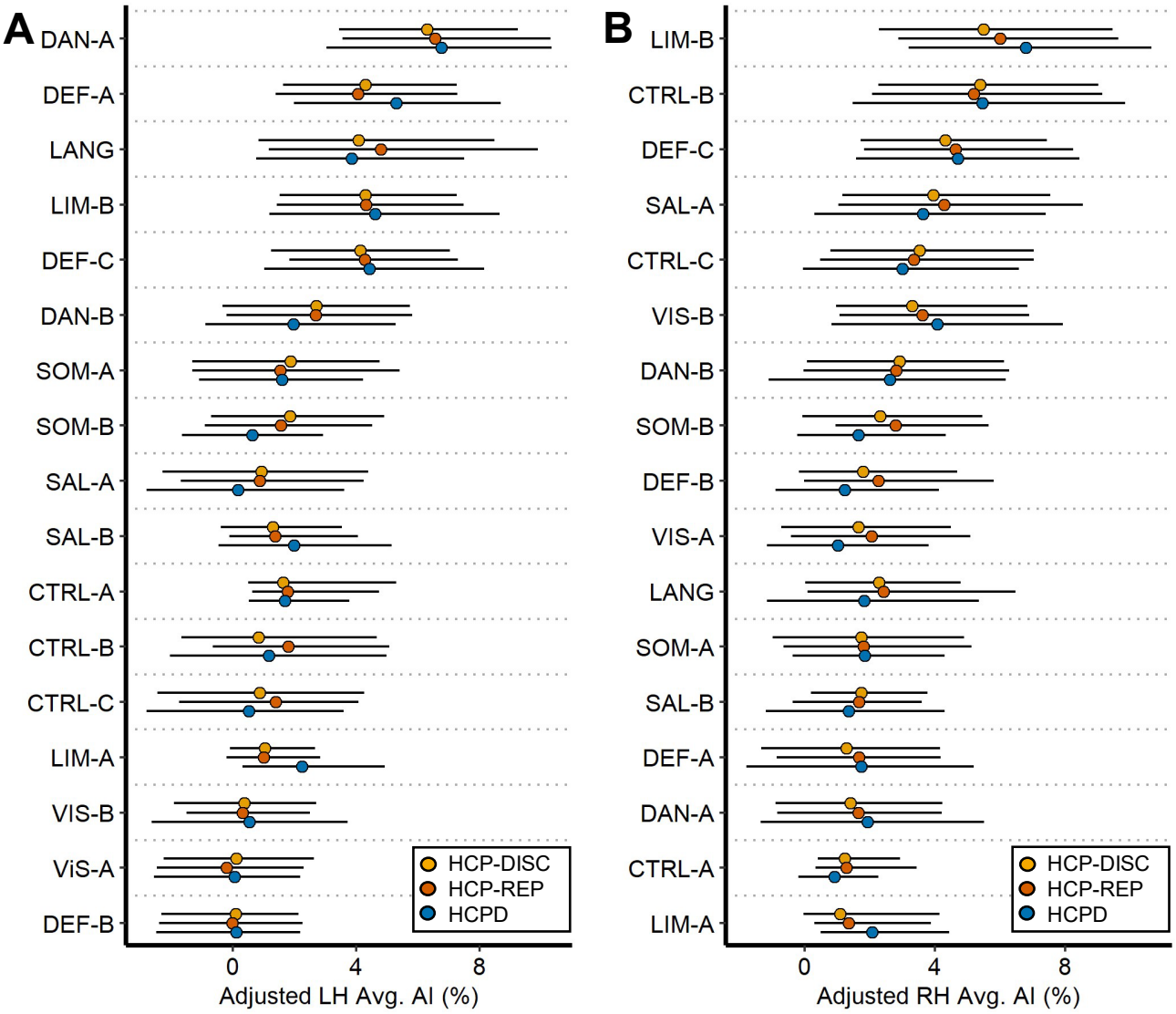

Note. For each panel, the y-axis displays the 17 networks and the x-axis displays the adjusted average autonomy index values, with greater values representing greater hemispheric specialization (left hemisphere on Panel A and right hemisphere on Panel B). Autonomy index values were adjusted by regressing out the effects of mean-centered age, mean-centered mean framewise displacement, sex, and handedness using the following formula: $AI_{adj} = AI_{nat}$ —

[β_1(mean-centered age_{nat} - mean of mean-centered age_{nat}) + β_2(mean-centered FD_{nat} - mean of mean-centered FD_{nat}) + β_3(sex_{nat} – mean sex_{nat}) + β_4($handedness_{nat}$ – mean $handedness_{nat}$)]. Autonomy index adjustment occurred separately for each network within each dataset for each hemisphere. Bars represent the 2.5 and 97.5 percentiles.

Within-Network Contributions to Specialization

To decompose network specialization and identify the greatest contributions to each network's specialization, deconstructed autonomy index values were averaged within the 17 networks for each target network. Visual examination of the top left- and right-lateralized networks initially indicated that within-network connections appear to be the greatest contributors (e.g., Language network connections contribute the most to Language network specialization; see Supplementary Figures S6-S11). Following within-network connections, other specialized networks appear to be the second largest contributor to specialization (see Figure 6). Matrices of mean dAI scores for all potential 17 seed networks confirmed these two principles (see Supplementary Figures S12-S14).

Figure 6

Deconstructed Autonomy Index Values Within and Between Specialized Networks for the HCP-Discovery, HCP-Replication, and HCPD Datasets

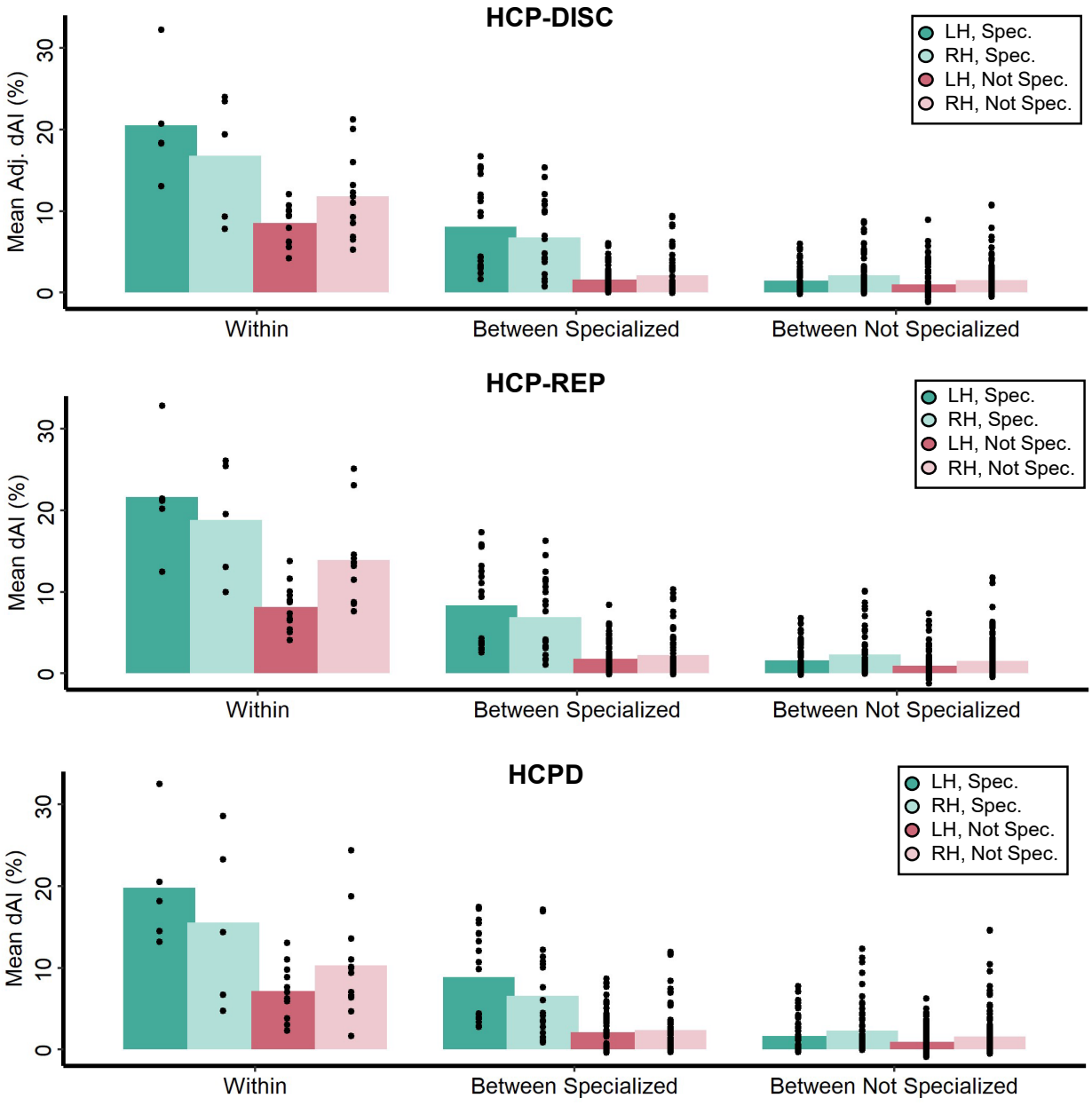

Note. For each row, the averaged dAI value for each category is given. dAI scores were grouped as being within-network (e.g., target network Language and averaged network Language), between specialized networks (e.g., target network Language and averaged network Dorsal

Attention-A), and between not specialized (e.g., target network Language and averaged network Visual-A). Next, dAI scores were further binned depending on the target network as being specialized or not specialized (specialized networks included the top five left- and right-lateralized networks). Finally, dAI scores were organized by hemisphere, left or right. Each point represents a single target and averaged network combination mean dAI score. Across each dataset, within-network contributions appear to be greatest followed by between-specialized network contributions.

Discussion

In the present study, we examined brain network specialization using a functional connectivity-based measure, replicating and expanding on the work of Wang et al. (2014). After directly replicating Wang et al. (2014) and addressing the reliability of a within-individual implementation, we identified specialized networks at a 17-network resolution and determined the greatest contributions to specialization. Inconsistent with our first hypothesis, we identified networks other than those directly associated with language, visuospatial attention, and executive control as being the most specialized. However, across three datasets, we found that within-network connections contributed most to a given network's specialization followed by connections from other specialized networks. Taken as a whole, these results provide evidence for guiding principles of brain organization generally and the specialization of macroscale brain networks specifically.

Evidence for the Reliability of the Autonomy Index

In the present study, we examined specialization using the autonomy index. However, the implementation of this measure differed from the original in two key ways: the use of a 17-

network parcellation scheme as opposed to seven networks, and the adoption of individual parcellations to delineate network boundaries as opposed to a single group-level network parcellation. While we contend that these differences facilitated the acquisition of novel insights into network specialization, it was uncertain as to whether they compromised the integrity of the autonomy index. The top five left- and right-specialized networks fell within moderate test-retest reliability. Additional reliability analyses indicated that the autonomy index is stable within individuals after approximately 20 minutes of resting-state fMRI data.

While the individual-level implementation of the autonomy index was found to be reliable, task effects were found. This finding replicates previously observed task effects on a different measure of functional connectivity-derived network specialization (see Study 1). This is likely due to the idea that the act of "resting" introduces greater variability in functional connectivity compared to that observed during task-based fMRI, potentially as a result of mind wandering (Elton & Gao, 2015). Furthermore, when it comes to predicting individual traits, task-based models outperform rest-based models, and this has been attributed to the "unconstrained nature" of the resting state (Greene et al., 2018).

Identification of Highly Specialized Networks

Notably, the top five greatest left-specialized networks included the Language, Dorsal Attention-A, Default-A, Default-C, and Limbic-B networks, while the right-specialized counterparts included the Salience/Ventral Attention-A, Control-B, Control-C, Default-C, and Limbic-B networks. Similar to previous work, several highly left-lateralized networks support language function (such as the Language, Default-A, and Default-C networks) and several highly right-lateralized networks support visuospatial attention and executive control functions (such as the Salience/Ventral Attention-A, Control-B, and Control-C networks; Wang et al., 2014).

Interestingly, while networks associated with language, attention, and executive control were highly specialized, they were not the most specialized left- and right-lateralized networks. Instead, the Dorsal Attention-A and Limbic-B networks were the most left- and right-lateralized networks, respectively. Corroborating this finding, a network surface area-based approach to specialization also using the Kong et al. (2019) 17-network parcellation identified these two networks as the most specialized (see Study 1). While it is unclear why language and visuospatial attention were not identified as the most lateralized networks, this may be due to differences in methodologies or even the failure to compare language and attentional networks against the large number of networks examined here.

An alternative explanation for the identification of the Dorsal Attention-A and Limbic -B networks as being most specialized comes from other within-individual investigations. Work on the default network found that the group-defined default network is split into two parallel yet interdigitated networks which subserve different functions on the individual level (Braga & Buckner, 2017; DiNicola et al., 2020). Thus, it may be that, by taking a fine-grained approach to network parcellations, networks which have previously been described as bilateral may be split into subnetworks, of which one may be left- or right-lateralized. In the case of dorsal attention, previously described as belonging to a bilateral network (Fox et al., 2006; Mengotti et al., 2020), this may have been split into a highly left-specialized network (Dorsal Attention-A) and a less specialized network (Dorsal Attention-B).

Interestingly, the present study failed to replicate dually-specialized frontoparietal control networks (Wang et al., 2014) within the 17-network parcellation. Instead, we identified the Control-B and Control-C networks as being highly right-lateralized with minimal specialization of the Control-A network. Additionally, we found that the Default-C and Limbic-B networks

were highly specialized to both hemispheres. While it is unclear why these specific networks would show this dual or coupling pattern of specialization, further investigation into these specific networks and their functional implications could provide valuable insights.

Contributions to Specialization

In order to better understand which functional connections contribute the most to a given network's specialization, we implemented a novel version of the within-individual implementation of the autonomy index: the deconstructed autonomy index. Resulting patterns of dAI values indicated that the greatest contributions to network specialization were from the same network (following a within-between network gradient) followed by other specialized networks (following a specialization gradient). This first principle of specialization contributions--that within-network contributions are greatest--is supported by the idea that hemispheric asymmetries increase the modularization of functions, thereby decreasing redundancy (Levy, 1969), processing speed (Ringo et al., 1994), and interhemispheric conflict (Andrew et al., 1982; Corballis, 1991; Gerrits et al., 2020; Vallortigara, 2006). A larger number of within-network connections would contribute to that network's specialization of function and likely increase the efficiency of that network. Support for the second principle of network contributions--that connections from other specialized networks make up the second largest contribution--can be found from graph theoretical analysis and so-called "rich clubs". These hubs are composed of high degree and high strength nodes, and are highly interconnected to one another (Colizza et al., 2006; Opsahl et al., 2008). Notably, rich club nodes have been identified in highly integrated brain regions, such as cingulate and pericingulate regions, as well as highly specialized brain regions including the orbitofrontal cortex, caudate, fusiform gyrus, and hippocampus (Kocher et al., 2015). Relevant to the present study, this work with rich club hubs evidences an interesting

idea: specialized brain regions can be highly interconnected with one another. While the specialized brain networks discussed in the present study are not necessarily the same as the specialized brain regions referenced in Kocher et al. (2015), our work suggests that the strength of between-network contributions is less than within-network contributions.

Limitations and Future Directions

In order to obtain individual parcellations that are reliable within individuals and comparable with previous work, the MS-HBM pipeline was selected. As a part of this pipeline, inter-subject variability is accounted for by way of group priors (derived from 40 GSP subjects). One risk with incorporating group priors is that they may constrain network boundaries in ways that do not necessarily reflect an individual's functional neurobiology. As noted in Kong et al. (2019), functional connectivity profiles derived from individuals are fairly noisy compared with those from a group-averaged profile. Thus, while the incorporation of group priors may reduce this noise, some signal may be lost as well.

An additional limitation with the selected method concerns the failure to capture the moment-to-moment dynamics of brain function. By creating static parcellations, we have oversimplified the temporal dimension of these large-scale networks. Relevant to the use of the autonomy index, which is based on correlations between vertices, one team found that brain activity between pairs of distributed regions fluctuates in and out of correlation over time (Zalesky et al., 2014). Future investigations may consider implementing approaches to specialization that account for temporal dynamics, such as multi-layer network approaches (Betzel & Bassett, 2017).

Further applications of the deconstructed autonomy index could involve studying populations other than neurotypical children, adolescents, and adults. For example, it would be

interesting to know how contributions to network specialization may be different in autism, for which atypical functional lateralization patterns have been reliably observed (Anderson et al., 2010; Cardinale et al., 2013; Eyler et al., 2012; Harris et al., 2006; Jouravlev et al., 2020; Kleinhans et al., 2008; X.-Z. Kong et al., 2022; Lindell & Hudry, 2013; Müller et al., 2003; Nielsen et al., 2014; Persichetti et al., 2022; Redcay & Courchesne, 2008) as well as schizophrenia (Agcaoglu et al., 2018; X.-Z. Kong et al., 2022; Ocklenburg et al., 2013; Sommer et al., 2001). Additionally, it is unknown when the patterns of network contributions are established or how they potentially change in older adulthood. Future research could provide valuable insights into potential variations of network contributions in individuals with neurodevelopmental conditions and shed light on the developmental trajectory and potential changes in network specialization throughout adulthood.

Conclusions

In the present study, we examined brain network organization on an individual level through the lens of specialization. We identified most networks as exhibiting greater within-hemisphere connectivity than between-hemisphere connectivity. Additionally, we found that the greatest contributors to network specialization were first within-network connections followed by connections with other specialized networks.

Acknowledgements

Data were provided in part by the Human Connectome Project, WU-Minn Consortium (principal Investigators: David Van Essen and Kamil Ugurbil; 1U54MH091657) funded by the 16 NIH Institutes and Centers that support the NIH Blueprint for Neuroscience Research; and by the McDonnell Center for Systems Neuroscience at Washington University. HCPD data reported in this publication were supported by the National Institute of Mental Health of the National

Institutes of Health under Award Number U01MH109589 and by funds provided by the McDonnell Center for Systems Neuroscience at Washington University in St. Louis. The HCP-Development 2.0 Release data used in this report came from DOI: 10.15154/1520708. Collection of the NSD dataset was supported by NSF IIS-1822683 and NSF IIS-1822929. Furthermore, we acknowledge the support of the Office of Research Computing at Brigham Young University.

References

Agcaoglu, O., Miller, R., Damaraju, E., Rashid, B., Bustillo, J., Cetin, M. S., Van Erp, T. G. M., McEwen, S., Preda, A., Ford, J. M., Lim, K. O., Manoach, D. S., Mathalon, D. H., Potkin, S. G., & Calhoun, V. D. (2018). Decreased hemispheric connectivity and decreased intra- and inter- hemisphere asymmetry of resting state functional network connectivity in schizophrenia. *Brain Imaging and Behavior*, *12*(3), 615–630. https://doi.org/10.1007/s11682-017-9718-7

Allen, E. J., St-Yves, G., Wu, Y., Breedlove, J. L., Prince, J. S., Dowdle, L. T., Nau, M., Caron, B., Pestilli, F., Charest, I., Hutchinson, J. B., Naselaris, T., & Kay, K. (2022). A massive 7T fMRI dataset to bridge cognitive neuroscience and artificial intelligence. *Nature Neuroscience*, *25*(1), Art. 1. https://doi.org/10.1038/s41593-021-00962-x

Anderson, J. S., Lange, N., Froehlich, A., DuBray, M. B., Druzgal, T. J., Froimowitz, M. P., Alexander, A. L., Bigler, E. D., & Lainhart, J. E. (2010). Decreased left posterior insular activity during auditory language in autism. *American Journal of Neuroradiology*, *31*(1), 131–139.

Andrew, R., Mench, J., & Rainey, C. (1982). Right-left asymmetry of response to visual stimuli in the domestic chick. *Analysis of Visual Behaviour*, 197–209.

Betzel, R. F., & Bassett, D. S. (2017). Multi-scale brain networks. *Neuroimage*, *160*, 73–83.

Braga, R. M., & Buckner, R. L. (2017). Parallel interdigitated distributed networks within the individual estimated by intrinsic functional connectivity. *Neuron*, *95*(2), 457-471.e5. https://doi.org/10.1016/j.neuron.2017.06.038

Braga, R. M., DiNicola, L. M., Becker, H. C., & Buckner, R. L. (2020). Situating the left-lateralized language network in the broader organization of multiple specialized large-

scale distributed networks. *Journal of Neurophysiology*, *124*(5), Art. 5. https://doi.org/10.1152/jn.00753.2019

Cardinale, R. C., Shih, P., Fishman, I., Ford, L. M., & Müller, R.-A. (2013). Pervasive rightward asymmetry shifts of functional networks in Autism Spectrum Disorder. *JAMA Psychiatry*, *70*(9), 975–982. https://doi.org/10.1001/jamapsychiatry.2013.382

Colizza, V., Flammini, A., Serrano, M. A., & Vespignani, A. (2006). Detecting rich-club ordering in complex networks. *Nature Physics*, *2*(2), Art. 2. https://doi.org/10.1038/nphys209

Corballis, M. C. (1991). *The lopsided ape: Evolution of the generative mind.* (pp. vii, 366). Oxford University Press.

Dale, A. M., Fischl, B., & Sereno, M. I. (1999). Cortical surface-based analysis: I. Segmentation and surface reconstruction. *NeuroImage*, *9*(2), 179–194. https://doi.org/10.1006/nimg.1998.0395

DiNicola, L. M., Braga, R. M., & Buckner, R. L. (2020). Parallel distributed networks dissociate episodic and social functions within the individual. *Journal of Neurophysiology*, *123*(3), Art. 3. https://doi.org/10.1152/jn.00529.2019

Dubois, J., & Adolphs, R. (2016). Building a science of individual differences from fMRI. *Trends in Cognitive Sciences*, *20*(6), 425–443. https://doi.org/10.1016/j.tics.2016.03.014

Elton, A., & Gao, W. (2015). Task-related modulation of functional connectivity variability and its behavioral correlations. *Human Brain Mapping*, *36*(8), 3260–3272.

Eyler, L. T., Pierce, K., & Courchesne, E. (2012). A failure of left temporal cortex to specialize for language is an early emerging and fundamental property of autism. *Brain*, *135*(3), 949–960.

Fedorenko, E. (2021). The early origins and the growing popularity of the individual-subject analytic approach in human neuroscience. *Current Opinion in Behavioral Sciences*, *40*, 105–112. https://doi.org/10.1016/j.cobeha.2021.02.023

Fedorenko, E., & Blank, I. A. (2020). Broca's area is not a natural kind. *Trends in Cognitive Sciences*, *24*(4), 270–284. https://doi.org/10.1016/j.tics.2020.01.001

Fischl, B., Rajendran, N., Busa, E., Augustinack, J., Hinds, O., Yeo, B. T. T., Mohlberg, H., Amunts, K., & Zilles, K. (2008). Cortical folding patterns and predicting cytoarchitecture. *Cerebral Cortex*, *18*(8), 1973–1980. https://doi.org/10.1093/cercor/bhm225

Fischl, B., Sereno, M. I., Tootell, R. B. H., & Dale, A. M. (1999). High-resolution intersubject averaging and a coordinate system for the cortical surface. *Human Brain Mapping*, *8*(4), 272–284. https://doi.org/10.1002/(SICI)1097-0193(1999)8:4<272::AID-HBM10>3.0.CO;2-4

Fox, M. D., Corbetta, M., Snyder, A. Z., Vincent, J. L., & Raichle, M. E. (2006). Spontaneous neuronal activity distinguishes human dorsal and ventral attention systems. *Proceedings of the National Academy of Sciences*, *103*(26), 10046–10051. https://doi.org/10.1073/pnas.0604187103

Friedrich, P., Patil, K. R., Mochalski, L. N., Li, X., Camilleri, J. A., Kröll, J.-P., Wiersch, L., Eickhoff, S. B., & Weis, S. (2022). Is it left or is it right? A classification approach for investigating hemispheric differences in low and high dimensionality. *Brain Structure and Function*, *227*(2), 425–440. https://doi.org/10.1007/s00429-021-02418-1

Frost, M. A., & Goebel, R. (2012). Measuring structural–functional correspondence: Spatial variability of specialised brain regions after macro-anatomical alignment. *NeuroImage*, *59*(2), 1369–1381. https://doi.org/10.1016/j.neuroimage.2011.08.035

Gazzaniga, M. S. (2000). Cerebral specialization and interhemispheric communication: Does the corpus callosum enable the human condition? *Brain*, *123*(7), 1293–1326. https://doi.org/10.1093/brain/123.7.1293

Gerrits, R., Verhelst, H., & Vingerhoets, G. (2020). Mirrored brain organization: Statistical anomaly or reversal of hemispheric functional segregation bias? *Proceedings of the National Academy of Sciences*, *117*(25), 14057–14065. https://doi.org/10.1073/pnas.2002981117

Gordon, E. M., Laumann, T. O., Gilmore, A. W., Newbold, D. J., Greene, D. J., Berg, J. J., Ortega, M., Hoyt-Drazen, C., Gratton, C., Sun, H., Hampton, J. M., Coalson, R. S., Nguyen, A. L., McDermott, K. B., Shimony, J. S., Snyder, A. Z., Schlaggar, B. L., Petersen, S. E., Nelson, S. M., & Dosenbach, N. U. F. (2017). Precision functional mapping of individual human brains. *Neuron*, *95*(4), Art. 4. https://doi.org/10.1016/j.neuron.2017.07.011

Gotts, S. J., Jo, H. J., Wallace, G. L., Saad, Z. S., Cox, R. W., & Martin, A. (2013). Two distinct forms of functional lateralization in the human brain. *Proceedings of the National Academy of Sciences*, *110*(36), E3435–E3444.

Gratton, C., Nelson, S. M., & Gordon, E. M. (2022). Brain-behavior correlations: Two paths toward reliability. *Neuron*, *110*(9), 1446–1449. https://doi.org/10.1016/j.neuron.2022.04.018

Greene, A. S., Gao, S., Scheinost, D., & Constable, R. T. (2018). Task-induced brain state manipulation improves prediction of individual traits. *Nature Communications*, *9*(1), Art. 1. https://doi.org/10.1038/s41467-018-04920-3

Greve, D. N., & Fischl, B. (2009). Accurate and robust brain image alignment using boundary-based registration. *NeuroImage*, *48*(1), 63–72. https://doi.org/10.1016/j.neuroimage.2009.06.060

Harris, G. J., Chabris, C. F., Clark, J., Urban, T., Aharon, I., Steele, S., McGrath, L., Condouris, K., & Tager-Flusberg, H. (2006). Brain activation during semantic processing in autism spectrum disorders via functional magnetic resonance imaging. *Brain and Cognition*, *61*(1), 54–68. https://doi.org/10.1016/j.bandc.2005.12.015

Holmes, A. J., Hollinshead, M. O., O'Keefe, T. M., Petrov, V. I., Fariello, G. R., Wald, L. L., Fischl, B., Rosen, B. R., Mair, R. W., Roffman, J. L., Smoller, J. W., & Buckner, R. L. (2015). Brain Genomics Superstruct Project initial data release with structural, functional, and behavioral measures. *Scientific Data*, *2*(1), Art. 1. https://doi.org/10.1038/sdata.2015.31

Jenkinson, M., Bannister, P., Brady, M., & Smith, S. M. (2002). Improved optimization for the robust and accurate linear registration and motion correction of brain images. *NeuroImage*, *17*(2), 825–841. https://doi.org/10.1006/nimg.2002.1132

Jouravlev, O., Kell, A. J. E., Mineroff, Z., Haskins, A. J., Ayyash, D., Kanwisher, N., & Fedorenko, E. (2020). Reduced language lateralization in autism and the broader autism phenotype as assessed with robust individual-subjects analyses. *Autism Research*, *13*(10), 1746–1761. https://doi.org/10.1002/aur.2393

Kleinhans, N. M., Müller, R.-A., Cohen, D. N., & Courchesne, E. (2008). Atypical functional lateralization of language in autism spectrum disorders. *Brain Research*, *1221*, 115–125. https://doi.org/10.1016/j.brainres.2008.04.080

Kocher, M., Gleichgerrcht, E., Nesland, T., Rorden, C., Fridriksson, J., Spampinato, M. V., & Bonilha, L. (2015). Individual variability in the anatomical distribution of nodes participating in rich club structural networks. *Frontiers in Neural Circuits*, *9*. https://www.frontiersin.org/articles/10.3389/fncir.2015.00016

Kong, R., Li, J., Orban, C., Sabuncu, M. R., Liu, H., Schaefer, A., Sun, N., Zuo, X.-N., Holmes, A. J., Eickhoff, S. B., & Yeo, B. T. T. (2019). Spatial topography of individual-specific cortical networks predicts human cognition, personality, and emotion. *Cerebral Cortex*, *29*(6), Art. 6. https://doi.org/10.1093/cercor/bhy123

Kong, X.-Z., Postema, M. C., Guadalupe, T., de Kovel, C., Boedhoe, P. S. W., Hoogman, M., Mathias, S. R., van Rooij, D., Schijven, D., Glahn, D. C., Medland, S. E., Jahanshad, N., Thomopoulos, S. I., Turner, J. A., Buitelaar, J., van Erp, T. G. M., Franke, B., Fisher, S. E., van den Heuvel, O. A., … Francks, C. (2022). Mapping brain asymmetry in health and disease through the ENIGMA consortium. *Human Brain Mapping*, *43*(1), 167–181. https://doi.org/10.1002/hbm.25033

Koo, T. K., & Li, M. Y. (2016). A guideline of selecting and reporting intraclass correlation coefficients for reliability research. *Journal of Chiropractic Medicine*, *15*(2), 155–163. https://doi.org/10.1016/j.jcm.2016.02.012

Kwong, K. K. (2012). Record of a single fMRI experiment in May of 1991. *NeuroImage*, *62*(2), 610–612. https://doi.org/10.1016/j.neuroimage.2011.07.089

Laumann, T. O., Gordon, E. M., Adeyemo, B., Snyder, A. Z., Joo, S. J., Chen, M.-Y., Gilmore, A. W., McDermott, K. B., Nelson, S. M., Dosenbach, N. U. F., Schlaggar, B. L., Mumford, J. A., Poldrack, R. A., & Petersen, S. E. (2015). Functional system and areal organization of a highly sampled individual human brain. *Neuron*, *87*(3), 657–670. https://doi.org/10.1016/j.neuron.2015.06.037

Levy, J. (1969). Possible basis for the evolution of lateral specialization of the human brain. *Nature*, *224*(5219), Art. 5219. https://doi.org/10.1038/224614a0

Li, J., Kong, R., Liégeois, R., Orban, C., Tan, Y., Sun, N., Holmes, A. J., Sabuncu, M. R., Ge, T., & Yeo, B. T. T. (2019). Global signal regression strengthens association between resting-state functional connectivity and behavior. *NeuroImage*, *196*, 126–141. https://doi.org/10.1016/j.neuroimage.2019.04.016

Lindell, A. K., & Hudry, K. (2013). Atypicalities in cortical structure, handedness, and functional lateralization for language in Autism Spectrum Disorders. *Neuropsychology Review*, *23*(3), 257–270. https://doi.org/10.1007/s11065-013-9234-5

Liu, H., Stufflebeam, S. M., Sepulcre, J., Hedden, T., & Buckner, R. L. (2009). Evidence from intrinsic activity that asymmetry of the human brain is controlled by multiple factors. *Proceedings of the National Academy of Sciences*, *106*(48), 20499–20503.

Marek, S., Tervo-Clemmens, B., Calabro, F. J., Montez, D. F., Kay, B. P., Hatoum, A. S., Donohue, M. R., Foran, W., Miller, R. L., Hendrickson, T. J., Malone, S. M., Kandala, S., Feczko, E., Miranda-Dominguez, O., Graham, A. M., Earl, E. A., Perrone, A. J., Cordova, M., Doyle, O., … Dosenbach, N. U. F. (2022). Reproducible brain-wide association studies require thousands of individuals. *Nature*, *603*(7902), Art. 7902. https://doi.org/10.1038/s41586-022-04492-9

MATLAB. (2018). *9.5.0.944444 (R2018b)*. The MathWorks Inc.

Mengotti, P., Käsbauer, A.-S., Fink, G. R., & Vossel, S. (2020). Lateralization, functional specialization, and dysfunction of attentional networks. *Cortex*, *132*, 206–222. https://doi.org/10.1016/j.cortex.2020.08.022

Milner, B. (1971). Interhemispheric differences in the localization of psychological processes in man. *British Medical Bulletin*, *27*, 272–277.

Mueller, S., Wang, D., Fox, M. D., Yeo, B. T. T., Sepulcre, J., Sabuncu, M. R., Shafee, R., Lu, J., & Liu, H. (2013). Individual variability in functional connectivity architecture of the human brain. *Neuron*, *77*(3), 586–595. https://doi.org/10.1016/j.neuron.2012.12.028

Mueller, S., Wang, D., Pan, R., Holt, D. J., & Liu, H. (2015). Abnormalities in hemispheric specialization of caudate nucleus connectivity in schizophrenia. *JAMA Psychiatry*, *72*(6), 552–560. https://doi.org/10.1001/jamapsychiatry.2014.3176

Müller, R.-A., Kleinhans, N., Kemmotsu, N., Pierce, K., & Courchesne, E. (2003). Abnormal variability and distribution of functional maps in autism: An fMRI study of visuomotor learning. *American Journal of Psychiatry*, *160*(10), 1847–1862. https://doi.org/10.1176/appi.ajp.160.10.1847

Newbold, D. J., & Dosenbach, N. U. (2021). Tracking plasticity of individual human brains. *Current Opinion in Behavioral Sciences*, *40*, 161–168. https://doi.org/10.1016/j.cobeha.2021.04.018

Newbold, D. J., Laumann, T. O., Hoyt, C. R., Hampton, J. M., Montez, D. F., Raut, R. V., Ortega, M., Mitra, A., Nielsen, A. N., Miller, D. B., Adeyemo, B., Nguyen, A. L., Scheidter, K. M., Tanenbaum, A. B., Van, A. N., Marek, S., Schlaggar, B. L., Carter, A. R., Greene, D. J., … Dosenbach, N. U. F. (2020). Plasticity and spontaneous activity

pulses in disused human brain circuits. *Neuron*, *107*(3), 580-589.e6. https://doi.org/10.1016/j.neuron.2020.05.007

Nielsen, J. A., Zielinski, B. A., Fletcher, P. T., Alexander, A. L., Lange, N., Bigler, E. D., Lainhart, J. E., & Anderson, J. S. (2014). Abnormal lateralization of functional connectivity between language and default mode regions in autism. *Molecular Autism*, *5*(1), 8. https://doi.org/10.1186/2040-2392-5-8

Ocklenburg, S., Westerhausen, R., Hirnstein, M., & Hugdahl, K. (2013). Auditory hallucinations and reduced language lateralization in schizophrenia: A meta-analysis of dichotic listening studies. *Journal of the International Neuropsychological Society*, *19*(4), 410–418. https://doi.org/10.1017/S1355617712001476

Oldfield, R. (1971). Oldfield, R. (1971). The assessment and analysis of handedness: The Edinburgh inventory. *Neuropsychologia*, *9*(1), 97-113.

Opsahl, T., Colizza, V., Panzarasa, P., & Ramasco, J. J. (2008). Prominence and control: The weighted rich-club effect. *Physical Review Letters*, *101*(16), 168702. https://doi.org/10.1103/PhysRevLett.101.168702

Penfield, W., & Jasper, H. (1954). *Epilepsy and the functional anatomy of the human brain.* Little, Brown.

Perez, D. C., Dworetsky, A., Braga, R. M., Beeman, M., & Gratton, C. (2023). Hemispheric asymmetries of individual differences in functional connectivity. *Journal of Cognitive Neuroscience*, *35*(2), 200–225. https://doi.org/10.1162/jocn_a_01945

Persichetti, A. S., Shao, J., Gotts, S. J., & Martin, A. (2022). Maladaptive laterality in cortical networks related to social communication in Autism Spectrum Disorder. *Journal of Neuroscience*, *42*(48), 9045–9052. https://doi.org/10.1523/JNEUROSCI.1229-22.2022

R Core Team. (2011). *Wilcoxon rank sum and signed rank tests*. R Documentation.[Online]. Available: http://stat. ethz. ch/R-manual/R ….

Rasmussen, T., & Milner, B. (1977). The role of early left-brain injury in determining lateralization of cerebral speech functions. *Annals of the New York Academy of Sciences*, *299*, 355–369.

Redcay, E., & Courchesne, E. (2008). Deviant functional magnetic resonance imaging patterns of brain activity to speech in 2–3-year-old children with autism spectrum disorder. *Biological Psychiatry*, *64*(7), 589–598.

Ringo, J. L., Doty, R. W., Demeter, S., & Simard, P. Y. (1994). Time is of the essence: A conjecture that hemispheric specialization arises from interhemispheric conduction delay. *Cerebral Cortex*, *4*(4), 331–343. https://doi.org/10.1093/cercor/4.4.331

Smith, S. M., Jenkinson, M., Woolrich, M. W., Beckmann, C. F., Behrens, T. E. J., Johansen-Berg, H., Bannister, P. R., De Luca, M., Drobnjak, I., Flitney, D. E., Niazy, R. K., Saunders, J., Vickers, J., Zhang, Y., De Stefano, N., Brady, J. M., & Matthews, P. M. (2004). Advances in functional and structural MR image analysis and implementation as FSL. *NeuroImage*, *23*, S208–S219. https://doi.org/10.1016/j.neuroimage.2004.07.051

Somerville, L. H., Bookheimer, S. Y., Buckner, R. L., Burgess, G. C., Curtiss, S. W., Dapretto, M., Elam, J. S., Gaffrey, M. S., Harms, M. P., Hodge, C., Kandala, S., Kastman, E. K., Nichols, T. E., Schlaggar, B. L., Smith, S. M., Thomas, K. M., Yacoub, E., Van Essen, D. C., & Barch, D. M. (2018). The Lifespan Human Connectome Project in Development: A large-scale study of brain connectivity development in 5–21 year olds. *NeuroImage*, *183*, 456–468. https://doi.org/10.1016/j.neuroimage.2018.08.050

Sommer, I., Aleman, A., Ramsey, N., Bouma, A., & Kahn, R. (2001). Handedness, language lateralisation and anatomical asymmetry in schizophrenia: Meta-analysis. *The British Journal of Psychiatry*, *178*(4), 344–351. https://doi.org/10.1192/bjp.178.4.344

Sun, J., Gao, X., Hua, Q., Du, R., Liu, P., Liu, T., Yang, J., Qiu, B., Ji, G.-J., Hu, P., & Wang, K. (2022). Brain functional specialization and cooperation in Parkinson's disease. *Brain Imaging and Behavior*, *16*(2), 565–573. https://doi.org/10.1007/s11682-021-00526-4

Vallortigara, G. (2006). The evolutionary psychology of left and right: Costs and benefits of lateralization. *Developmental Psychobiology*, *48*(6), 418–427. https://doi.org/10.1002/dev.20166

Vázquez-Rodríguez, B., Suárez, L. E., Markello, R. D., Shafiei, G., Paquola, C., Hagmann, P., van den Heuvel, M. P., Bernhardt, B. C., Spreng, R. N., & Misic, B. (2019). Gradients of structure–function tethering across neocortex. *Proceedings of the National Academy of Sciences*, *116*(42), 21219–21227. https://doi.org/10.1073/pnas.1903403116

Wada, J., & Rasmussen, T. (1960). Intracarotid injection of sodium amytal for the lateralization of cerebral speech dominance: Experimental and clinical observations. *Journal of Neurosurgery*, *17*(2), 266–282.

Wang, D., Buckner, R. L., & Liu, H. (2014). Functional specialization in the human brain estimated by intrinsic hemispheric interaction. *Journal of Neuroscience*, *34*(37), Art. 37. https://doi.org/10.1523/JNEUROSCI.0787-14.2014

Wilcoxon, F. (1945). Individual comparisons by ranking methods. *Biometrics Bulletin*, *1*(6), 80–83. https://doi.org/10.2307/3001968

Yeo, B. T. T., Krienen, F. M., Sepulcre, J., Sabuncu, M. R., Lashkari, D., Hollinshead, M., Roffman, J. L., Smoller, J. W., Zöllei, L., Polimeni, J. R., Fischl, B., Liu, H., & Buckner,

R. L. (2011). The organization of the human cerebral cortex estimated by intrinsic functional connectivity. *Journal of Neurophysiology*, *106*(3), 1125–1165. https://doi.org/10.1152/jn.00338.2011

Zalesky, A., Fornito, A., Cocchi, L., Gollo, L. L., & Breakspear, M. (2014). Time-resolved resting-state brain networks. *Proceedings of the National Academy of Sciences*, *111*(28), 10341–10346. https://doi.org/10.1073/pnas.1400181111

Study 3 Supplementary Materials

Figure S1

Direct Replication of Wang et al. (2014) Across the HCP-Discovery and HCP-Replication Datasets

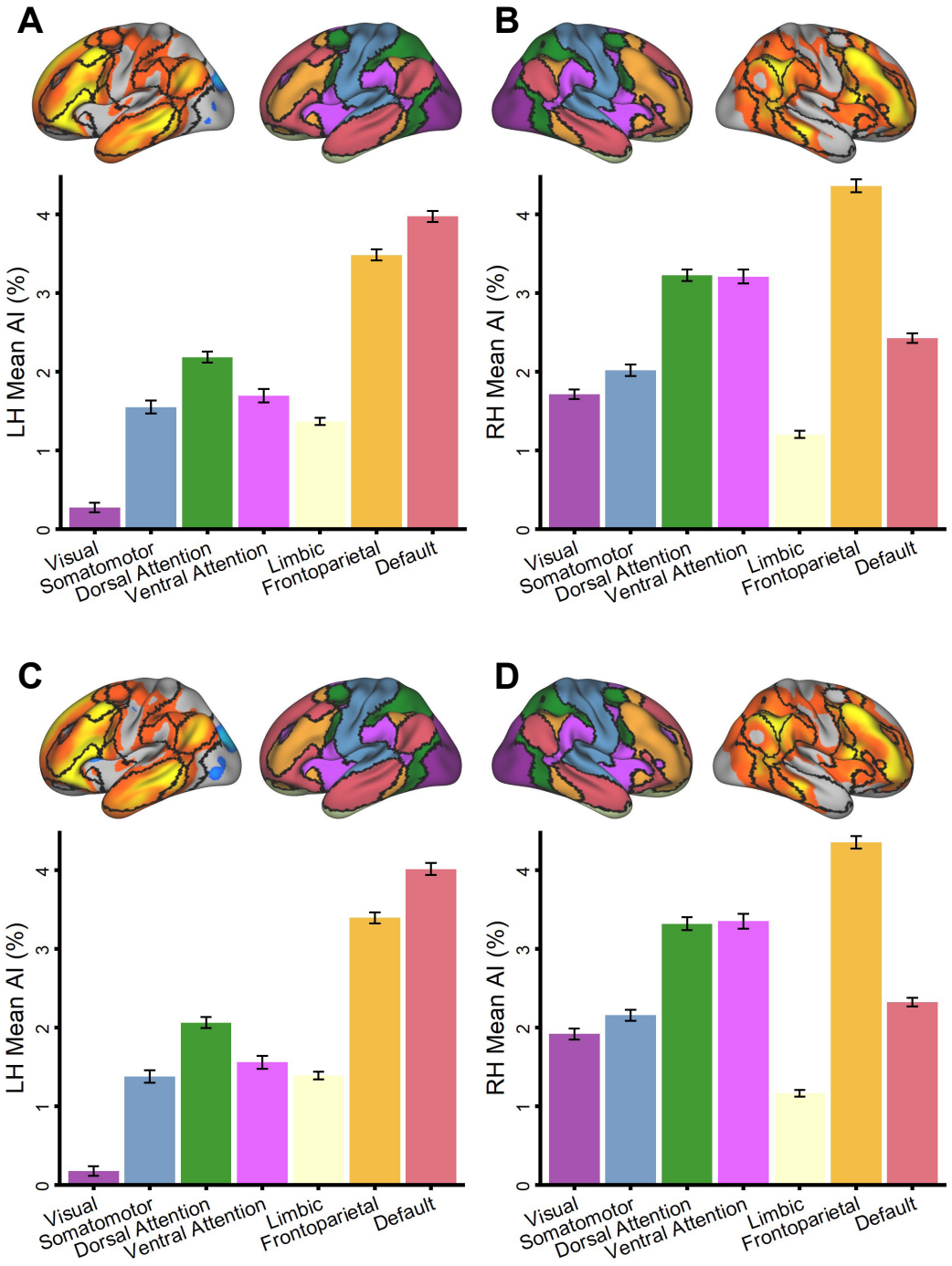

Note. Panel A depicts autonomy index (AI) values averaged within the left hemisphere networks of the HCP-Discovery dataset. Panel B depicts AI values averaged within the right hemisphere networks of the HCP-Discovery dataset. Panel C depicts AI values averaged within the left hemisphere networks of the HCP-Replication dataset. Panel D depicts AI values averaged within the right hemisphere networks of the HCP-Replication dataset. Network boundaries came from a 1000-subject parcellation (Yeo et al., 2011). Error bars represent the standard error of the mean.

Figure S2

Replication of Wang et al. (2014) Across 17 Networks in the HCP-Discovery and HCP-Replication Datasets

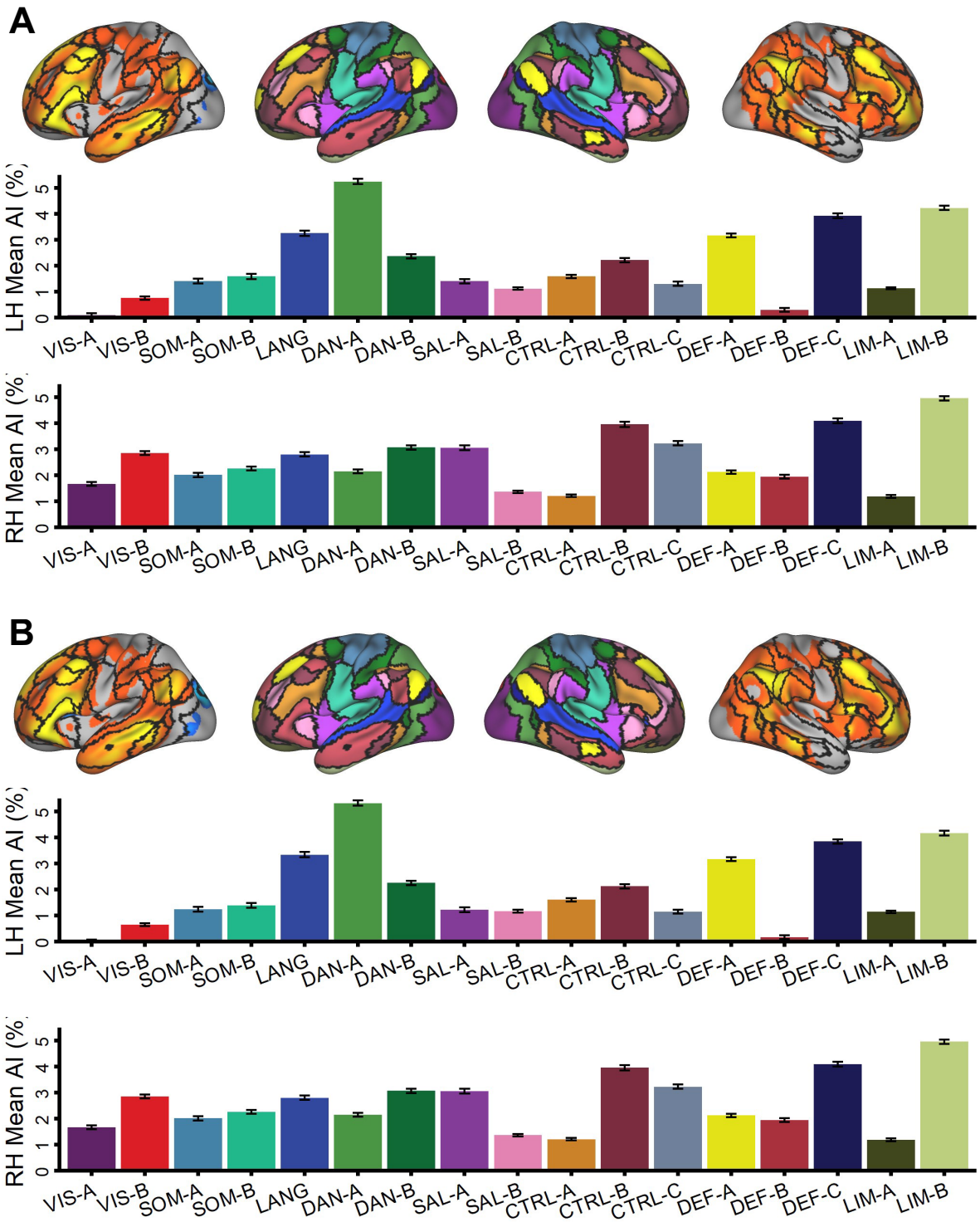

Note. Panel A depicts the average autonomy index (AI) values for each of 17 networks in the left and right hemispheres for the HCP-Discovery dataset. Panel B depicts the average AI values for each of 17 networks in the left and right hemispheres for the HCP-Replication datasets. Network boundaries came from a 1000-subject parcellation (Yeo et al., 2011). Error bars represent the standard error of the mean.

Figure S3

Test-Retest Reliability and Temporal Signal-to-Noise Ratio (tSNR) by Network

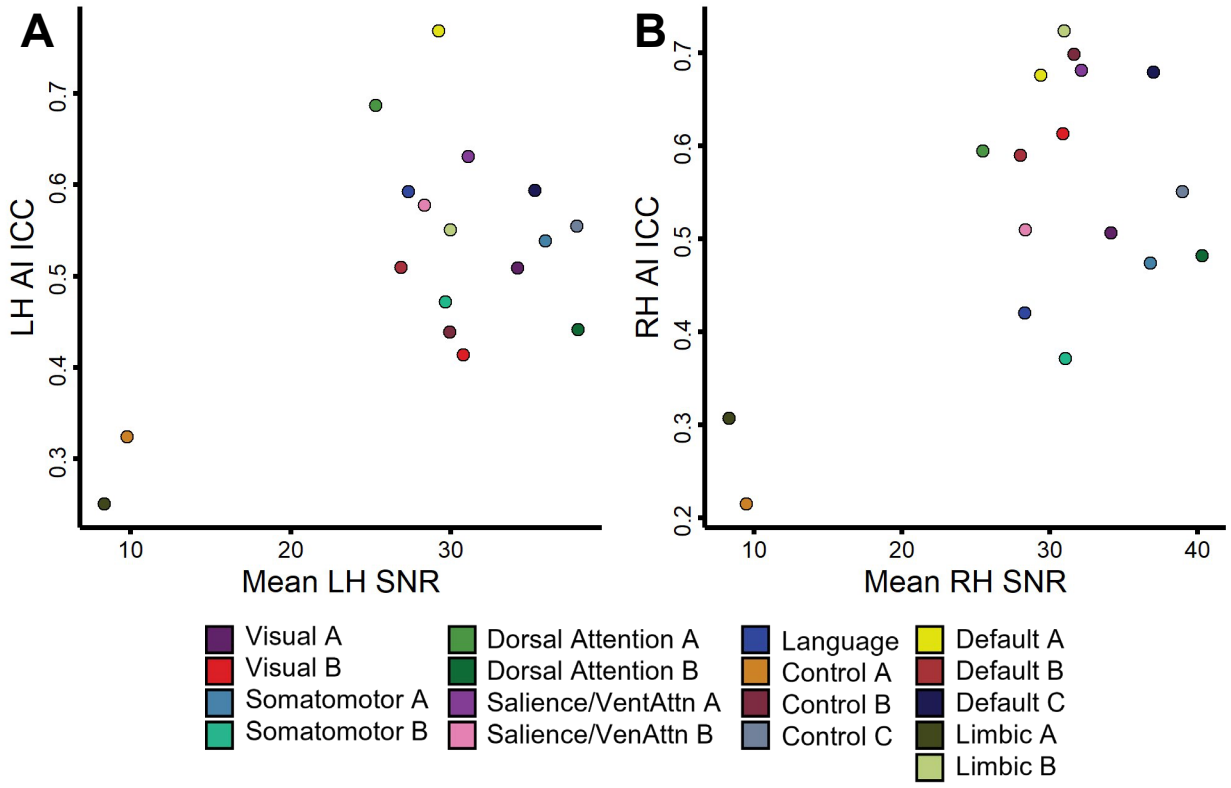

Note. tSNR was calculated by taking the mean BOLD signal and dividing it by the standard deviation in BOLD signal across all vertices for each participant. The tSNR was then averaged within network boundaries for each participant before being averaged across participants. Spearman rank correlations identified no relationship between intraclass correlation coefficients and network-averaged temporal signal-to-noise ratios in the left hemisphere ($r(15) = 0.11$, $p =$

.68; Panel A) and right hemisphere (r(15) = .27, p = .29; Panel B). Each circle represents a single network.

Figure S4

Autonomy Index Network Reliability

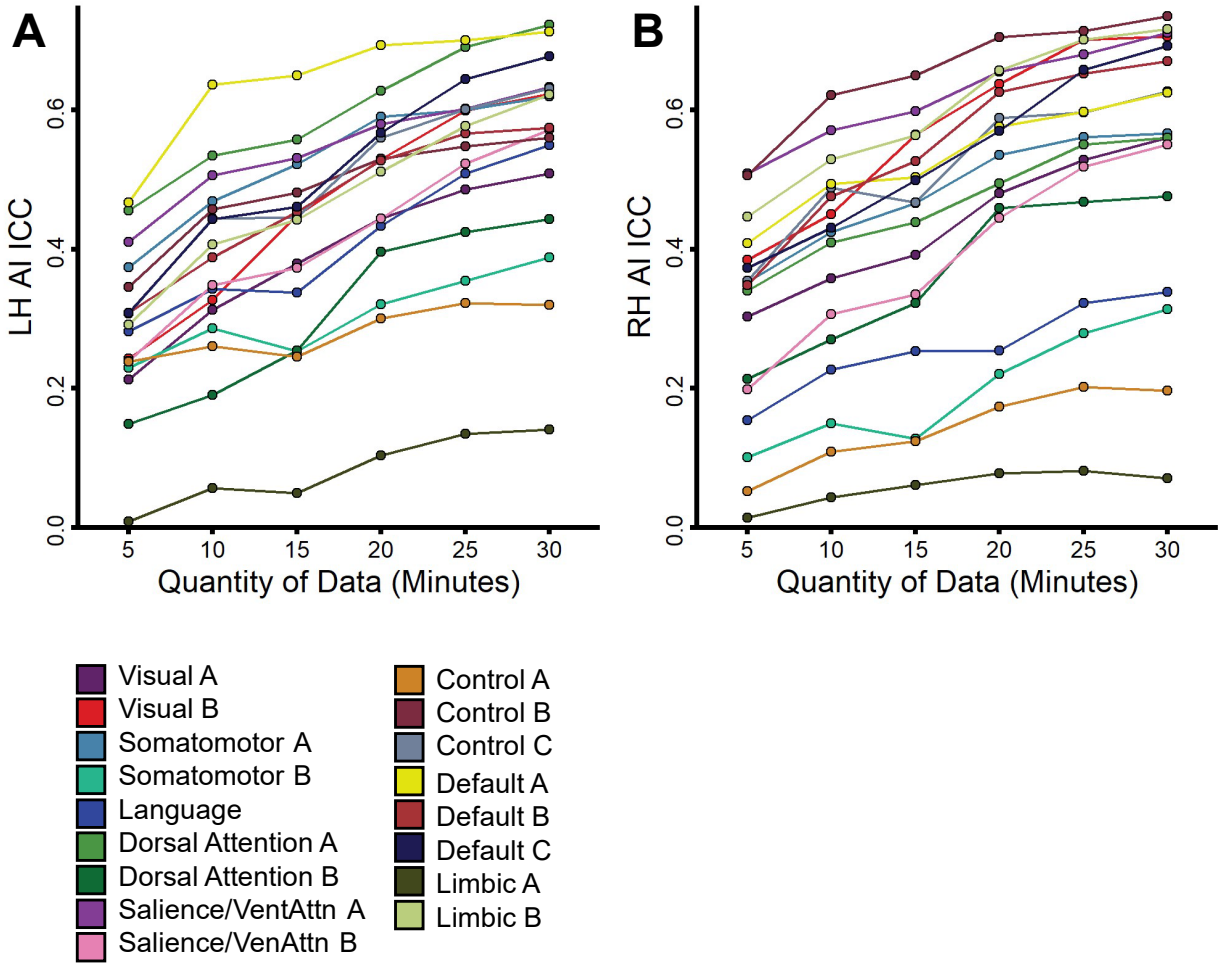

Note. Depicted is the intraclass correlation coefficient calculated for each network's mean autonomy index value between the 30 independent minutes of data and each increment of data. Panel A depicts the intraclass correlation coefficients for networks in the left hemisphere while Panel B depicts the intraclass correlation coefficients for networks in the right hemisphere.

Figure S5

Negative Relationship Between Handedness and Salience/Ventral Attention-A Left Hemisphere Mean Autonomy Index

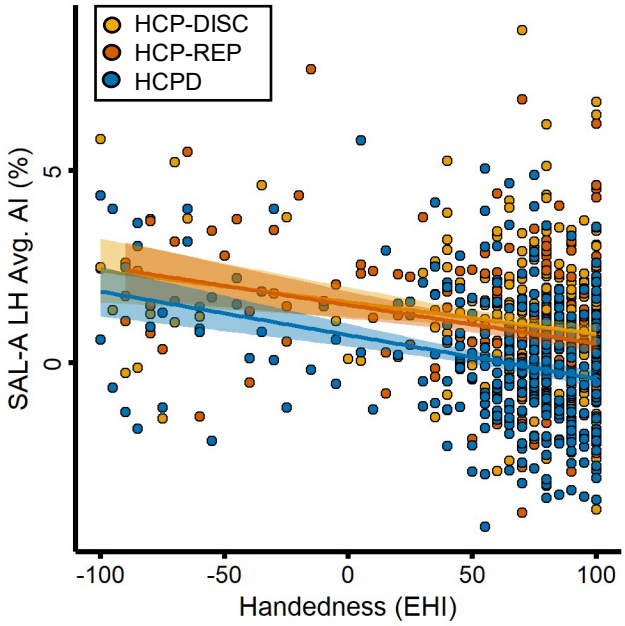

Note. Across the HCP-Discovery, HCP-Replication, and HCPD datasets, handedness (measured via the Edinburgh Handedness Inventory) was a significant covariate for the left hemisphere Salience/Ventral Attention-A mean autonomy index. Each point represents a subject.

Figure S6

Deconstructed Autonomy Index (dAI) for the Top Five Left-Lateralized Networks in the HCP-Discovery Dataset

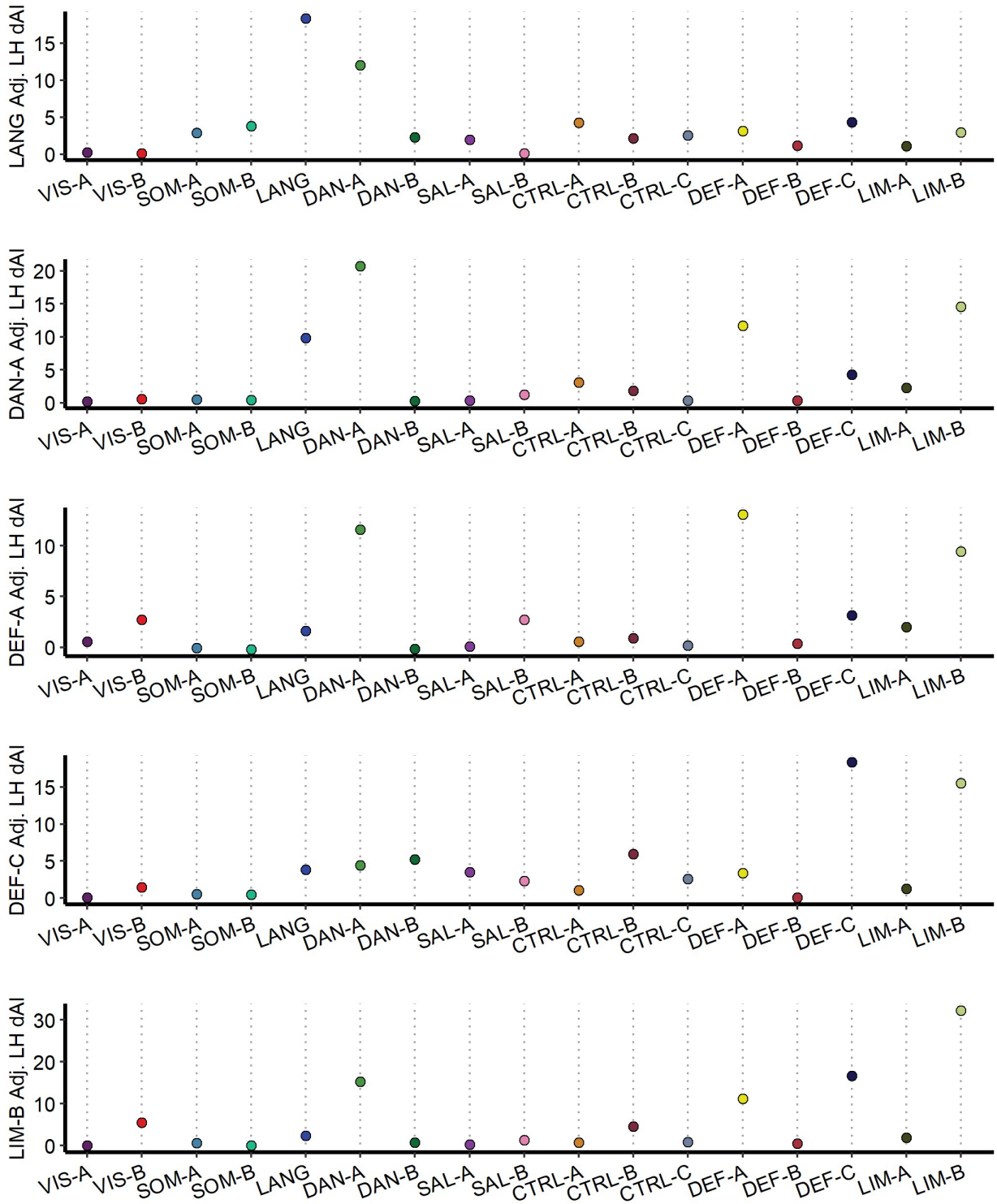

Note. dAI values were averaged within each network (1-17) for each target network (Language, Dorsal Attention-A, Default-A, Default-C, and Limbic-B). Points represent mean dAI values.

Figure S7

Deconstructed Autonomy Index (dAI) for the Top Five Right-Lateralized Networks in the HCP-Discovery Dataset

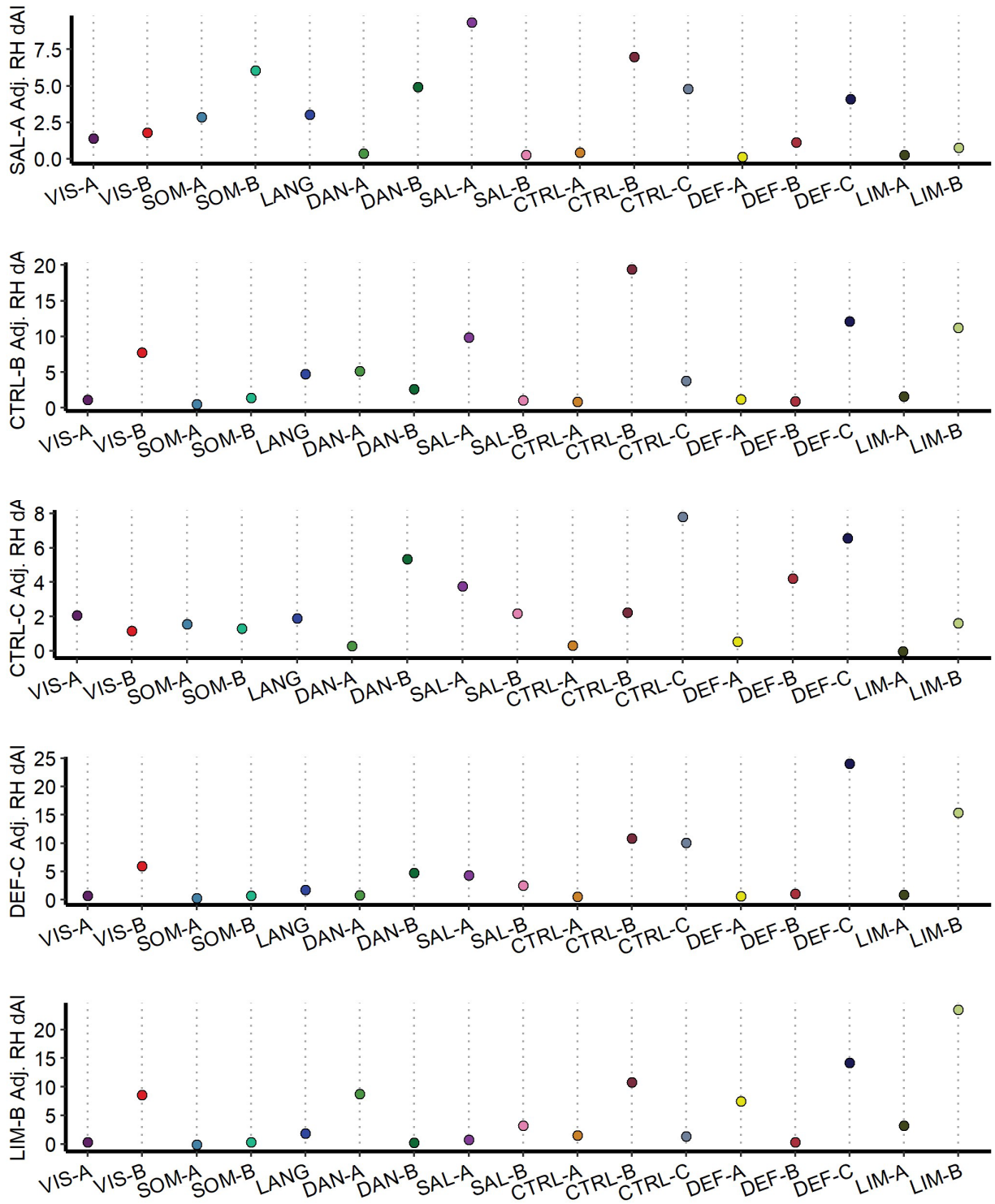

Note. dAI values were averaged within each network (1-17) for each target network (Salience/Ventral Attention-A, Control-B, Control-C, Default-C, and Limbic-B). Points represent mean dAI values.

Figure S8

Deconstructed Autonomy Index (dAI) for the Top Five Left-Lateralized Networks in the HCP-Replication Dataset

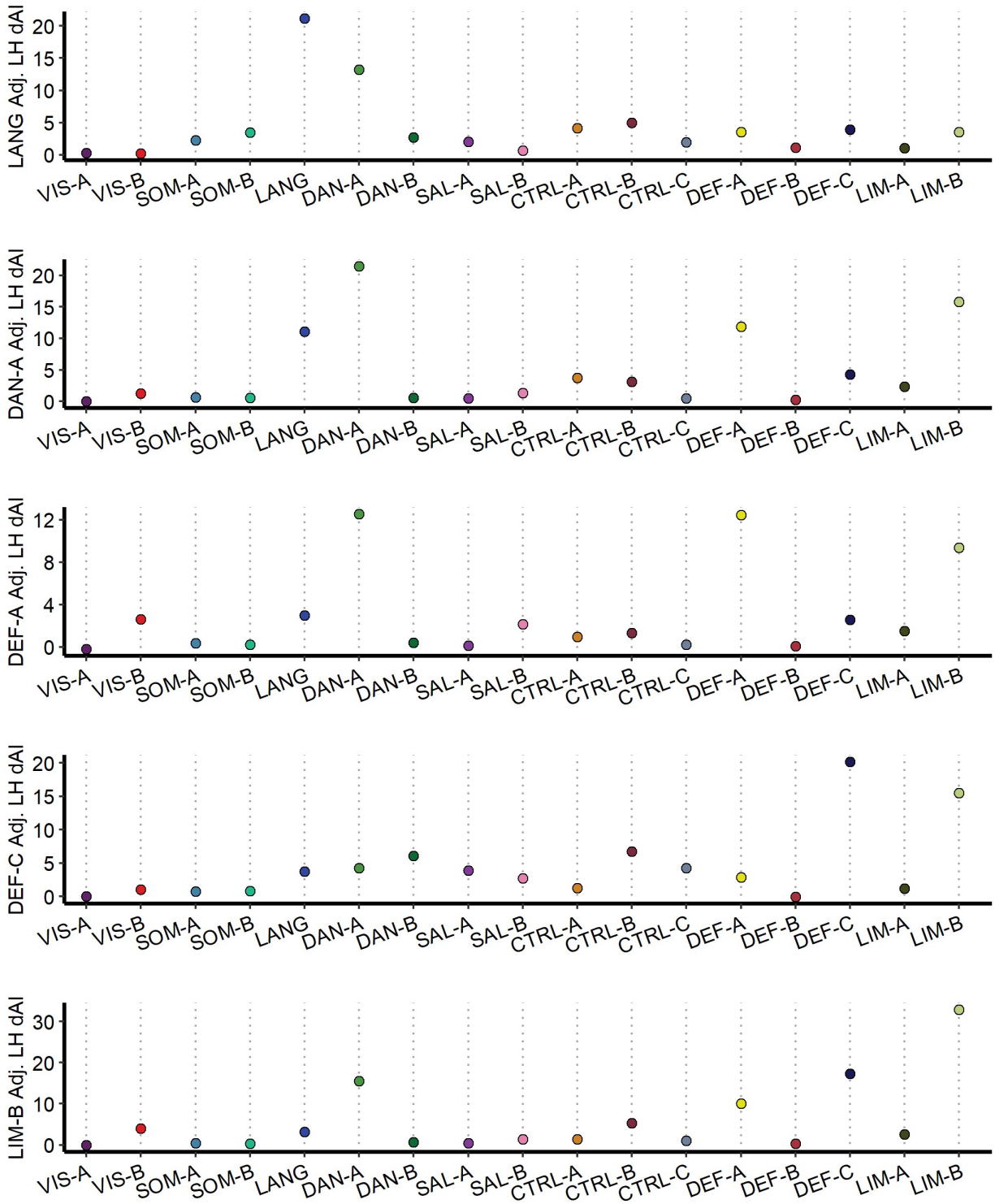

Note. dAI values were averaged within each network (1-17) for each target network (Language, Dorsal Attention-A, Default-A, Default-C, and Limbic-B). Points represent mean dAI values.

Figure S9

Deconstructed Autonomy Index (dAI) for the Top Five Right-Lateralized Networks in the HCP-Replication Dataset

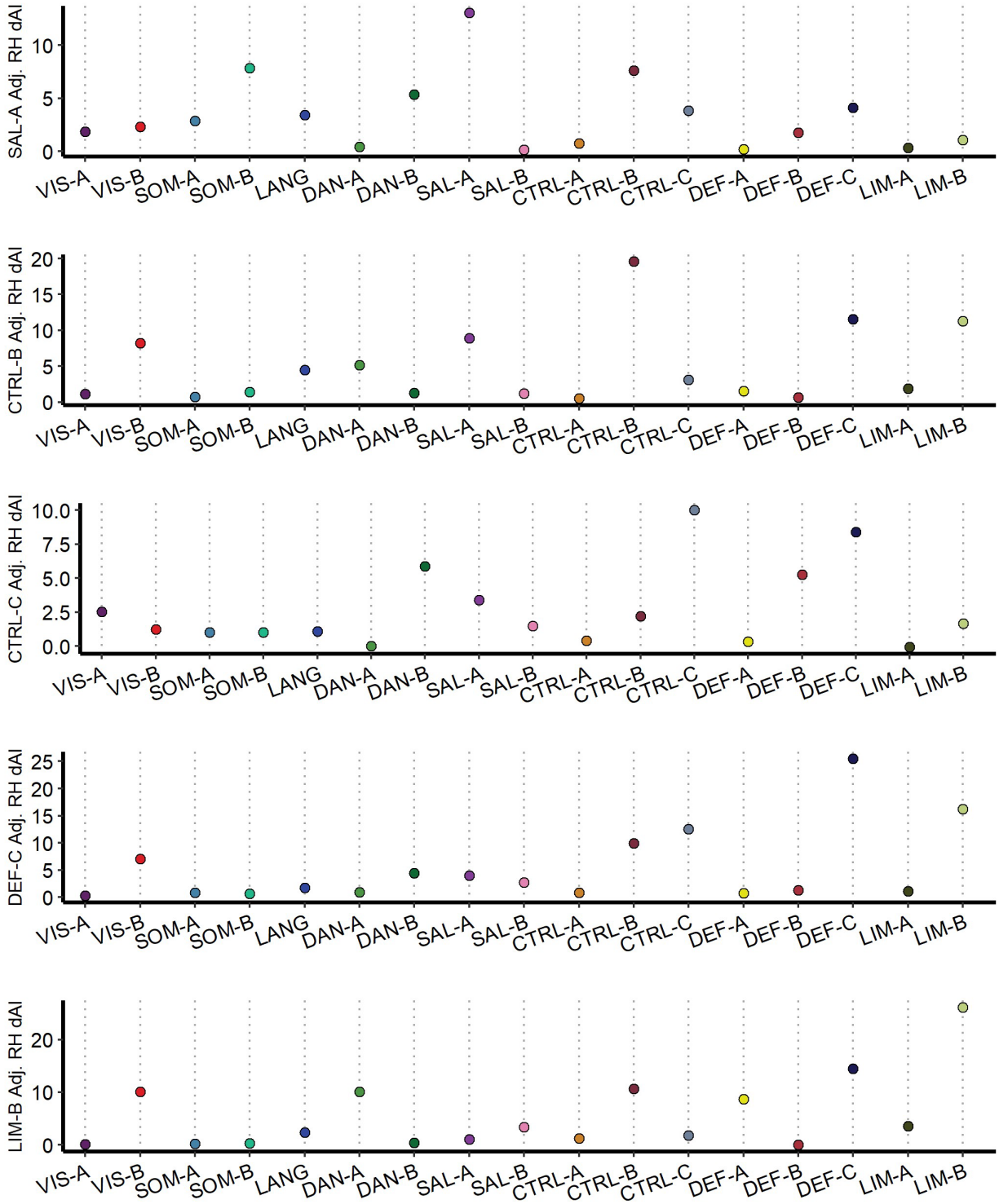

Note. dAI values were averaged within each network (1-17) for each target network (Salience/Ventral Attention-A, Control-B, Control-C, Default-C, and Limbic-B). Points represent mean dAI values.

Figure S10

Deconstructed Autonomy Index (dAI) for the Top Five Left-Lateralized Networks in the HCPD Dataset

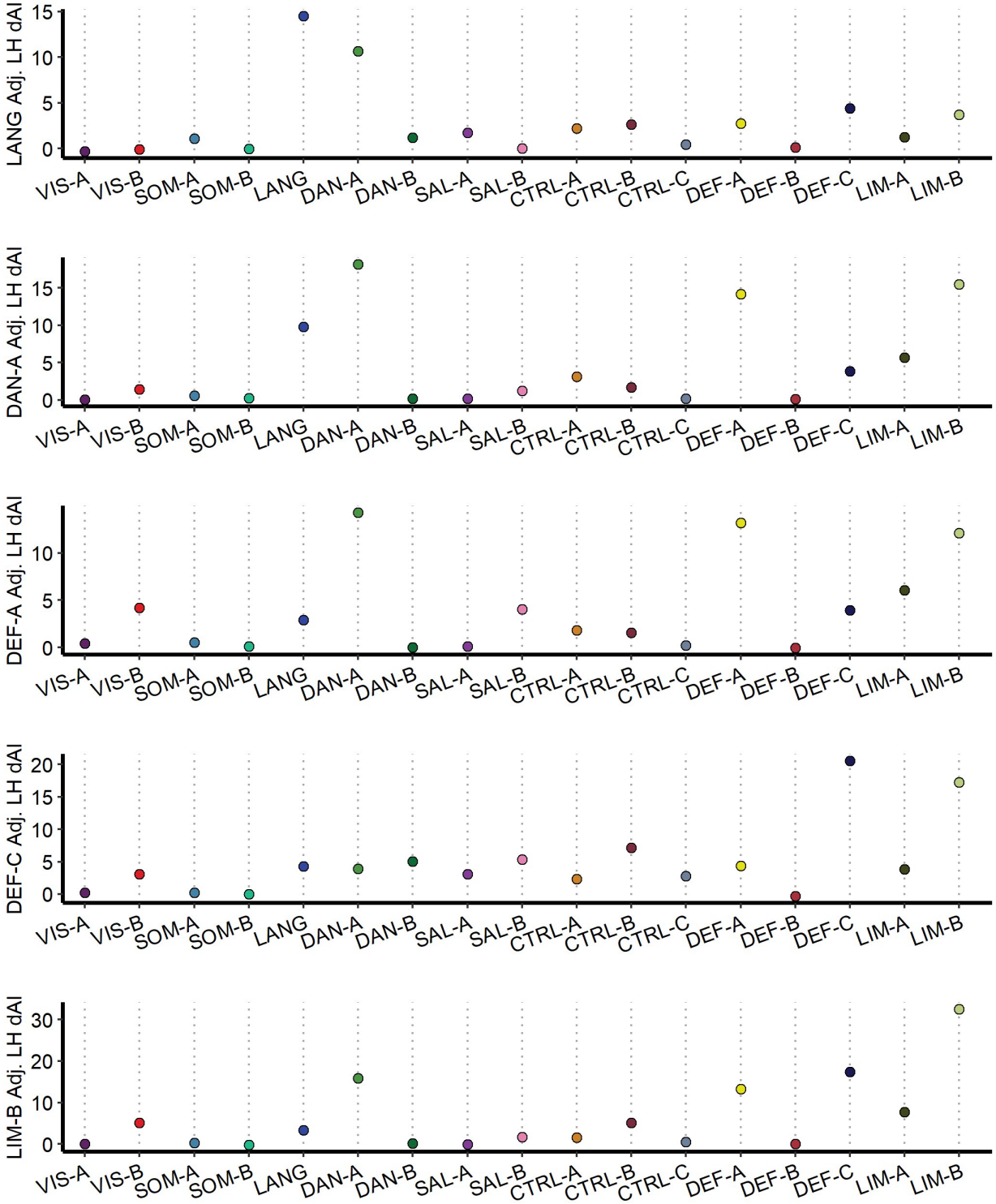

Note. dAI values were averaged within each network (1-17) for each target network (Language, Dorsal Attention-A, Default-A, Default-C, and Limbic-B). Points represent mean dAI values.

Figure S11

Deconstructed Autonomy Index (dAI) for the Top Five Right-Lateralized Networks in the HCPD Dataset

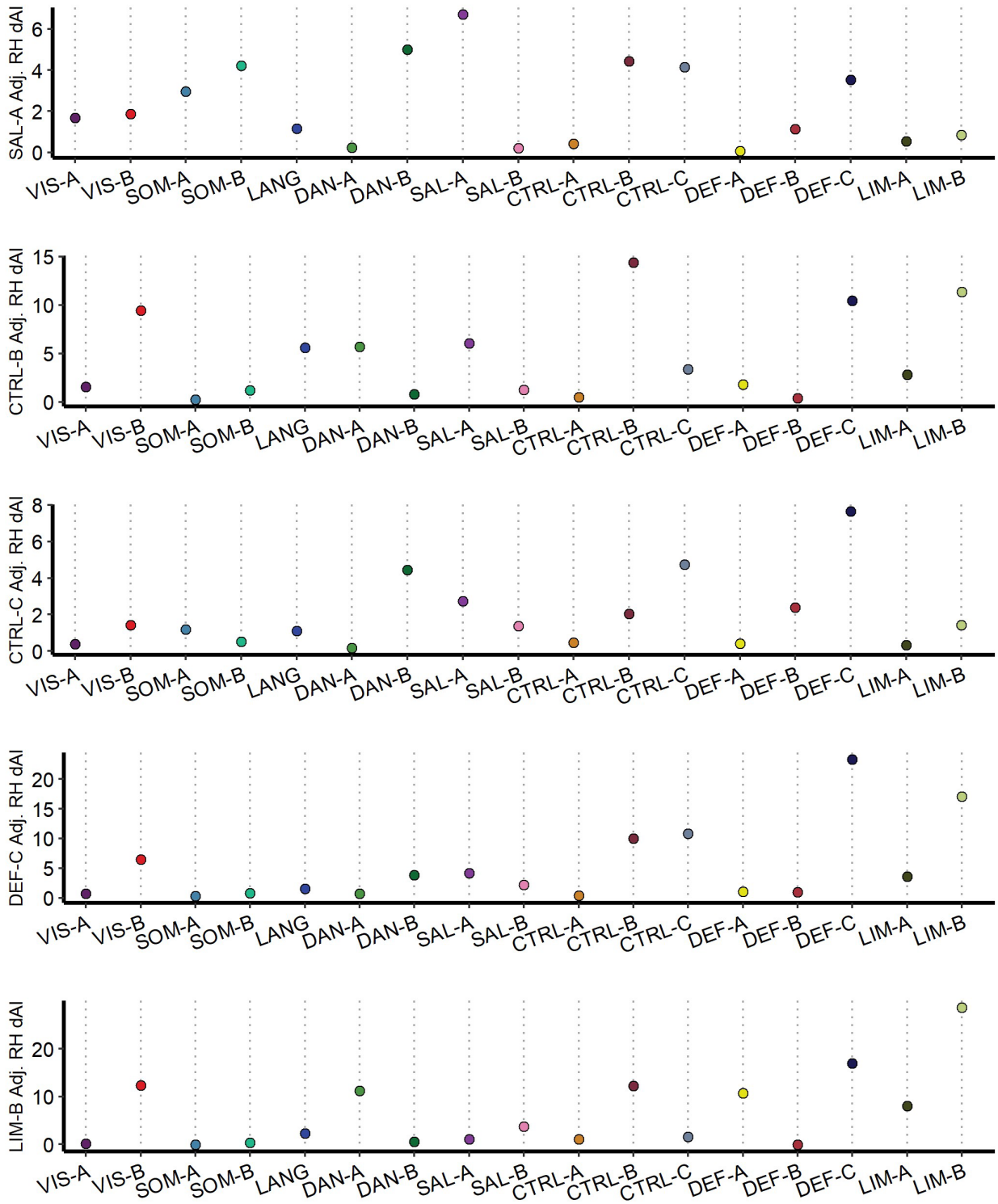

Note. dAI values were averaged within each network (1-17) for each target network (Salience/Ventral Attention-A, Control-B, Control-C, Default-C, and Limbic-B). Points represent mean dAI values.

Figure S12

Deconstructed Autonomy Index (dAI) for All 17 Target Networks in the HCP-Discovery Dataset

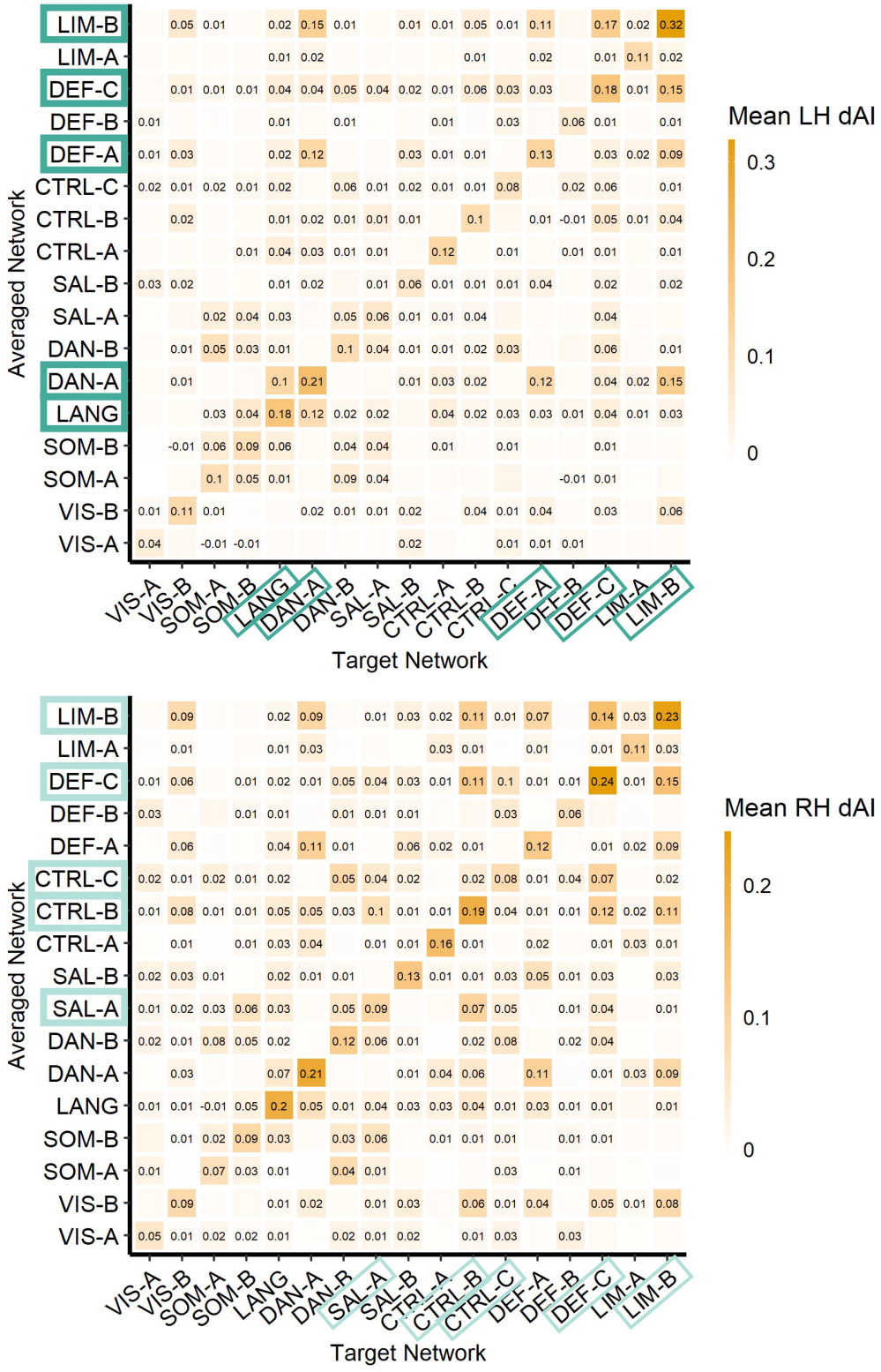

Note. dAI values were averaged within each network (1-17) for each target network (1-17). The diagonal represents within-network contributions, which appear to make the strongest contributions to network specialization. These are followed by contributions from other specialized networks.

Figure S13

Deconstructed Autonomy Index (dAI) for All 17 Target Networks in the HCP-Replication Dataset

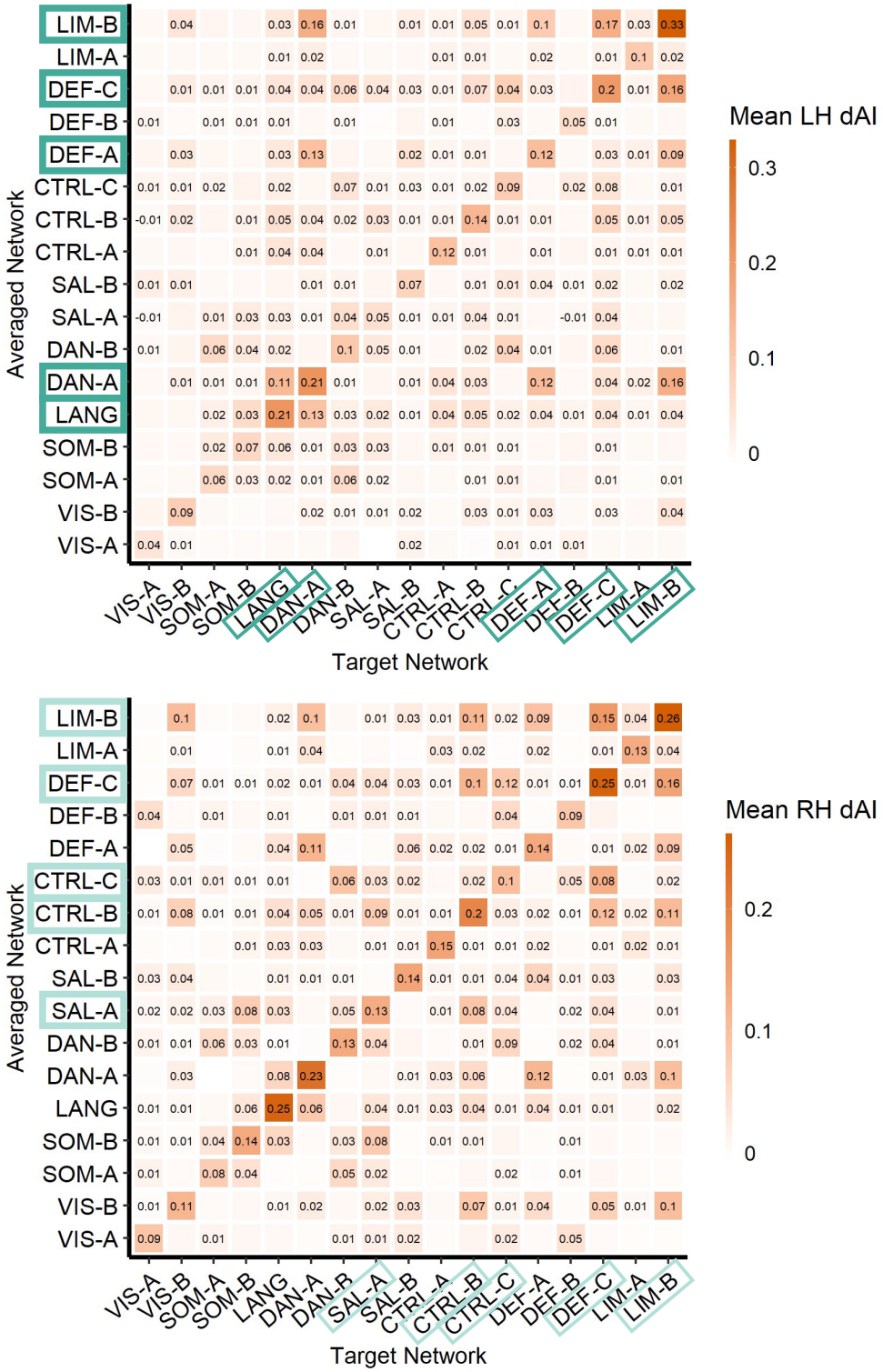

Note. dAI values were averaged within each network (1-17) for each target network (1-17). The diagonal represents within-network contributions, which appear to make the strongest contributions to network specialization. These are followed by contributions from other specialized networks.

Figure S14

Deconstructed Autonomy Index (dAI) for All 17 Target Networks in the HCPD Dataset

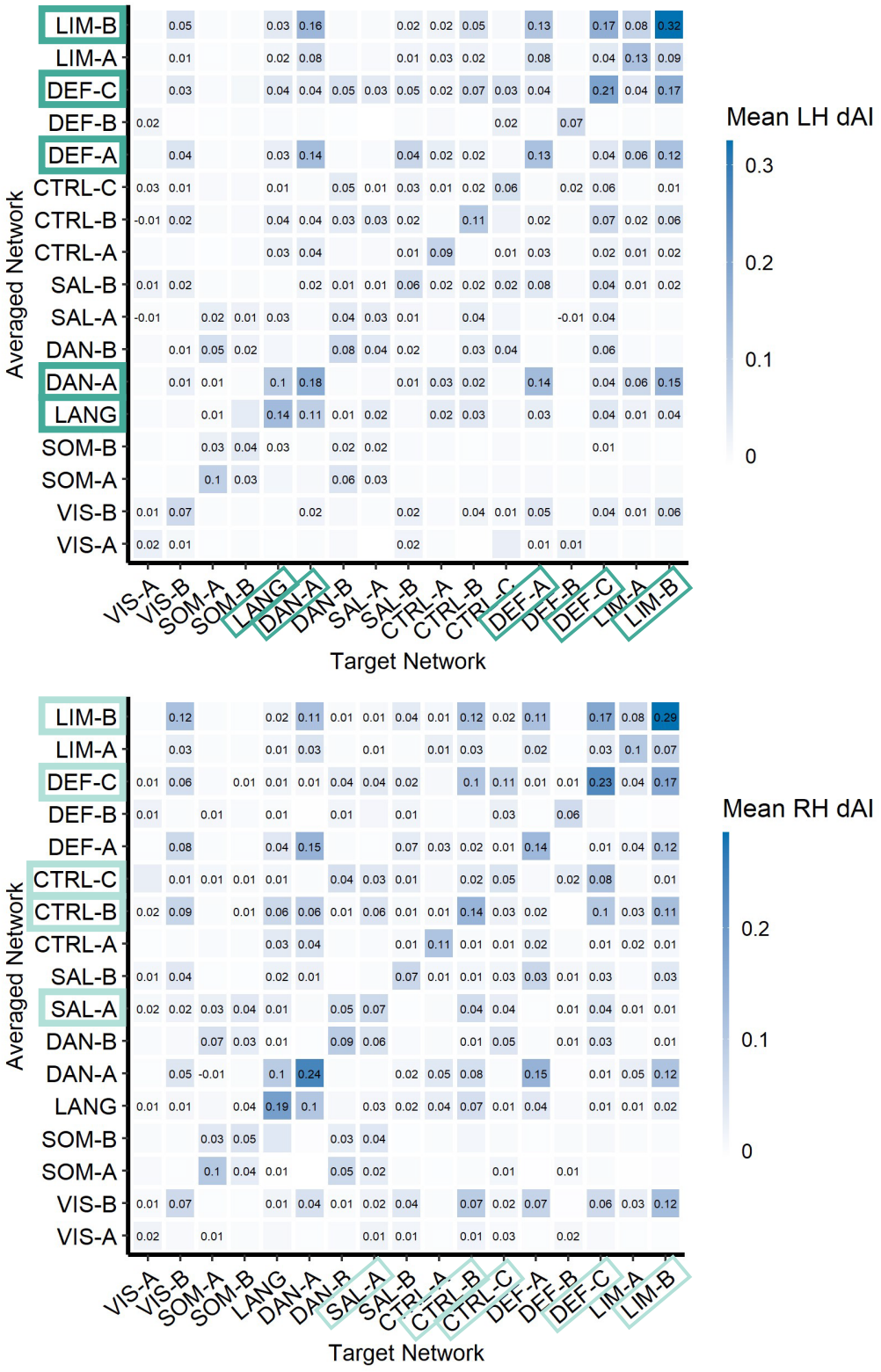

Note. dAI values were averaged within each network (1-17) for each target network (1-17). The diagonal represents within-network contributions, which appear to make the strongest contributions to network specialization. These are followed by contributions from other specialized networks.

Supplementary Table 1

Identifying Left-Specialized Networks Using Multiple Regressions in the HCP-Discovery Dataset (N = 276), HCP-Replication Dataset (N = 277), and the HCPD Dataset (N = 343)

Network Intercept	Dataset	β	*SE*	*t*	*p*
Visual-A					
	HCP-DISC	0.19	0.18	1.07	.29
	HCPD-REP	0.01	0.02	0.29	.14
	HCPD	0.11	0.13	0.84	.39
Visual-B					
	HCP-DISC	0.99	0.16	6.4	< .001
	HCPD-REP	0.75	0.15	5.06	< .001
	HCPD	0.97	0.18	5.3	< .001
Somatomotor-A					
	HCP-DISC	1.66	0.21	7.52	< .001
	HCPD-REP	1.44	0.23	6.28	< .001
	HCPD	1.3	0.14	9.33	< .001
Somatomotor-B					
	HCP-DISC	1.78	0.24	7.48	< .001
	HCPD-REP	1.79	0.19	-0.68	< .001
	HCPD	0.63	0.12	5.3	< .001
Language					
	HCP-DISC	3.53	0.32	11.12	< .001
	HCPD-REP	4.22	0.32	13.16	< .001
	HCPD	3.87	0.21	18.14	< .001
Dorsal Attention-A					
	HCP-DISC	5.13	0.22	23.79	< .001
	HCPD-REP	5.79	0.24	24.09	< .001
	HCPD	5.89	0.22	27.09	< .001
Dorsal Attention-B					
	HCP-DISC	2.57	0.22	11.44	< .001
	HCPD-REP	2.7	0.22	12.09	< .001
	HCPD	1.73	0.18	9.81	< .001
Salience/VenAttn-A					

	HCP-DISC	1.55	0.23	6.76	< .001
	HCPD-REP	1.58	0.22	7.29	< .001
	HCPD	0.76	0.17	4.38	< .001
Salience/VenAttn-B					
	HCP-DISC	1.07	0.13	7.89	< .001
	HCPD-REP	1.24	0.15	8.36	< .001
	HCPD	1.77	0.16	11.28	< .001
Control-A					
	HCP-DISC	1.32	0.18	7.14	< .001
	HCPD-REP	1.59	0.16	9.79	< .001
	HCPD	1.57	0.09	16.75	< .001
Control-B					
	HCP-DISC	1.56	0.24	6.46	< .001
	HCPD-REP	1.97	0.24	8.36	< .001
	HCPD	1.94	0.19	9.91	< .001
Control-C					
	HCP-DISC	1.19	0.23	5.19	< .001
	HCPD-REP	1.25	0.21	6.07	< .001
	HCPD	0.58	0.18	3.28	0.001
Default-A					
	HCP-DISC	3.16	0.2	15.54	< .001
	HCPD-REP	3.59	0.22	16.67	< .001
	HCPD	4.42	0.21	20.78	< .001
Default-B					
	HCP-DISC	0.4	0.16	2.57	0.01
	HCPD-REP	0.39	0.17	2.24	0.03
	HCPD	0.14	0.13	1.07	0.28
Default-C					
	HCP-DISC	4.06	0.21	19.47	< .001
	HCPD-REP	3.85	0.2	18.91	< .001
	HCPD	4.33	0.2	21.17	< .001
Limbic-A					
	HCP-DISC	0.92	0.09	10.09	< .001
	HCPD-REP	1.01	0.11	9.26	< .001
	HCPD	2.12	0.13	16.16	< .001
Limbic-B					
	HCP-DISC	4.11	0.21	19.27	< .001
	HCPD-REP	3.91	0.22	18.09	< .001
	HCPD	4.7	0.21	22.31	< .001

Note: Coefficients and *p*-values for the intercept are shown. Networks with reliably significant (Bonferroni-corrected alpha level of .001) intercepts are bolded.

Supplementary Table 2

Identifying Right-Specialized Networks Using Multiple Regressions in the HCP-Discovery Dataset (N = 276), HCP-Replication Dataset (N = 277), and the HCPD Dataset (N = 343)

Network Intercept	Dataset	β	*SE*	*t*	*p*
Visual-A					
	HCP-DISC	1.39	0.18	7.69	< .001
	HCPD-REP	1.52	0.19	7.76	< .001
	HCPD	0.93	0.14	6.72	< .001
Visual-B					
	HCP-DISC	2.4	0.2	11.97	< .001
	HCPD-REP	2.79	0.21	13.48	< .001
	HCPD	3.27	0.21	15.89	< .001
Somatomotor-A					
	HCP-DISC	1.84	0.2	9	< .001
	HCPD-REP	1.86	0.2	9.29	< .001
	HCPD	1.78	0.13	13.46	< .001
Somatomotor-B					
	HCP-DISC	2.02	0.18	11.07	< .001
	HCPD-REP	2.33	0.17	14.01	< .001
	HCPD	1.46	0.13	11.64	< .001
Language					
	HCP-DISC	2.41	0.18	13.45	< .001
	HCPD-REP	2.75	0.21	13.03	< .001
	HCPD	1.61	0.18	8.91	< .001
Dorsal Attention-A					
	HCP-DISC	2.15	0.19	11.32	< .001
	HCPD-REP	1.84	0.19	9.93	< .001
	HCPD	2.12	0.19	10.72	< .001
Dorsal Attention-B					
	HCP-DISC	2.76	0.22	12.56	< .001
	HCPD-REP	2.67	0.24	11.15	< .001
	HCPD	2.54	0.19	13.21	< .001
Salience/VenAttn-A					
	HCP-DISC	2.83	0.24	11.82	< .001
	HCPD-REP	3.14	0.26	11.95	< .001
	HCPD	2.74	0.21	13.05	< .001
Salience/VenAttn-B					
	HCP-DISC	1.73	0.14	12.61	< .001
	HCPD-REP	1.75	0.14	12.45	< .001
	HCPD	1.49	0.14	10.63	< .001
Control-A					
	HCP-DISC	1.22	0.11	11.56	< .001
	HCPD-REP	1.24	0.1	11.9	< .001
	HCPD	0.84	0.06	13.14	< .001
Control-B					

	HCP-DISC	4.09	0.26	15.68	< .001
	HCPD-REP	4.09	0.26	15.79	< .001
	HCPD	4.22	0.24	17.89	< .001
Control-C					
	HCP-DISC	2.91	0.22	13.03	< .001
	HCPD-REP	3.14	0.23	13.67	< .001
	HCPD	2.84	0.19	15.15	0.001
Default-A					
	HCP-DISC	1.98	0.21	9.64	< .001
	HCPD-REP	1.83	0.18	9.95	< .001
	HCPD	1.97	0.19	9.98	< .001
Default-B					
	HCP-DISC	1.46	0.17	8.51	< .001
	HCPD-REP	1.91	0.19	9.87	< .001
	HCPD	1.19	0.14	8.38	< .001
Default-C					
	HCP-DISC	3.62	0.22	16.21	< .001
	HCPD-REP	4.12	0.23	17.92	< .001
	HCPD	4.33	0.2	21.44	< .001
Limbic-A					
	HCP-DISC	1.14	0.15	7.85	< .001
	HCPD-REP	1.24	0.14	9.16	< .001
	HCPD	2.01	0.11	17.59	< .001
Limbic-B					
	HCP-DISC	5.06	0.26	19.69	< .001
	HCPD-REP	5.7	0.23	24.29	< .001
	HCPD	6.07	0.22	27.85	< .001

Note: Coefficients and *p*-values for the intercept are shown. Networks with reliably significant (Bonferroni-corrected alpha level of .001) intercepts are bolded.

References

Wang, D., Buckner, R. L., & Liu, H. (2014). Functional specialization in the human brain estimated by intrinsic hemispheric interaction. *Journal of Neuroscience*, *34*(37), Art. 37. https://doi.org/10.1523/JNEUROSCI.0787-14.2014

Yeo, B. T. T., Krienen, F. M., Sepulcre, J., Sabuncu, M. R., Lashkari, D., Hollinshead, M., Roffman, J. L., Smoller, J. W., Zöllei, L., Polimeni, J. R., Fischl, B., Liu, H., & Buckner, R. L. (2011). The organization of the human cerebral cortex estimated by intrinsic functional connectivity. *Journal of Neurophysiology*, *106*(3), 1125–1165. https://doi.org/10.1152/jn.00338.2011

Overall Conclusion

The primary aim of this dissertation was to estimate specialization in individuals using methodologically robust approaches. Together, the findings from the three studies have shed light on the organization of specialized brain networks in neurotypical and autistic individuals.

Study 1 introduced a novel measure of specialization, the Network Surface Area Ratio (NSAR), which was used to identify the most specialized networks and explore their relationships. Of the 17 networks examined, eight were found to be significantly specialized. Surprisingly, the most left-specialized network was the Dorsal Attention-A network, while the most right-specialized network was the Limbic-B network, contradicting our initial hypothesis that the language, visuospatial attention, and executive control networks would be the most specialized. Moreover, evidence supported a covariation pattern of specialization between left- and right-specialized networks, such as between the Limbic-B and Dorsal Attention-A networks, as well as evidence for compensation between networks specialized to the same hemisphere, such as between Language and Dorsal Attention-A.

After establishing NSAR as a reliable method in neurotypical adolescents and adults in Study 1, we investigated specialization in autism. Group differences in specialization between the autism and neurotypical groups were found for the Language, Salience/Ventral Attention-A, and Control-B networks. This was contrary to our original hypothesis that group differences would be limited to the Language network. Additionally, we examined the relationship between language specialization and three behavioral phenotypes and found no significant relationships between language specialization and verbal ability or autism symptom severity. However, we did find that language delay stratified language specialization, with group differences between the autism with language delay and neurotypical groups.

Study 3 took a deeper dive into within-individual specialization using the autonomy index, which had been previously implemented at the group level. We replicated group-level findings at the 7-network level and then implemented the autonomy index at the individual level with 17 networks. The most left-specialized network was the Dorsal Attention-A network while the Limbic-B network was the most right-specialized network. Then, to understand contributing factors to specialization, a novel method, the deconstructed autonomy index, was implemented to identify the specific connections contributing to each network's specialization. The greatest contributors to specialization included first within-network connections followed by connections with other specialized networks.

When considering the main takeaways from all three studies, it becomes evident that robust measures were crucial in achieving the proposed research objectives. NSAR provided spatially specific information with a clear and intuitive interpretation and required no scaling or normalization factor. In contrast, the autonomy index allowed us to explore functional connectivity differences between hemispheres, focusing on within- versus between-hemisphere connectivity. Both measures captured specialization in distinct ways, but arrived at the identification of the Dorsal Attention-A and Limbic-B networks as the most specialized networks, although the ranking following these two networks varied depending on the method.

Another integral aspect of these studies was the focus on exploring specialization at multiple levels. On the macroscale, Study 1 examined specialized network relationships, such as how the degree of specialization in left-specialized networks might influence the degree of specialization of right-specialized networks. On the microscale, Study 3 delved into vertex-level connections, identifying the specific connections that contributed to specialization, which were first along a within-between network gradient and then along a specialization gradient.

Additionally, this research provides valuable insights into the implications of atypical specialization in autism. Interestingly, no age-related effects were consistently observed in Studies 1 and 3 across the HCP-Discovery, HCP-Replication, and HCPD datasets. Moreover, no relationship was found between language specialization and verbal ability in Study 2. However, language delay stratified language specialization. Together, these three pieces of evidence suggest that disruptions in language specialization occurring early in development may be responsible for behavioral differences observed in autism later in adolescence and adulthood.

In conclusion, this dissertation has contributed significantly to our understanding of specialization within individuals using two distinct measures. By examining 17 networks for specialization, we confirmed that both NSAR and the autonomy index supported the Dorsal Attention-A network and the Limbic-B network as the most specialized networks. Furthermore, our investigation of specialization in autism uncovered group differences across three networks and highlighted the relationship between language delay and language specialization. The identification of connections contributing to specialization provides a potential benchmark for further exploration in different developmental stages and neurodevelopmental conditions such as schizophrenia. Overall, this research has extended our comprehension of large-scale brain network organization within individuals, offering insights into their relationships with each other and their underpinnings.

Appendix: Deviations from the Prospectus and Justification

Overview

While carrying out the analyses proposed in the prospectus, several large and small deviations emerged due to a variety of factors. Several of these larger differences came after a crucial conversation with a collaborator, which shaped a research question and added a previously unconsidered hypothesis. Other changes arose following denial of access to a proposed dataset and the review of data quality. But most significantly, after examining preliminary results, some questions and hypotheses were grouped together in a different configuration, more conducive to a logical storyline and eventual publication. Regardless of the reason, changes to the three aims, their associated hypotheses, and proposed datasets from the accepted prospectus are outlined below.

Aim 1

In the prospectus, Aim 1 encapsulated estimating hemispheric specialization within adult neurotypical individuals using the autonomy index in conjunction with various parcellation schemes. This aim was updated to investigating hemispheric specialization in neurotypical individuals using a different metric of specialization: the network surface area ratio (NSAR). After a conversation with a colleague, we decided to adapt a measure of specialization based on network surface area. However, including results from both the autonomy index and NSAR proved to be too cumbersome for one paper. Since there were enough interesting results with NSAR, it made more sense to split this off as its own paper. Results from estimating specialization using the autonomy index became Aim 3. Additionally, only one parcellation scheme was adopted: the multi-session hierarchical Bayesian modeling algorithm (MS-HBM; Kong et al., 2019). Preliminary results in ten subjects showed extremely low test-retest reliability

for the other proposed parcellation scheme, *k*-means, so this was dropped from the analysis pipeline.

Given the changes in the overall goal of Aim 1, it is unsurprising that significant changes were made to the hypotheses and datasets used to test these hypotheses. The proposed Hypothesis 1.1 centered around identifying the most specialized networks, which were hypothesized to be language and visuospatial attention. This was updated to also include networks involved in executive control, which was neglected due to oversight. Previously, a frontoparietal control network was found to be highly specialized (in addition to networks involved in language and attention; Wang et al., 2014). Changes were also made to the proposed Hypothesis 1.2, which hypothesized that a greater relationship between language laterality and language specialization would be found using a within-individual approach. We were not able to acquire the proposed Harvard dataset, which included the large quantity of language task data needed to compare language laterality and language specialization within individuals. However, we were able to examine how an Human Connectome Project (HCP) group parcellation aligned with a language atlas (Lipkin et al., 2022) as part of examining the validity of NSAR. Additionally, the second hypothesis was reframed as investigating specialized network relationships, which we hypothesized would follow one of three patterns: covariation, compensation, or independence.

Neither the Harvard dataset (Braga et al., 2020) nor the Midnight Scan Club dataset (Gordon et al., 2020) were included in Study 1 as proposed. The Harvard dataset was dropped due to access issues while the Midnight Scan Club dataset was dropped due to unusually large voxel sizes (4 mm isotropic; Gordon et al., 2017), which resulted in a poor group parcellation as assessed by a colleague. In place of these datasets, the HCP, Human Connectome Project-

Development (HCPD; Somerville et al., 2018), and the Natural Scenes Dataset (NSD; Allen et al., 2022) were selected. The HCP dataset includes approximately one hour of resting-state fMRI data per individual with relatively low motion per participant. The HCPD dataset was brought in as an additional replication dataset in a younger population (5-21 years). The NSD dataset was used to examine task effects on the individual parcellations and NSAR, since there are multiple hours of resting-state fMRI and task fMRI data available per participant (although the number of participants is reduced at $N = 8$).

Aim 2

Originally, Aim 2 was proposed as estimating hemispheric specialization in a neurodevelopmental population (autism) and exploring the relationship between hemispheric specialization and verbal ability. The second part of this aim was expanded to include the relationship between language specialization and three behavioral phenotypes instead of one. Those additional behavioral phenotypes included autism symptom severity and language delay, which were added to enable us to better understand which, if any, of these were driving a hypothesized group difference in language specialization. Thus, while the first two hypotheses of this study were unchanged, two were added. We hypothesized that language specialization would be negatively related to autism symptom severity. We also hypothesized that language delay would stratify language specialization (based on work by Floris et al., 2016, 2021).

In the prospectus, two datasets were proposed for Aim 2: the Utah dataset and the Healthy Brain Network dataset (HBN; Alexander et al., 2017). The HBN dataset was originally included as a replication dataset for any findings identified with the Utah dataset. However, the HBN dataset was processed with the inclusion of task and rest data, which were rendered obsolete since task effects on individual parcellations and estimates of specialization were found.

Rather than continue with these data, the HBN dataset was dropped and a within-dataset replication using first and second runs in the Utah dataset (forthcoming) will be used as a replacement.

Aim 3

The greatest discrepancy in aims between the prospectus and the final dissertation can be found with Aim 3. It was proposed that we examine specialization in neurotypical development, across later childhood, adolescence, and early adulthood. However, preliminary analyses using the HCPD dataset found no consistent age-related effects on specialization. So, as previously described, Aim 1 was split into two studies: one estimating specialization using NSAR and another estimating specialization using the autonomy index. Thus, the new aim became estimating specialization in individuals using the autonomy index by first replicating Wang et al. (2014) using a group parcellation, estimating specialization in individuals, and then examining which connections contribute the most to a given networks specialization.

In the prospectus, only one hypothesis was proposed for Aim 3, and this was regarding the direction of functional specialization for left- and right-specialized networks across development. Keeping with the updated aim, this was replaced with two hypotheses. First, that the most specialized networks identified in neurotypical individuals using the autonomy index would be the language, visuospatial attention, and executive control networks (following Hypothesis 1.1). Second, we hypothesized that connections contributing to specialization would follow one of three gradients: a within-between networks gradient, a specialization gradient, or a sensorimotor-association cortex gradient. This second hypothesis was included with the goal of deconstructing specialization and examining which connections contribute the most to

specialization. To address this hypothesis, a new method was developed: the deconstructed autonomy index.

Proposed datasets for Aim 3 included the HCPD dataset with the Adolescent Brain Cognitive Development (ABCD) Study® (Casey et al., 2018) as a replication dataset. This was altered to include the same datasets as Aim 1: HCP, HCPD, and NSD. This allows us to directly compare results from the two measures of specialization. And, since no reliable effects of age on specialization for any of the networks were identified, the HCPD dataset was included as an additional replication dataset in a younger population.

References

Alexander, L. M., Escalera, J., Ai, L., Andreotti, C., Febre, K., Mangone, A., Vega-Potler, N., Langer, N., Alexander, A., Kovacs, M., Litke, S., O'Hagan, B., Andersen, J., Bronstein, B., Bui, A., Bushey, M., Butler, H., Castagna, V., Camacho, N., … Milham, M. P. (2017). An open resource for transdiagnostic research in pediatric mental health and learning disorders. *Scientific Data*, *4*(1), Art. 1. https://doi.org/10.1038/sdata.2017.181

Allen, E. J., St-Yves, G., Wu, Y., Breedlove, J. L., Prince, J. S., Dowdle, L. T., Nau, M., Caron, B., Pestilli, F., Charest, I., Hutchinson, J. B., Naselaris, T., & Kay, K. (2022). A massive 7T fMRI dataset to bridge cognitive neuroscience and artificial intelligence. *Nature Neuroscience*, *25*(1), Art. 1. https://doi.org/10.1038/s41593-021-00962-x

Braga, R. M., DiNicola, L. M., Becker, H. C., & Buckner, R. L. (2020). Situating the left-lateralized language network in the broader organization of multiple specialized large-scale distributed networks. *Journal of Neurophysiology*, *124*(5), Art. 5. https://doi.org/10.1152/jn.00753.2019

Casey, B. J., Cannonier, T., Conley, M. I., Cohen, A. O., Barch, D. M., Heitzeg, M. M., Soules, M. E., Teslovich, T., Dellarco, D. V., Garavan, H., Orr, C. A., Wager, T. D., Banich, M. T., Speer, N. K., Sutherland, M. T., Riedel, M. C., Dick, A. S., Bjork, J. M., Thomas, K. M., … Dale, A. M. (2018). The Adolescent Brain Cognitive Development (ABCD) study: Imaging acquisition across 21 sites. *Developmental Cognitive Neuroscience*, *32*, 43–54. https://doi.org/10.1016/j.dcn.2018.03.001

Floris, D. L., Lai, M.-C., Auer, T., Lombardo, M. V., Ecker, C., Chakrabarti, B., Wheelwright, S. J., Bullmore, E. T., Murphy, D. G. M., Baron-Cohen, S., & Suckling, J. (2016). Atypically rightward cerebral asymmetry in male adults with autism stratifies individuals

with and without language delay. *Human Brain Mapping*, *37*(1), 230–253. https://doi.org/10.1002/hbm.23023

Floris, D. L., Wolfers, T., Zabihi, M., Holz, N. E., Zwiers, M. P., Charman, T., Tillmann, J., Ecker, C., Dell'Acqua, F., Banaschewski, T., Moessnang, C., Baron-Cohen, S., Holt, R., Durston, S., Loth, E., Murphy, D. G. M., Marquand, A., Buitelaar, J. K., Beckmann, C. F., … Zwiers, M. P. (2021). Atypical brain asymmetry in autism—A candidate for clinically meaningful stratification. *Biological Psychiatry: Cognitive Neuroscience and Neuroimaging*, *6*(8), 802–812. https://doi.org/10.1016/j.bpsc.2020.08.008

Gordon, E. M., Laumann, T. O., Gilmore, A. W., Newbold, D. J., Greene, D. J., Berg, J. J., Ortega, M., Hoyt-Drazen, C., Gratton, C., Haoxin Sun, Hampton, J. M., Coalson, R. S., Nguyen, A., McDermott, K. B., Shimony, J. S., Snyder, A. Z., Schlaggar, B. L., Petersen, S. E., Nelson, S. M., & Dosenbach, N. U. F. (2020). *The Midnight Scan Club (MSC) dataset* [dataset]. Openneuro. https://doi.org/10.18112/OPENNEURO.DS000224.V1.0.3

Gordon, E. M., Laumann, T. O., Gilmore, A. W., Newbold, D. J., Greene, D. J., Berg, J. J., Ortega, M., Hoyt-Drazen, C., Gratton, C., Sun, H., Hampton, J. M., Coalson, R. S., Nguyen, A. L., McDermott, K. B., Shimony, J. S., Snyder, A. Z., Schlaggar, B. L., Petersen, S. E., Nelson, S. M., & Dosenbach, N. U. F. (2017). Precision functional mapping of individual human brains. *Neuron*, *95*(4), Art. 4. https://doi.org/10.1016/j.neuron.2017.07.011

Kong, R., Li, J., Orban, C., Sabuncu, M. R., Liu, H., Schaefer, A., Sun, N., Zuo, X.-N., Holmes, A. J., Eickhoff, S. B., & Yeo, B. T. T. (2019). Spatial topography of individual-specific cortical networks predicts human cognition, personality, and emotion. *Cerebral Cortex*, *29*(6), Art. 6. https://doi.org/10.1093/cercor/bhy123

Lipkin, B., Tuckute, G., Affourtit, J., Small, H., Mineroff, Z., Kean, H., Jouravlev, O., Rakocevic, L., Pritchett, B., Siegelman, M., Hoeflin, C., Pongos, A., Blank, I. A., Struhl, M. K., Ivanova, A., Shannon, S., Sathe, A., Hoffmann, M., Nieto-Castañón, A., & Fedorenko, E. (2022). *LanA (Language Atlas): A probabilistic atlas for the language network based on fMRI data from >800 individuals* (p. 2022.03.06.483177). bioRxiv. https://doi.org/10.1101/2022.03.06.483177

Somerville, L. H., Bookheimer, S. Y., Buckner, R. L., Burgess, G. C., Curtiss, S. W., Dapretto, M., Elam, J. S., Gaffrey, M. S., Harms, M. P., Hodge, C., Kandala, S., Kastman, E. K., Nichols, T. E., Schlaggar, B. L., Smith, S. M., Thomas, K. M., Yacoub, E., Van Essen, D. C., & Barch, D. M. (2018). The Lifespan Human Connectome Project in Development: A large-scale study of brain connectivity development in 5–21 year olds. *NeuroImage*, *183*, 456–468. https://doi.org/10.1016/j.neuroimage.2018.08.050

Wang, D., Buckner, R. L., & Liu, H. (2014). Functional specialization in the human brain estimated by intrinsic hemispheric interaction. *Journal of Neuroscience*, *34*(37), Art. 37. https://doi.org/10.1523/JNEUROSCI.0787-14.2014